Numerical computation of the acoustic radiation force exerted by a standing wave on an object immersed in a fluid by using a Lattice Boltzmann method for waves

Esteban Castro Ávila

Universidad Nacional de Colombia
Facultad de Ciencias, Departamento de Física
Bogotá D.C, Colombia
2023

Numerical computation of the acoustic radiation force exerted by a standing wave on an object immersed in a fluid by using a Lattice Boltzmann method for waves

Esteban Castro Ávila

Thesis submitted in partial fulfillment of the requirements for the degree of:

Master in science - Physics

Thesis advisor:
Dr. Ret-Nat. José Daniel Muñoz Castaño
Thesis co-advisor:
Dr. PhD. Paolo Malgaretti

Simulation of physic systems group Universidad Nacional de Colombia

Facultad de Ciencias, Departamento de Física
Bogotá D.C, Colombia
2023

To my family.

"The imagination of nature is far, far greater than the imagination of man."
-Richard P. Feynman

Acknowledgements

First, I wish to express my gratefulness to the National University of Colombia for letting me to be formed as scientist and supporting me with opportunities as the Academic rights Exception and the Auxiliary Professor scholarships. In the second place, to thank the Helmholtz Institute of Erlangen-Nürmberg for renewable energy (HI-ERN), especially to Prof. Dr. Jens Harting and Dr. Paolo Malgaretti, for inviting me as guest scientist for a four mnth research stay in Erlangen, Germany, and to collaborate in the development of the software LB3D. In the same manner I would like to thank the University Center of Bayern for Latin-America (BAYLAT) for its finnancial support during my research stay in Erlangen, and Prof. Harting, Dr. Malgaretti and the Jülich Forschungzentrum for financing my flight tickets. Also, I would like to give of course gratefulness to my family who was supporting me emotionally during these recent years to learn new things and grow professionally. I wish also thank my Thesis advisor, Dr. Ret-Nat José Daniel Muñoz, for the numerous lessons taught to me in the academics and professional life, ad my Thesis co-advisor, Dr. Paolo Malgaretti, for his essential contribution to this project and by providing knowledge about academic research strategies. In the same manner I wish to thank to all colleagues and partners at HI-ERN who guided me through the completion of this project, such as Dr. Othmane Aouane and Johannes Hielscher, among others, and finally to all colleagues from the National University of Colombia for the given emotional support during my M.Sc. studies.

Abstract

Title: Numerical computation of the acoustic radiation force exerted by a standing wave on an object immersed in a fluid by using a Lattice Boltzmann method for waves

The present work introduces a numerical procedure to compute the acoustic radiation force produced by standing waves on a compressible object immersed in an inviscid fluid. Instead of simulating the fluid mechanics equations directly, the proposal uses a Lattice Boltzmann model for waves to compute the first-order perturbations of the pressure and velocity fields, and it use them to compute the second-order acoustic radiation force on each surface element of the object, and it employs an interpolation scheme with kernel to increase the accuracy. The computed force can later be used to integrate the object's motion by using molecular dynamics. The method is implemented in the LB3D lattice Boltzmann simulation software and in a self-developed C++ code, and it is employed to integrate the total force on a sphere and a disk, respectively. The results reproduce with good accuracy the theoretical expressions by Gor'kov and Wei for the sphere and the disk, respectively, even with a modest number of Lattice-Botzmann cells. In addition, the force computed in the 2D case, when coupled to a molecular dynamics integration scheme, reproduces the motion of the disk to the standing wave nodes, when the disk is denser than the surrounding medium. The proposed procedure shows to be a promising tool for simulating phenomena where the acoustic radiation force plays a relevant role, like acoustic tweezers and the acoustic manipulation of microswimmers, with applications in medicine, biology, pharmaceutic industry and hydraulic engineering.

Keywords: Computational Acoustics, Microfluidics, Acoustofluidics, Computational methods, Paralellization, acoustical tweezers, Acoustic radiation force, Gor'kov potential, Lattice-Boltzmann method, discrete transport Boltzmann equation, conservation laws, wave equation.

Resumen

Título: Cómputo numérico de la fuerza de radiación acústica ejercida por una onda estacionaria en un objeto inmerso en un fluido usando un método de Lattice Boltzmann para ondas

El presente trabajo introduce un procedimiento numérico para calcular la fuerza de radiación acústica producida por ondas estacionarias sobre un objeto comprimible sumergido en un fluido no viscoso. En lugar de simular directamente las ecuaciones de la mecánica de fluidos, la propuesta utiliza un modelo Lattice Boltzmann para ondas para calcular las perturbaciones de primer orden de los campos de presión y velocidad, y las utiliza para calcular la fuerza de radiación acústica de segundo orden sobre cada elemento de la superficie del objeto, empleando un esquema de interpolación con kernel para aumentar la precisión. La fuerza calculada se puede utilizar posteriormente para integrar el movimiento del objeto mediante dinámica molecular. El método se implementa en el software de simulación Lattice Boltzmann LB3D y en un código C++ de desarrollo propio, y se emplea para integrar la fuerza total sobre una esfera y un disco, respectivamente. Los resultados reproducen con buena precisión las expresiones teóricas de Gor'kov y Wei para la esfera y el disco, respectivamente, incluso con un número modesto de celdas de Lattice-Botzmann. Adicionalmente, la fuerza calculada en el caso 2D, cuando se combina con un esquema de integración de dinámica molecular, reproduce el movimiento del disco hacia los nodos de la onda estacionaria, cuando el disco es más denso que el medio circundante. El procedimiento propuesto se muestra como una herramienta prometedora para simular fenómenos donde la fuerza de la radiación acústica juega un papel relevante, como las pinzas acústicas y la manipulación acústica de micronadadores, con aplicaciones en medicina, biología, industria farmacéutica e ingeniería hidráulica.

Palabras clave: Acústica computacional, Microfluídica, Acustofluídica, métodos computacionales, paralelización, pinzas acústicas, fuerza de radiación acústica, potencial de Gor'kov, métodos de Lattice-Boltzmann, ecuación de transporte de Boltzmann discreta, leyes de conservación, ecuacuión de ondas.

Contents

List of Figures

chart index

Chapter 1

Introduction

The study of the motion of microswimmers in aqueous media has won relevance in the recent years, because of its applications in biotechnology, biodiversity, health research, marine research and earth science, among others [1]. Microswimmers are microscopical bodies in a fluid usually transported without contact through external acoustic, magnetic or electrostatic fields [2–4]. One way of controlling the motion of microswimmers is by using acoustical tweezers, i.e. sets of ultrasound transducers and reflectors that are able to generate standing acoustic waves with pressure nodes focused on the object to be moved (Fig. 1.2a, [4]). Acoustic tweezers can be built with a piezoelectric (PZT) transducer and a reflecting surface (figure 1.1) or with an array of phase-modulated transducers [5]. Just like optical tweezers use standing electromagnetic waves to manipulate microscopical objects like viruses, cells or bacteria, acoustic tweezers can manipulate particles as soon as it size is much smaller than the wavelength of the standing wave. Nevertheless, acoustic tweezers requires 5×10^5 times less power than optical tweezers. Indeed, they can move objects from 100 nm to 10 mm large with intensities from 10^{-2} to 10 W/cm^2 for the input source, whereas optical tweezers requires more than 10^6 W/cm^2 [6].

The manipulation of small objects with standing waves began with the 2018 Nobel Prize study on optical tweezers, developed by Ashkin in 1970, who showed the possibility of trap and accelerate dielectric particles by using the stable potential well of a focused continuous

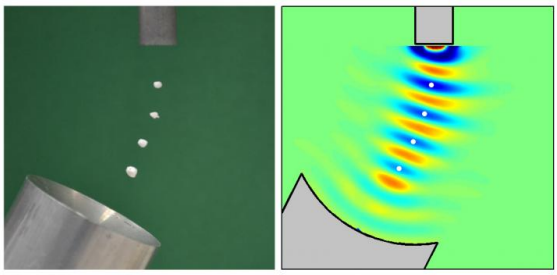

Fig. 1.1. Example of acoustic levitation using acoustical tweezers (from [1, pag. 204]).

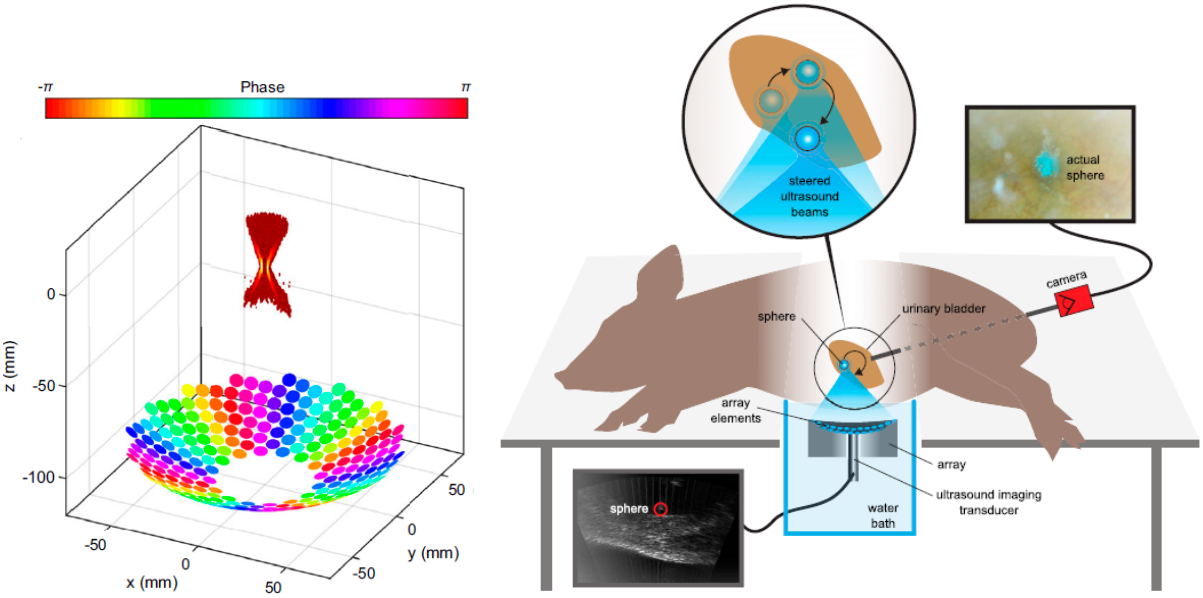

(a) **(b)**

Fig. 1.2. (a) Focal acoustic tweezer made of an array of transducers to develop surgeries; (b) surgery for the extraction of a urinary stone of a pig.(from [7]).

laser [8]. Parallel to this research, in 1962 the Russian physicist Lev Petrovich Gor'kov, based on previous works by Louis V. King on acoustical radiation forces [9, 10], studied the force exerted by an acoustical field on a spherical particle immersed in an ideal (non-viscous, isentropic and irrotational) fluid and deduced the so-called Gor'kov potential, which is the basic principle of acoustical tweezers [11]. The two-dimensional case was first studied by J. Wu and G. Du in 1990 [12], validating their results with experiments on a glass microneedle confined in a chamber with piezo-electric (PZT) transducers. Another study of the two-dimensional case was performed by Wei Wei et al. in 2004 [13], who used scattering theory to solve the wave equation for a compressible cylinder of infinite height in a standing wave. A complete and solid theoretical review can be found in the book *Theoretical Microfluidics* [14] and the thematic series *Acoustofluidics*, both written by Henrik Bruus, where most of the theoretical content of the acoustic radiation force can be found in chapters 1, 2 and 7 of the series. [15–17]. Later experiments created lab chips with acoustical traps that move an array of colloidal particles in the three orthogonal directions of space [4]. On a larger scale, in 2020 transducer arrays were used to extract kidney stones from a pig in a non-invasive surgery, as seen in figure 1.2. The surgery was accomplished without damages in the organ tissues, demonstrating the potential of acoustical tweezers for medicine applications [7].

Acoustic tweezers has also been explored as a supporting ground for transporting swarms of self-assembling micro-bots that, inspired by nature, could be used for surgery or drug de-

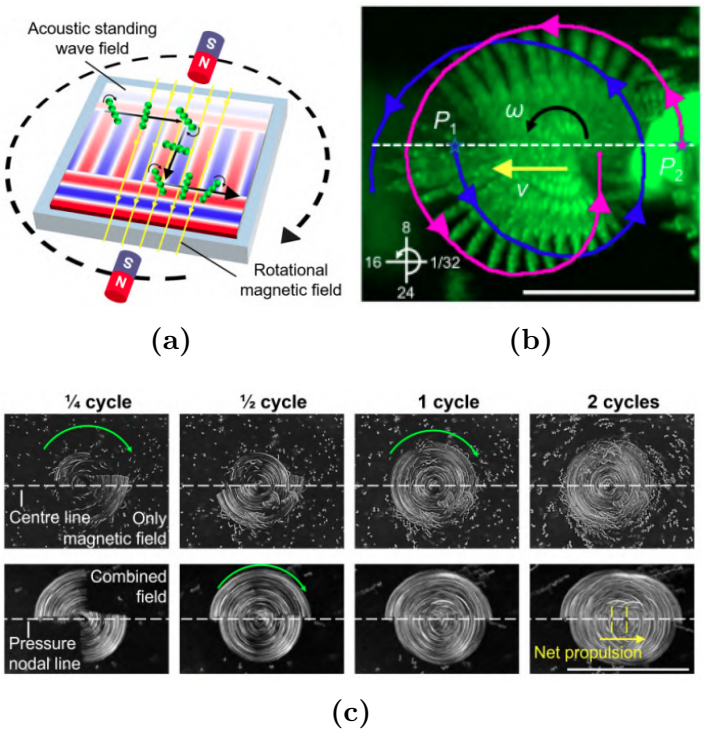

Fig. 1.3. General sketch of the rolling Microswimmers experiment (a). Graphical definition of the angular and linear speed of the Microswimmers (b) and comparison of the motion with and without standing waves (c).

livery [18]. One way to produce swarms or self-assembling micro-bots is to use external rotating magnetic fields to align paramagnetic beads in a liquid and form chains or ribbons. The same rotating field can drive the micro-bots to roll on the walls of the container [19, 20]. Nevertheless, rolling on the walls of a blood vessel could damage the tissue, and some alternative should be found to support the rolling motion. In a recent work, Zhang et. al. [21] used the nodal planes of acoustic standing waves as virtual walls where the micro-bots can roll on. The results show that acoustic standing waves are a promising alternative to guide swarms of self-assembled micro-bots through blood vessels for future medical applications, without damaging the vessels walls tissues. The theoretical studies of acoustic radiation phenomena have been developed for irrotational, non-viscous and isentropic fluids by assuming that the bodie's motion is much slower than the acoustic oscillations. Within this frame, all theoretical studies rely on the assumption that the relevant macroscopic fields, like pressure and velocity, can be written as a perturbative expansion, where the first-order contributions p_1 for the pressure and $\vec{u}_1$ for the velocity satisfy the wave equation. Although the acoustic radiation force depends on second-order contributions, they can be written in terms of p_1 and $\vec{u}_1$. This fact opens the possibility of simulate the wave equation - instead of solving

the Navier-Stokes equations - to compute p_1 and $\vec{u}_1$, and use those results to compute the acoustic radiation force. Moreover, the assumption of slow motion for the immersed body suits perfectly for the experiments with microswimmers, which move with typical speeds of a few μm/s, whereas the ultrasound frequencies lay around MHz.

The analytical computation of the acoustic radiation force on particles immersed in a fluid is only possible for simple geometries, and complex shapes of today's microswimmers require suited numerical simulation tools. One of this tools is the Lattice-Boltzmann model (LBM), a numeric scheme that solves the Boltzmann transport equation for a set of distribution functions on a discrete lattice of cubic cells, so that the macroscopic moments obtained from those functions satisfy a bunch of conservation laws in the macroscopic limit, written as partial differential equations. One of the main advantages of this model is that the evolution of one cell is independent from the information of the neighboring cells, making parallelization much easier to implement on processors and graphics cards than for other numeric approaches like finite differences or finite volumes. The LBM have been widely used to simulate fluids with excellent results [22, 23], even for multiphase and multicomponent systems [24, 25]. A simple Lattice-Boltzmann model with a single relaxation time, known as LBGK, is able to simulate viscous fluids with Reynolds numbers up to 10^3, and special techniques like Multiple relaxation Time [26] and Entropic Lattice Boltzmman [27, 28] allows to go with Reynolds numbers up to 10^6. Originally developed for fluids, LBM are also capable to compute more general systems, like electromagnetic fields [29], wave functions in quantum mechanics with a DFT [30] and general relativity [31].

In 2004 J.A. Cosgrove et al. [32] used a LBGK Lattice-Boltzmann for fluids to simulate in two-dimensions the motion of a disk by standing acoustic waves. They calculated the force exerted by the waves and were able to reproduce the theoretical predictions by Wu and Du. However a LBGK for fluids computes the density and velocity fields of the fluid up to second order precision and the perturbations p_1 and $\vec{u}_1$, to fist order precision; thus, simulating acoustical tweezers with the desired precision will require very small cells, making it harder to implement it for three-dimensional simulations. Although there exist very efficient LBM for acoustics [33], even for curved cells [34], they have never been used to calculate the acoustic radiation force. In addition, there are very efficient software packages for computational fluid dynamics with Lattice-Boltzmann. One of them is LB3D, developed by the Dynamics of Complex Fluids and Interfaces group of the Helmholtz Institute of Erlangen-Nürmberg for Renewable Energy (HI-ERN), under the leadership of the professor Dr. Jens Harting [35]. This software includes a series of features apart from the Lattice-Boltzmann method, such as external forcing, colloids, Ladd particles, an immersed boundary method, among others. Its code is written in FORTRAN90 and parallelized using MPI, and it runs efficiently in clusters with hundred of processors. LB3D is able to perform simulations of multicomponent and multiphase fluids, as well as capillarity, but it does not include features to simulate acoustic waves yet.

Inspired in the mentioned study about rolling microswimmers in standing waves and based on the theory regarding acoustic radiation force, the present work develops a numerical methodology with lattice-Boltzmann to compute the acoustic radiation force on a immersed

body in a fluid with acoustic standing waves, and implement it in LB3D. Our proposal uses a Lattice-Boltzmann method to simulate the wave equation and compute the first-order perturbation fields p_1 and $\vec{u}_1$. Next, it uses those fields to compute the time-averaged acoustic radiation forces. The proposal uses a kernel-based interpolation method [36] to compute the perturbation fields close to the body with higher precision. The numerical algorithm is implemented in LB3D for the sphere and in a C++ code for the disk. Both codes are tested by setting a standing acoustic wave with a single node, integrating the total force on a sphere, in 3D, and a dis, in 2D, and comparing the results with the theoretical solutions by Gor'kov [11] and Wei [13]. The numerical results make an excellent agreement with the analytical values in both cases, even by using a relatively small number of cells. Finally, that force can be used to integrate via molecular dynamics the movement of the body and reproduce its displacement to the node, which is predicted when the body's density is larger than those of the surrounding medium. The proposed methodology is, therefore, a promising tool for the numerical simulation of microswimmers driven by standing acoustic waves.

The document is organized as follows: A short review on fluid mechanics and acoustics fundamentals is given in 2. Thereafter, the theory behind the acoustic radiation force will be fully explained in 3, such that the most important aspects on how the acoustic manipulation works are detailed explained. The chapter 4 provides a well detailed summary of what the Lattice-Boltzmann method is, how does it work and how to implement it. At this point all the theoretical topics of this work have been covered, and the numerical implementation follows. The numeric computation is fully explained and illustrated in chapter 5, giving details on how LB3D was modified to simulate acoustics and how to measure the acoustic radiation force, by using implemented tools and creating new ones. Chapter 6 reports the numerical tests and benchmarks to ensure the proper functionality of the two implementations: One standard code written in C++ for the two-dimensional case and the modification of the LB3D software for the three dimensional one. The LB3D development team contributed to this project with advice and support. Finally, the results reached with this methodology are discussed in chapter 7, where it is shown that the proposed approach is able to perform a simulation of the acoustic radiation force on an object immersed in standing waves, without high amounts of computation power.

Part I

Theoretical development

Chapter 2

Concepts on fluid dynamics and acoustics

2.1 Fluid dynamics concepts

To study the motion of fluids and elastic materials, it is necessary to describe this kind of physical system as a continuous medium where macroscopic variable are attributed, such as volume, density, pressure or other scalar or vector fields that may evolve in time and space ([37] and [15]). The key reason behind the continuum hypothesis relies on the length scale of the total system to study. On lab-on-a-chip applications, where characteristic length scales are in the order of 100 μm similar to the magnetic microrotors experiment, there are already more than 10^{23} molecules per each space element of this size, thus, the system will be considered macroscopic. Although inter-molecular distances are around 0.3 nm for fluids and 3 nm for gases, a minimum length for a continuous fluid mechanics description is usually taken around 10 μm [14, sec. 1.1.2]. To be able to distinguish from one length scale to another, the Knudsen number ϵ is introduced as

$$\epsilon = \frac{l_{\text{mfp}}}{L} \quad , \tag{2.1}$$

with l_{mfp} the mean free path for the particles and L the characteristic system size. When Knudsen number is much less than unity, the continuum hypothesis is a valid treatment for fluids [38, sec. 1.1]. In that hypothesis any infinitesimal volume element is small compared to system size but large compared to the particles' mean free path, and it is not necessary to follow the dynamics of individual fluid particles, but the time evolution of macroscopic fields. Those fields will be defined at any fixed position $\vec{r} = (x, y, z)$ of coordinates $r_1 = x$, $r_2 = y$ and $r_3 = z$ in three-dimensional euclidean space, and Cartesian index notation is convenient to describe them. So, any vector $\vec{A}$ can be written as A_i with $i = \{x_1, x_2, x_3\} \equiv \{x, y, z\}$ and any matrix shall be written as $\mathbb{M} = M_{ij}$. In index notation, some useful symbols are: the Kronecker Delta δ_{ij}, as a way to denote an identity matrix, and the Levi-Civita symbol

ϵ_{ijk}, which is valued 1 for any even permutation of 123, -1 for any odd permutation of 123 and 0 for any other case.

Let us consider than an infinitesimal fluid volume element moves through space from $\vec{r}(t)$ at time t to $\vec{r}(t+\Delta t)$ at time $t+\Delta t$. That movement can be described by the displacement vector $\vec{D}(\vec{r},t) = \vec{r}(t+\Delta t) - \vec{r}(t)$ and the instantaneous velocity vector

$$\vec{u}(\vec{r},t) = \frac{\partial \vec{D}}{\partial t} \quad . \tag{2.2}$$

This velocity, considered as a *field* is assigned to the spatial point $\vec{r}$, not to the fluid volume. This way of describing the evolution of velocity or other fields is called an *Eulerian picture* [15], which is the usual frame to describe the dynamic behavior of a fluid.

Other relevant macroscopic fields to describe the fluid are the density $\rho(\vec{r},t)$, as the total mass of all particles in the fluid element divided by its volume ΔV,

$$\rho(\vec{r},t) = \frac{\sum_{n\in\Delta V} m_n}{\Delta V} \quad ; \tag{2.3}$$

the momentum $\vec{J}(\vec{r},t)$ per unit volume, which is naturally defined as

$$\vec{J}(\vec{r},t) = \rho(\vec{r},t)\vec{u}(\vec{r},t) \quad , \tag{2.4}$$

and fluid's thermodynamics variables as the pressure $P(\vec{r},t)$ or the temperature $T(\vec{r},t)$.

Those macroscopic fields are evolved in time and space by partial differential equations, and the two most relevant are: the mass conservation law and the momentum conservation law (for a detailed derivation of those two laws, see [14, 37]). Although energy conservation must also be included, it can be replaced by a thermodynamic state equation. The mass conservation can be written as

$$\frac{\partial \rho}{\partial t} + \vec{\nabla}\cdot\vec{J} = 0 \quad , \tag{2.5}$$

and the momentum conservation law, known as the Navier-Stokes equation, as

$$\rho\left[\frac{\partial \vec{u}}{\partial t} + \left(\vec{u}\cdot\vec{\nabla}\right)\vec{u}\right] = -\vec{\nabla}P + \eta\nabla^2\vec{u} + (\eta+\eta')\,\vec{\nabla}\left(\vec{\nabla}\cdot\vec{u}\right) \quad . \tag{2.6}$$

This is just Newton's Second Law for a fluid element. The term between square brackets on the left is just the acceleration of that element, written as function of the velocity field $\vec{u}$. The first term on the right is the force exerted by the pressure, and the next two terms are the forces due to the first (η) and second (η') viscosity coefficients for the fluid. Those two terms can be neglected in the limit cases of this work, leading to a special form of the momentum conservation law called the *Euler's equation*,

$$\rho\left[\frac{\partial \vec{u}}{\partial t} + \left(\vec{u}\cdot\vec{\nabla}\right)\vec{u}\right] = -\vec{\nabla}P \quad . \tag{2.7}$$

Euler's equation can be rewritten in several equivalent ways. By replacing Eq. 2.4 into Eq. 2.7 and using the identity

$$\vec{\nabla}\cdot\left(\vec{u}\otimes\vec{J}\right)=\left(\vec{J}\cdot\vec{\nabla}\right)\vec{u}+\vec{u}\left(\vec{\nabla}\cdot\vec{J}\right)\quad , \tag{2.8}$$

which, in components, reads

$$\partial_k\left(u_iJ_k\right)=J_k\partial_k u_i+u_i\partial_k J_k \tag{2.9}$$

(with $\partial_t\equiv\partial/\partial t$ and $\partial_i\equiv\partial/\partial x_i$), Eq. 2.7 transforms into

$$\frac{\partial\vec{J}}{\partial t}=-\vec{\nabla}P+\vec{\nabla}\cdot\left(\vec{u}\otimes\vec{J}\right)\quad . \tag{2.10}$$

Since $\vec{\nabla}P=\vec{\nabla}\cdot(\mathbf{1}P)$ (or $\partial_k P=\partial_i\left(\delta_{ik}P\right)$, in components), Euler's equation takes the form of a conservation law, indeed,

$$\frac{\partial\vec{J}}{\partial t}=-\vec{\nabla}\cdot\Pi\quad , \tag{2.11}$$

with

$$\Pi=\mathbf{1}P+\vec{u}\otimes\vec{J}\quad ,\quad (\text{ or }\Pi_{ik}=\delta_{ik}P+\rho U_iU_k\text{ , in components}), \tag{2.12}$$

known as the *moment flux tensor*.

The force exerted by a fluid to an immersed object is a momentum exchange between the fluid and the object. If the force per unit volume acting on the object is $\vec{f}$ then the momentum change would be

$$\vec{f}=\frac{\partial\vec{J}}{\partial t}=-\vec{\nabla}\cdot\Pi\quad , \tag{2.13}$$

and the total force on the object is obtained by integrating that force over the entire volume V_p of the object [37, sec. 6],

$$\vec{F}=\int_{V_p}\vec{f}\,dV=-\int_{V_p}\vec{\nabla}\cdot\Pi\,dV=-\oint_{\partial V_p}\Pi\cdot\hat{n}\,dS\quad , \tag{2.14}$$

where we have used the divergence theorem, ∂V_p is the object's surface and $\hat{n}$ is a unitary vector perpendicular to that surface. This expression will be the key to deduce the acoustic radiation force, and for this reason its derivation has been fully explained (see [39, app. A]).

Another form of Euler's Equation can be obtained by using the identity

$$\left(\vec{u}\cdot\vec{\nabla}\right)\vec{u}=\vec{\Omega}\times\vec{u}+\frac{1}{2}\vec{\nabla}u^2\quad , \tag{2.15}$$

with $\vec{\Omega}=\vec{\nabla}\times\vec{u}$ the *vorticity*, to obtain

$$\frac{\partial\vec{u}}{\partial t}+\vec{\Omega}\times\vec{u}=-\frac{\vec{\nabla}P}{\rho}-\frac{1}{2}\vec{\nabla}u^2\quad . \tag{2.16}$$

If, in addition the fluid can be approximated as incompressible $\rho = cte$, the whole right-hand side can be set into a single gradient [1]

$$\frac{\partial \vec{u}}{\partial t} + \vec{\Omega} \times \vec{u} = -\vec{\nabla}\left[\frac{P}{\rho} + \frac{1}{2}u^2\right] \quad . \tag{2.17}$$

Finally, if the flux is irrotational ($\vec{\Omega} = 0$) there exist a velocity potential ϕ such that

$$\nabla\phi = \vec{u} \quad . \tag{2.18}$$

Thus,

$$\vec{\nabla}\left[\frac{\partial \phi}{\partial t} + \frac{P}{\rho} + \frac{1}{2}u^2\right] = 0 \quad , \tag{2.19}$$

and the term between square brackets is uniform everywhere. That is another form of *Bernoulli's principle* [40, sec. 4.16], which will be very useful to calculate the radiation force.

2.2 Acoustic waves in an inviscid fluid

It is pretty well known that sound is essentially a perturbation of pressure in air or any other material which propagates in the form of waves. As any other fluid, air is described by the mass and momentum conservation equations introduced in the previous section (usually called Navier-Stokes - NSE - equations). That set of equations is non-linear; so, how the wave equation - which is linear - can be obtained from them? To answer this question it is necessary to explain sound as small changes in density which produces small perturbations in pressure that, at first order, are linearly related. This relationship is established by the elastic response of the material and, in the case of gases, by the equation of state. As viscous forces are neglected, the pressure is the only component contributing to the dynamics of the fluid. The pressure is steady and constant where the fluid is static and no net motion is carried on. If the steady values for pressure and density are p_0 and ρ_0, respectively, then an acoustic wave is basically a perturbation of the pressure around this constant value. The total pressure P an density ρ would be their steady values p_0 and ρ_0 plus the small perturbations p_1 and ρ_1 due to the acoustic wave, respectively ([41, p. 136] and [37, p. 251]), that is

$$\rho = \rho_0 + \rho_1 \quad , \quad P = p_0 + p_1 \quad , \tag{2.20}$$

The variation of p_1 is strictly related to the deformation or strain of a small spatial element of the fluid, while ρ_1 to the aggregation or absence of matter, but to understand more deeply into this association, it is necessary a volume element of the fluid as part of an elastic material. Consider this elastic material being stretched in direction x by an external force.

[1] The same trick can be performed if the process is adiabatic. Indeed, because $\vec{\nabla}h = T\vec{\nabla}S + v\vec{\nabla}P$, with h the enthalpy S the entropy and $v = 1/\rho$ the specific volume, if $\vec{\nabla}S = 0$, then $\vec{\nabla}P/\rho = \vec{\nabla}h$, and the whole right side can be also gathered into a single gradient [37].

Each point in the material with coordinate x moves to a point $x+\xi(x)$, with $\xi(x)$ the point's *displacement*. Another point with coordinate $x+\Delta x$ moves to $(x+\Delta x)+\xi(x+\Delta x)$. The final distance between the two points is $\xi(x+\Delta x)-\xi(x) \simeq \frac{\partial \xi}{\partial x}\Delta x$, whereas the original one was Δx. The *strain* ϵ_{xx} is defined as the fractional elongation of the material element between those two points,

$$\epsilon_{xx} = \frac{\partial \xi}{\partial x} \quad . \tag{2.21}$$

The same occurs in three dimensions. Under an external force field, each point of coordinates (x, y, z) moves by a displacement vector $\vec{D} = (\xi, \eta, \zeta)$. Thus, an element of initial volume $V = \Delta x \Delta y \Delta z$ expands to a final volume $V + \Delta V$ such that, at first order,

$$\theta = \frac{\Delta V}{V} = \frac{\left(\Delta x + \frac{\partial \xi}{\partial x}\Delta x\right)\left(\Delta y + \frac{\partial \eta}{\partial y}\Delta y\right)\left(\Delta z + \frac{\partial \zeta}{\partial z}\Delta z\right) - \Delta x \Delta y \Delta z}{\Delta x \Delta y \Delta z} = \frac{\partial \xi}{\partial x} + \frac{\partial \eta}{\partial y} + \frac{\partial \zeta}{\partial z} = \nabla \cdot \vec{D}\,. \tag{2.22}$$

The quantity θ is known as the *dilation*.

Let us divide the total pressure P as a steady value p_0 plus a small perturbation p_1

$$P = p_0 + p_1 \quad . \tag{2.23}$$

The variation p_1 must be related to the deformation of a small spatial element of the fluid. Under isotropic compression, the dilation (that would be negative) is proportional to the increments in pressure (Hooke's Law),

$$p_1 = -B\theta = -B\left(\nabla \cdot \vec{D}\right) \quad , \tag{2.24}$$

with B the Bulk's modulus [41, p. 136]. Notice that the left side of 2.24 is the small perturbation of the total pressure P introduced in 2.23. This means that any small change in pressure will cause a small proportional and relative change in volume, giving the following definition for the Bulk's modulus:

$$B = -V\frac{\Delta P}{\Delta V} \to -V\frac{dP}{dV} \quad , \tag{2.25}$$

that will be useful to describe sound propagation in gases, as it will be see later.

Let us come back to the forces on our volume element $\Delta x \Delta y \Delta z$ at (x, y, z). At first order, the total force in the x direction is the one exerted by the pressure $p1 = p_1(x, y, z)$ on the surface of area $\Delta y \Delta z$ at x minus the one exerted by the pressure $p_1(x+\Delta x, y, z) \simeq p_1 + \frac{\partial p_1}{\partial x}\Delta x$ on the opposite surface of area $\Delta y \Delta z$ at $x + \Delta x$,

$$F_x = p_1(x, y, z)\Delta y \Delta z - \left(p_1(x) + \frac{\partial p_1}{\partial x}\Delta x\right)\Delta y \Delta z = -\frac{\partial p_1}{\partial x}\Delta x \Delta y \Delta z \quad . \tag{2.26}$$

The same occurs in the y and z directions; therefore, the vector force applied to the volume element is

$$\vec{F} = (F_x, F_y, F_z) = -\left(\frac{\partial p_1}{\partial x}, \frac{\partial p_1}{\partial y}, \frac{\partial p_1}{\partial z}\right)\Delta x \Delta y \Delta z = -\vec{\nabla} p_1 \Delta V \quad . \tag{2.27}$$

This force produces an acceleration $\partial^2\vec{D}/\partial t^2$ on the volume element of mass $\rho_0\Delta V$ given by Newton's Second Law as

$$\vec{F} = \rho_0 \frac{\partial^2 \vec{D}}{\partial t^2}\Delta V \quad , \tag{2.28}$$

which may be rewritten using 2.27 as

$$-\vec{\nabla} p_1 = \rho_0 \frac{\partial^2 \vec{D}}{\partial t^2} \quad . \tag{2.29}$$

By taking the divergence on both sides and using 2.24 we get,

$$-\nabla^2 p_1 = \rho_0 \frac{\partial^2}{\partial t^2}\left(\vec{\nabla}\cdot\vec{D}\right) = -\frac{\rho_0}{B}\frac{\partial^2 p_1}{\partial t^2} \quad . \tag{2.30}$$

That is the wave equation (2.31) with $c = \sqrt{B/\rho_0}$ the speed of sound.

With this linear approximation it is possible to describe the behavior of the acoustic wave propagation in an elastic medium with the wave equation

$$\nabla^2 p_1 = \frac{1}{c^2}\frac{\partial^2 p_1}{\partial t^2} \quad , \quad \text{with } c = \sqrt{\frac{B}{\rho_0}} \quad , \tag{2.31}$$

where B is the bulk modulus defined in (2.25).

2.3 The speed of sound in air

Although the constant c is determined under mathematical consistency, the physical meaning as a speed of sound waves must be detailed treated from the Thermodynamics of an ideal gas. As a common example, we tend to hear sound from gases like air, thus, it will be a good example to consider.

Air under room temperature and standard pressure conditions can be considered as an ideal gas, governed by the equation of state

$$PV = Nk_BT \quad , \tag{2.32}$$

with pressure P, volume V temperature T and total number of particles N , and as thermodynamic quantities and $k_B = 1.38 \times 10^{-23}$ J/K the Boltzmann's constant.

We saw in that the speed of sound in an elastic material is given by $c = \sqrt{B/\rho}$, with B the bulk modulus and ρ the density, and the bulk modulus by $B = -V\frac{dP}{dV}$ (Eq. 2.25). Thus, the bulk modulus can be deduced by considering an expansion or contraction of the gas, but what kind of thermodynamic process is behind this compression or expansion? A first idea was given by Isaac Newton in 1686, who proposed that the expansion and contraction of sound waves was *isothermic*, arguing negligible changes of temperature. With this in mind, 2.32 becomes

$$PV = \text{constant} \quad , \tag{2.33}$$

and, therefore,

$$B = -V\frac{dP}{dV} = P = \rho_0 \frac{k_B T}{m_{\text{mol}}} \quad . \tag{2.34}$$

Thus, the isothermic speed of sound c_0 becomes

$$c_0 = \sqrt{\frac{k_B T}{m_{\text{mol}}}} \quad . \tag{2.35}$$

The value of the sound speed on air using 2.35 at a room temperature of 300 K is about 293 m/s, which is pretty far from the actual value, which is close to 343 m/s at this same temperature. Something was wrong in the Newton's deduction and no correction was developed until 1816 by Laplace, who concluded that the mistake was to consider an isothermic expansion. Instead, he argued that the expansion and contraction of sound waves is so fast that there is no time for thermalization and heat transfer $\delta Q = 0$, keeping entropy constant rather than temperature, implying an adiabatic process. For this kind of process the following relationship is valid:

$$PV^{\gamma} = \text{constant} \quad , \tag{2.36}$$

being γ the adiabatic constant defined as the quotient between the heat capacities at constant volume and constant pressure ($\gamma = C_p/C_v$). For a gas of diatomic molecules, like most of the molecules in air, this value is $\gamma = 1.4$. With 2.36 on hand, we get

$$\begin{aligned} dPV^{\gamma} + \gamma\frac{PV^{\gamma}}{V}dV = 0 \quad , \quad -V\frac{dP}{dV} = \gamma P \\ B_{\text{ad}} = -\gamma P \quad . \end{aligned} \tag{2.37}$$

Thus, the adiabatic sound speed c_{ad} becomes

$$c_{\text{ad}} = \sqrt{\frac{\gamma k_B T}{m_{\text{mol}}}} \quad . \tag{2.38}$$

This last expression gives a value close to 347 m/s at a temperature of 300 K, which agrees pretty well with the measured value. If we want to obtain a closer value, dissipation of sound due to viscosity must be considered.

It is interesting to note that the equation of state for the ideal gas (Eq. 2.32) can be rewritten in terms of the isotermical speed of sound c_{iso} (Eq. 2.35). By multiplying and dividing the right-hand side by the molecular weight m_{mol} and dividing by V on both sides, one obtains

$$P = \left(\frac{N m_{\text{mol}}}{V}\right)\left(\frac{K_B T}{m_{\text{mol}}}\right) = \rho c_0^2 \quad , \tag{2.39}$$

with $c_0 = \sqrt{\frac{k_B T}{m_{\text{mol}}}}$. This linear relationship is useful investigate how acoustical waves also affect the density and other macroscopic quantities of the medium [41, p. 139-142].

In general, there are compressible fluids where the pressure depends on the density only, but without a strict linear dependence. This kind of fluids are considered *barotropic* [17, 37] and the pressure in this case can be written as a Taylor expansion in the density around ρ_0

$$P = p_0 + (\rho - \rho_0)\left(\frac{\partial P}{\partial \rho}\bigg|_{p_0}\right)_S + \frac{1}{2}(\rho - \rho_0)^2\left(\frac{\partial^2 P}{\partial \rho^2}\bigg|_{p_0}\right)_S + \dots \tag{2.40}$$

From 2.42 is easy to notice that

$$c_0^2 = \left(\frac{\partial P}{\partial \rho}\bigg|_{p_0}\right)_S \quad , \tag{2.41}$$

which is a most general expression to obtain c_0, consistent with the result for an ideal gas. Eq. 2.40 also gives a general expression to compute p_1 as $p_1 = (\rho - \rho_0)c_0^2$, and the sub-index notation of this quantity will be from now on related to the first order term of 2.40. The small variations of pressure obey to a version of an ideal gas equation state which may be written as follows:

$$p_1 = c_0^2 \rho_1 \quad , \tag{2.42}$$

with $c_0 = \sqrt{k_b T/m}$ the isothermal speed of sound. Thus, up to first order, it is possible to rewrite (2.20) as

$$\rho = \rho_0 + \rho_1 \quad , \tag{2.43a}$$

$$P = p_0(\rho_0) + c_0^2 \rho_1 \quad , \tag{2.43b}$$

$$\vec{u} = \vec{0} + \vec{u}_1 \quad , \tag{2.43c}$$

Although we have already shown how the wave equation is derived from elastic theory, it is also fruitful to see how the same equation can be deducted from the NSE equations. NSE equations were introduced in section 2.1 as a general description for the dynamics of any fluid. Here, as viscous effects are neglected, the equations to are the conservation of mass ((2.5)) and the Euler's equation ((2.7)). By replacing (2.43) and (2.43c) into those equations, and keeping only first order terms, we obtain [17]

$$\frac{\partial \rho_1}{\partial t} + \rho_0 \nabla \cdot \vec{u}_1 = 0 \quad , \tag{2.44a}$$

$$\rho_0 \frac{\partial \vec{u}_1}{\partial t} + \nabla p_1 = 0 \quad . \tag{2.44b}$$

By taking the diveregence on both sides of 2.44b, we obtain

$$\rho_0 \frac{\partial}{\partial t}(\nabla \cdot \vec{u}_1) + \nabla^2 p_1 = 0 \quad . \tag{2.45}$$

By replacing 2.44a, the wave equation is obtained,

$$\begin{aligned} \rho_0 \frac{\partial}{\partial t}\left(-\frac{1}{\rho_0}\frac{\partial \rho_1}{\partial t}\right) + \nabla^2 p_1 &= 0 \\ \frac{\partial^2 \rho_1}{\partial t^2} &= \nabla^2 p_1 \\ \frac{1}{c_0^2}\frac{\partial^2 p_1}{\partial t^2} &= \nabla^2 p_1 \end{aligned} \tag{2.46}$$

where (2.42) was used. The reader would notice that the perturbations in density ρ_1 also fulfills the wave equation, because they grow proportional to the pressure (see (2.42)).

Summarizing, the wave equation for the acoustic waves in a non-viscous gas has been obtained in two ways: by computing the propagation of linear deformations in an gas, considered as an elastic and isotropic medium, and by linearizing up to fist order the NSE equations for this case, that is the mass conservation and Euler equations. Both paths are equivalent in the sense that both rely on small adiabatic compressions and expansions of the medium, and only linear relations between the deformation and the stress ara assumed. However, if one wants to calculate the hydrodynamic force produced by an acoustic wave on an object immersed in the fluid, experimental observations such as acoustic radiation force are not visible if we work with first order approximations. Indeed, those effects are only measurable as quantities averaged in time, and any field with first-order dependence on a harmonic oscillation will have a null average over time. In order to explain these effects, it is necessary to develop an expansion for the fields at least to second order [16, sec. III]. This will be fully explained in the next chapter. The acoustic radiation force have a general expression dependent of the small perturbations of the macroscopic field which satisfy the waves equation, as we have shown in this chapter, meaning that by solving the waves equation for those fields the acoustic radiation force is calculated. The solution of the waves equation will depend on the geometry of the immersed object as well as the incident waves, thus, in the following chapter we will develop the case of an sphere between standing waves, called the Gor'kov acoustic radiation force, as well as the analogous two-dimensional case of an infinite cylinder immersed in a bi-dimensional fluid.

Chapter 3

The acoustic radiation force theory

3.1 A first order expansion

As we discussed in section 2.1 (Eq. (2.14)), the total force on an immersed object can be expressed as the integration of the *moment flux tensor* through a surface enclosing the particle. Any particle or small body immersed in a fluid with the presence of a standing acoustic pressure fields will experience a time-averaged force once the acoustic field has reached a steady state. This force is known as the *acoustic radiation force* and, it is responsible for displacing the particle towards the node (or anti-node) in an acoustic tweezer when the particle size is much smaller than the wavelength. In section 2.2 it was shown how the wave equation is obtained by expanding at first order the continuity and Euler equations; however, if we try to determine the acoustic radiation force via 2.14 by neglecting the second term of 2.12, we would get

$$\vec{F}(t) = -\oint_{\partial V_p} p_1(\vec{r},t)\hat{n}dS \quad , \tag{3.1}$$

which depends only on the harmonic oscillating pressure $p_1 = \cos(\omega t)$ and, therefore, the time-averaged value of this force, defined as

$$\langle \vec{F}(t) \rangle = \frac{1}{T}\int_0^T \vec{F}(t)dt \tag{3.2}$$

will be zero [1].

Since the linear contribution is not enough, it is necessary to develop a perturbative expansion for the pressure up to second order, such that the computed force includes non-linear terms that will eventually remain in the time-averaged force. This development will be shown in this chapter, by combining an completing the deductions in [11, 17, 39]. First, a non-viscous irrotational flow is considered and the second-order perturbative expansion

[1] Indeed, the time averages of $\langle cos(\omega t - \beta)\rangle = \langle sin(\omega t - \beta)\rangle = 0$. In contrast, time averages of quadratic contributions like $\langle cos^2(\omega t - \beta)\rangle = \langle sin^2(\omega t - \beta)\rangle = \frac{1}{2}$ are no null.

is developed. Then, it will be shown that the second order contributions to the force are expressed only in terms of the first order contributions to the pressure and velocity fields, i.e. those which satisfy the wave equation. Therefore, it is not necessary to solve the non-linear equations 2.5 and 2.7 to compute the force; only by solving the wave equation (analytically or numerically) the first order contributions, the radiation force can be computed. Next, the wave equation shall be solved, using the proper boundary conditions at the object's surface, and their results are used to compute the radiation acoustic force due to the pressure and velocity field scattered by the particle in terms of the known incident fields.

3.2 The second order acoustic radiation force

Now it is time to develop a perturbative expansion up to second order as done in 2.43. Then

$$\rho = \rho_0 + \rho_1 + \rho_2 \quad , \tag{3.3a}$$

$$P = p_0(\rho_0) + p_1 + p_2 \quad \text{and} \tag{3.3b}$$

$$\vec{u} = \vec{0} + \vec{u}_1 + \vec{u}_2 \quad . \tag{3.3c}$$

By replacing those expansions into the mass (Eq. (2.5)) and momentum (Eq. (2.6)) conservation law, using Eq. (2.44) and taking the second-order terms only, we obtain

$$\frac{\partial \rho_2}{\partial t} + \rho_0 \nabla \cdot \vec{u}_2 + \nabla \cdot (\rho_1 \vec{u}_1) = 0 \quad , \tag{3.4a}$$

$$\rho_0 \frac{\partial \vec{u}_2}{\partial t} + \rho_1 \frac{\partial \vec{u}_1}{\partial t} + \nabla p_2 + \rho_0 (\vec{u}_1 \cdot \nabla)\vec{u}_1 = 0 \quad . \tag{3.4b}$$

The last term of the left side of Eq. (3.4b) can be rewritten by using the next mathematical property:

$$\frac{1}{2}\nabla(\vec{u}_1 \cdot \vec{u}_1) = (\vec{u}_1 \cdot \nabla)\vec{u}_1 + \vec{u}_1 \times (\nabla \times \vec{u}_1) \quad , \tag{3.5}$$

where the term $\vec{u}_1 \times (\nabla \times \vec{u}_1) = 0$, because the flux is irrotational.Then (3.4b) becomes

$$\rho_0 \frac{\partial \vec{u}_2}{\partial t} + \rho_1 \frac{\partial \vec{u}_1}{\partial t} + \nabla p_2 + \frac{\rho_0}{2}\nabla(u_1^2) = 0 \quad . \tag{3.6}$$

By using (2.42) and (2.44b) the second term of the left hand side may be written as

$$\rho_0 \frac{\partial \vec{u}_2}{\partial t} - \frac{p_1}{\rho_0 c^2}\nabla p_1 + \nabla p_2 + \frac{\rho_0}{2}\nabla(u_1^2) = 0 \quad , \tag{3.7}$$

and using the product derivative property for gradients we end up with

$$\rho_0 \frac{\partial \vec{u}_2}{\partial t} + \nabla p_2 = \frac{1}{2\rho_0 c_0^2}\nabla(p_1^2) - \frac{\rho_0}{2}\nabla(u_1^2) \quad . \tag{3.8}$$

Because we are interested in writing the total velocity and pressure fields in terms of only first-order terms, let us add equation (2.44b) as a null term such that, by using 3.3b and (3.3c) we have

$$\rho_0\frac{\partial\vec{u}_2}{\partial t}+\rho_0\frac{\partial\vec{u}_1}{\partial t}+\nabla p_2+\nabla p_1=\frac{1}{2\rho_0c_0^2}\nabla(p_1^2)-\frac{\rho_0}{2}\nabla(u_1^2)$$
$$\rho_0\frac{\partial\vec{u}}{\partial t}+\nabla(P-p_0)=\nabla\left(\frac{1}{2\rho_0c^2}p_1^2-\frac{\rho_0}{2}u_1^2\right) \quad . \tag{3.9}$$

Now by using (2.18) we end up with a total non-static pressure written as follows:

$$\nabla(P-p_0)=\nabla\left(\frac{p_1^2}{2\rho_0c_0^2}-\frac{\rho_0}{2}u_1^2-\rho_0\frac{\partial\phi}{\partial t}\right) \quad , \tag{3.10}$$

that can be plugged into (2.14) to obtain a second order force by also including the dyadic product of the velocities in (2.12), since it is a second order term. So, the second order radiation acoustic force becomes

$$\langle F_i\rangle=-\oint\left\langle\left(-\rho_0\frac{u_1^2}{2}+\frac{p_1^2}{2\rho_0c_0^2}\right)\delta_{ij}+\rho_0v_iv_j\right\rangle dS_j \quad . \tag{3.11}$$

Since we are assuming that the fluid is non-rotational ($\Omega=\vec{\nabla}\times\vec{v}=0$), the velocity field is the gradient of a scalar velocity potential ϕ (Eq. (2.18)) and, the first order velocity and pressure fields can be written in terms of such potential as

$$\vec{u}_1=\nabla\phi \quad , \tag{3.12}$$

$$p_1=-\rho_0\frac{\partial\phi}{\partial t} \quad , \tag{3.13}$$

and Eq. (3.11) becomes

$$\langle F_i\rangle=-\oint\left\langle\left(-\frac{\rho_0}{2}|\nabla\phi|^2+\frac{\rho_0}{2c_0^2}\left[\frac{\partial\phi}{\partial t}\right]^2\right)\delta_{ij}+\rho_0\partial_i\phi\partial_j\phi\right\rangle dS_j \quad , \tag{3.14}$$

The potential ϕ also obeys a wave equation. By replacing (3.12) and (3.13) into Eq. (2.44a), one obtains

$$\frac{1}{c_0^2}\frac{\partial^2\phi}{\partial t^2}=\nabla^2\phi \quad . \tag{3.15}$$

That opens the possibility of computing the force just by solving the velocity scalar potential - which satisfies only one wave equation - with the proper boundary conditions. In the next section we will show, with all possible details, how to solve this equation for a compressible disk by following the Gor'kov approach and completing the intermediate steps of his celebrated paper [11].

3.3 The Gor'kov acoustic radiation force on a sphere

Incident, scattered and interference terms

We want to compute the average force acting on a spherical object immersed in a liquid by a standing acoustic wave. Let us assume that the object's radius R_p is much smaller that the wavelength λ,

$$R_p \ll \lambda \quad , \tag{3.16}$$

With this approximation it is possible to solve (3.15) by dividing the potential field into an incident field and a scattered field [11], that is

$$\phi = \phi_{\text{in}} + \phi_{\text{sc}} \quad , \quad \vec{u}_1 = \vec{u}_{\text{in}} + \vec{u}_{\text{sc}} \quad , \quad p_1 = p_{\text{in}} + p_{\text{sc}} \quad . \tag{3.17}$$

The incident field ϕ_{in} would be the solution for the ongoing waves as if there was no spherical particle, while the scattered field ϕ_{sc} is the difference between the actual field and the incident field.

With the velocity potential divided into an incident and a scattered field, the average force Eq. (3.14) will have three contributions. The first one, due to ϕ_{in} only,

$$\langle F_{i,\text{IN}} \rangle = -\rho_0 \oint \left\langle \left(-\frac{\rho_0}{2} |\nabla \phi_{\text{in}}|^2 + \frac{\rho_0}{2c_0^2} \left[\frac{\partial \phi_{\text{in}}}{\partial t} \right]^2 \right) \delta_{ij} + \rho_0 \partial_i \phi_{\text{in}} \partial_j \phi_{\text{in}} \right\rangle dS_i \quad , \tag{3.18}$$

should be zero, because the incident field (which is the solution in absence of the object) does not receive any physical effect from the particle. In the case of plane waves, the incident field $\phi_{\text{in}} = \phi_0 \cos\left(\vec{k} \cdot \vec{r} - \omega t\right)$ is spatially homogeneous, implying a symmetry over the surface, and the closed integral will yield zero [39, p.79][17, p.] (see Appendix A for a detailed verification of this prediction).

The other two contributions containing information about the scattered wave are

$$\langle F_{i,\text{SC}} \rangle = -\rho_0 \oint \left\langle \left(-\frac{\rho_0}{2} |\nabla \phi_{\text{sc}}|^2 + \frac{\rho_0}{2c_0^2} \left[\frac{\partial \phi_{\text{sc}}}{\partial t} \right]^2 \right) \delta_{ij} + \rho_0 \partial_i \phi_{\text{sc}} \partial_j \phi_{\text{sc}} \right\rangle dS_i \tag{3.19}$$

and

$$\langle F_{i,\text{IN-SC}} \rangle = -\rho_0 \oint \left\langle \left(-\rho_0 \nabla \phi_{\text{in}} \cdot \nabla \phi_{\text{sc}} + \frac{\rho_0}{c_0^2} \left[\frac{\partial \phi_{\text{in}}}{\partial t} \right] \left[\frac{\partial \phi_{\text{sc}}}{\partial t} \right] \right) \delta_{ij} + \rho_0 \partial_i \phi_{\text{in}} \partial_j \phi_{\text{sc}} + \rho_0 \partial_i \phi_{\text{sc}} \partial_j \phi_{\text{in}} \right\rangle dS_i \ . \tag{3.20}$$

The contribution $\langle F_{i,\text{SC}} \rangle$, is much smaller than the interference term $\langle F_{i,\text{IN-SC}} \rangle$, because the scattering cross-section of a spherical particle is proportional to $(kR_p)^4$, which is negligible due to (3.16), and because the scattered potential field solution is proportional to R_p^3, as will be shown later; thus, the interference term (3.20) is the most relevant, and that is the one to be developed next [39, p.79].

By using (3.12) and (3.13)

$$\nabla\phi_{in}\cdot\nabla\phi_{sc}=\vec{u}_{in}\cdot\vec{u}_{sc}\quad , \tag{3.21a}$$

$$\frac{\rho_0}{c_0^2}\frac{\partial\phi_{in}}{\partial t}\frac{\partial\phi_{sc}}{\partial t}=\frac{c_0^2}{\rho_0}\rho_{in}\rho_{sc}\quad \text{and} \tag{3.21b}$$

$$\partial_i\phi_{\text{in}}\partial_j\phi_{\text{sc}}=u^i_{\text{in}}u^j_{\text{sc}}\quad , \tag{3.21c}$$

the interference term becomes

$$\langle F_{i,\text{IN-SC}}\rangle=-\rho_0\oint\left\langle\left(-\rho_0\vec{u}_{\text{in}}\cdot\vec{u}_{\text{sc}}+\frac{c_0^2}{\rho_0}\rho_{in}\rho_{sc}\right)\delta_{ij}+\rho_0u^i_{\text{in}}u^j_{\text{sc}}+\rho_0u^i_{\text{sc}}u^j_{\text{in}}\right\rangle dS_i\ . \tag{3.22}$$

By using Gauss theorem, the surface integral transforms into a volume integral,

$$\begin{aligned}\langle F_{i,\text{IN-SC}}\rangle=-\rho_0\int\Big\langle\Big(&-\rho_0(\partial_iu^m_{\text{in}})u^m_{\text{sc}}-\rho_0(\partial_iu^m_{\text{sc}})u^m_{\text{in}}+\frac{c_0^2}{\rho_0}\partial_i\rho_{in}\rho_{sc}+\frac{c_0^2}{\rho_0}\rho_{in}\partial_i\rho_{sc}\Big)\delta_{ij}+\\&\rho_0(\partial_iu^i_{\text{in}})u^j_{\text{sc}}+\rho_0u^i_{\text{in}}(\partial_iu^j_{\text{sc}})+\rho_0(\partial_iu^i_{\text{sc}})u^j_{\text{in}}+\rho_0u^i_{\text{sc}}(\partial_iu^j_{\text{in}})\Big\rangle dV\end{aligned} \tag{3.23}$$

the first two terms may be rewritten as

$$\begin{aligned}&(\partial_iu^m_{\text{in}})u^m_{\text{sc}}+(\partial_iu^m_{\text{sc}})u^m_{\text{in}}=(\partial_i\partial_m\phi_{\text{in}})u^m_{\text{sc}}+(\partial_i\partial_m\phi_{\text{sc}})u^m_{\text{in}}\\&=(\partial_m\partial_i\phi_{\text{in}})u^m_{\text{sc}}+(\partial_m\partial_i\phi_{\text{sc}})u^m_{\text{in}}=(\partial_mu^i_{\text{in}})u^m_{\text{sc}}+(\partial_mu^i_{\text{sc}})u^m_{\text{in}}\quad ,\end{aligned} \tag{3.24}$$

and the interference term simplifies to

$$\langle F_{i,\text{IN-SC}}\rangle=-\rho_0\int\left\langle\frac{c_0^2}{\rho_0}\partial_j\rho_{in}\rho_{sc}+\frac{c_0^2}{\rho_0}\rho_{in}\partial_j\rho_{sc}+\rho_0(\partial_iu^i_{\text{in}})u^j_{\text{sc}}+\rho_0(\partial_iu^i_{\text{sc}})u^j_{\text{in}}\right\rangle dV \tag{3.25}$$

Now, by using (2.44) for the incident and scattered fields on all terms but the last one, we obtain

$$\begin{aligned}\langle F_{i,\text{IN-SC}}\rangle=-\rho_0\int\Big\langle&-\frac{\partial u^j_{\text{in}}}{\partial t}\rho_{sc}-\frac{\partial u^j_{\text{sc}}}{\partial t}\rho_{in}-\frac{\partial\rho_{\text{in}}}{\partial t}u^j_{\text{sc}}+\rho_0(\partial_iu^i_{\text{sc}})u^j_{\text{in}}\Big\rangle dV\\&-\int\Big\langle-\frac{\partial u^j_{\text{in}}}{\partial t}\rho_{sc}-\frac{\partial}{\partial t}(u^j_{\text{sc}}\rho_{in})+\rho_0(\partial_iu^i_{\text{sc}})u^j_{\text{in}}\Big\rangle dV\end{aligned} \tag{3.26}$$

Since

$$-\frac{\partial u^j_{\text{in}}}{\partial t}\rho_{sc}=-\frac{\partial}{\partial t}(u^j_{\text{in}}\rho_{sc})+u^j_{\text{in}}\frac{\partial\rho_{sc}}{\partial t}\quad , \tag{3.27}$$

the averaged force simplifies to

$$\langle F_{i,\text{IN-SC}}\rangle=-\rho_0\int\left\langle-\frac{\partial}{\partial t}(u^j_{\text{sc}}\rho_{in}+u^j_{\text{in}}\rho_{sc})+u^j_{\text{in}}\frac{\partial\rho_{sc}}{\partial t}+\rho_0(\partial_iu^i_{\text{sc}})u^j_{\text{in}}\right\rangle dV\quad . \tag{3.28}$$

Because the time-average of the time derivatives of any periodic function is identically zero, the force simplifies further to

$$\langle F_i \rangle = -\rho_0 \int \left\langle u^i_{\text{in}} \left(\nabla^2 \phi_{sc} - \frac{1}{c_0^2} \frac{\partial^2 \phi_{sc}}{\partial t^2} \right) \right\rangle dV \quad . \tag{3.29}$$

Therefore, the time averaged force on the small sphere can be found if we compute the scattered velocity potential ϕ_{sc}. That will be done in the next section.

The scattered field

Because the outgoing reflected waves due to the presence of the object must be decreasing functions of the distance of the particle, the scattered field can be written as a multipolar expansion, as follows [37, sec. 11]:

$$\phi_{sc} = -\frac{a(t_{\text{ret}})}{r} + (\vec{A}(t_{\text{ret}}) \cdot \nabla)\frac{1}{r} + \dots \tag{3.30}$$

where $t_{\text{ret}} = t - r/c_0$ is the retarded time. The reader can notice that this is a retarded solution of the Poisson equation with a small source. Indeed, it can be shown that (3.30) is also a solution of the wave equation where the source is localized in a small region of space around the origin (see [42, sec. 6.4] for details).

Since $R_p \ll \lambda$, the action of the object on the medium closed to the film (where $r \approx R_p$) is almost instantaneous and,

$$t_{\text{ret}} = t - \frac{R_p}{c_0} = t - \frac{R_p}{\lambda} T \approx t \quad , \tag{3.31}$$

and the scattered potential ϕ can be expressed as the sum of a monopolar, ϕ_{mp}, and a dipolar, ϕ_{dip} contributions,

$$\phi_{sc} = \phi_{\text{mp}} + \phi_{\text{dip}} \quad , \tag{3.32}$$

with

$$\phi_{\text{mp}}(\vec{r}, t) = -\frac{a(t)}{r} \quad , \tag{3.33a}$$

$$\phi_{\text{dip}}(\vec{r}, t) = \vec{A}(t) \cdot \nabla \left(\frac{1}{r} \right) = -\vec{A}(t) \cdot \frac{\vec{r}}{r^3} \quad . \tag{3.33b}$$

Furthermore, the potential ϕ_{sc} will satisfy a Laplace equation

$$\nabla^2 \phi_{sc} = \nabla \cdot (\nabla \phi_{sc}) = \nabla \cdot \vec{u}_1 = 0 \quad . \tag{3.34}$$

This reflects the fact that close to the object the outer fluid behaves nearly incompressible.

The scalar field a and vector field $\vec{A}$ will be computed in the following sections with all the mathematical details.

The scalar field a(t)

Let us assume that the sphere of volume V_p is elastic, shrinking or expanding isotropically just by simply enlarging or decreasing its radius R_p in response to the incident pressure p_{in}. In that case, the volume change dV_p is related to p_{in} by

$$dp_{in} = -B_p \frac{dV_p}{V_p} \quad \text{, or} \quad \frac{\partial p_{in}}{\partial t} = -\frac{B}{V_p}\frac{dV_p}{dt} \quad , \tag{3.35}$$

with $B_p = c_p^2 \rho_p$ the particle's bulk modulus, c_p the particle's speed of sound and ρ_p the particle's density. Furthermore, because $p_{in} = \rho_{in} c_0^2$, with c_0 the speed of sound in the fluid,

$$\frac{dV_p}{dt} = -V_p \frac{c_0^2}{\rho_p c_p^2}\frac{\partial \rho_{\text{in}}}{\partial t} \quad . \tag{3.36}$$

Now, let us consider a mathematical spherical region Ω of radius R_Ω concentric to the sphere with $\lambda \gg R_\Omega > R_p$. When the sphere expands, the mass flux leaving Ω through its surface $\partial\Omega$ equals the rate at which the sphere pushes fluid out of it,

$$\oint_{\partial\Omega} (\rho_0 \vec{u}_1)\cdot \hat{r} dS = \oint_{\partial\Omega} (\rho_0 \vec{\nabla}\phi_{sc})\cdot \hat{r} dS = \frac{\partial}{\partial t}[(\rho_0 + \rho_{\text{in}})V_p] \quad , \tag{3.37}$$

with $\hat{r}$ the radial unitary vector.

By replacing the monopolar field (3.33a) and the volume time derivative (3.36) into (3.37), one obtains (See Appendix B for details)

$$a(t) = \frac{R_p^3}{3\rho_0}\frac{\partial \rho_{in}}{\partial t} f_1 \quad \text{, with} \quad f_1 = 1 - \frac{\kappa_p}{\kappa_0} \quad , \tag{3.38}$$

where $\kappa_0 = 1/(\rho_0 c_0^2)$ and $\kappa_p = 1/(\rho_p c_p^2)$ are the particle and fluid compressibility, respectively.

The vectorial field A(t)

Now let us consider the dipole contribution for the potential. Consider a sphere that moves with velocity $\vec{v}$ immersed to the fluid, and let us assume that the potential has the form

$$\phi_{\text{dip}} = \vec{A}\cdot\nabla\left(\frac{1}{r}\right) = -\vec{A}\cdot\frac{\vec{r}}{r^3} \quad , \tag{3.39}$$

where the position vector is measured between an observation point and the center of the sphere. The sphere is moving with a velocity $\vec{v}$ such that the vector $\vec{r}$ is

$$\vec{r} = \vec{r}_0 - t\vec{v} \quad , \tag{3.40}$$

where $\vec{r}_0$ is the sphere's position measured in a static reference frame. A first boundary condition is the fact that during the motion of the sphere there is no flow passing through the body, that is the normal velocities matches

$$\vec{u}\cdot\hat{r} = \vec{v}\cdot\hat{r} \quad , \tag{3.41}$$

Now the velocity $\vec{u}$ will be a fluid velocity around the sphere due to the disturbance of the sphere, but it is measured in reference frame where there is no external flow. Then

$$\vec{u} = \nabla\left(-\vec{A}\cdot\frac{\hat{r}}{r^2}\right) = -(\vec{A}\cdot\nabla)\frac{\hat{r}}{r^2} = \frac{3(\vec{A}\cdot\hat{r})\hat{r}-\vec{A}}{r^3} \quad . \tag{3.42}$$

By replacing (3.42) into (3.41), we obtain (see Appendix C for details)

$$\vec{A} = \frac{R_p^3}{2}\vec{v} \quad . \tag{3.43}$$

The vector $\vec{A}$ is related now to the dipolar moment of a *Doublet* and the fluid velocity written at (3.42) would take the following form:

$$\vec{u} = \frac{R_p^3}{2}\frac{3(\vec{v}\cdot\hat{r})\hat{r}-\vec{v}}{r^3} = \frac{R_p^3}{2}\left(\frac{3(\vec{v}\cdot\vec{r})\vec{r}}{r^5} - \frac{\vec{v}}{r^3}\right) \tag{3.44}$$

But the motion occurs due to the interaction between the fluid and the object immersed to it, meaning that the momentum must be conserved between them and the considered boundary condition is not enough. In order to take into account this interaction, we shall calculate the **drag** force made by the fluid on the object; but this time, as mentioned earlier, the fluid was assumed incompressible due to the length-scale separation between the wavelength and the radius of the object (3.16) and with this the force made by the fluid is

$$\vec{F}_i^{(\text{drag})} = -\oint\left(-\frac{\rho_0}{2}|\nabla\phi_{\text{dip}}|^2 - \frac{\partial\phi_{\text{dip}}}{\partial t}\right)\Big|_{r=R_p}\hat{n}dS \quad , \tag{3.45}$$

where the Bernoulli principle has been used [40]. (This expression is basically (3.14) but taking away the squared pressure term du to incompressinility and the dyadic tensor term because only the normal contribution contributes to the drag). Then, by using (3.39) and (3.43) we get (see Appendix C for details)

$$\begin{aligned}\vec{F}^{(\text{drag})} &= -\rho_0\oint\left(\frac{1}{2}\left(R_p\hat{r}\cdot\frac{\partial\vec{v}}{\partial t} + 3(\hat{r}\cdot\vec{v})^2 - v^2\right) - \frac{1}{8}\left(3(\hat{r}\cdot\vec{v})^2 + v^2\right)\right)\hat{n}dS \\ &= -\oint\frac{R_p}{2}\hat{r}\cdot\frac{\partial\vec{v}}{\partial t}\hat{n}dS - \oint\frac{v^2}{2}\left(\frac{9}{4}\frac{(\hat{r}\cdot\vec{v})^2}{v^2} - \frac{5}{4}\right)\hat{n}dS \quad .\end{aligned} \tag{3.46}$$

Then, by taking θ as the angle between the sphere's velocity $\vec{v}$ and its position $\vec{r}$, we have for the second integral, and

$$\hat{r}\cdot\vec{v} = v\cos\theta \tag{3.47}$$

and, after some algebra (see Appendix C for details), we obtain

$$\vec{F}^{(\text{drag})} = -\frac{2\pi R_p^3\rho_0}{3}\frac{\partial v}{\partial t}\hat{e}_z \equiv -M_{\text{add}}\frac{\partial v}{\partial t}\hat{e}_z \quad , \tag{3.48}$$

where we define $M_{\text{add}} = \frac{2\pi R_p^3 \rho_0}{3}$ as the *added mass* due to the motion of the fluid. With that force, the equation of motion for the particle becomes

$$m_p \frac{\partial \vec{v}}{\partial t} = \vec{f} - M_{\text{add}} \frac{\partial \vec{v}}{\partial t} \quad , \tag{3.49}$$

By Newton's Third Law $-\vec{f}$ is the force acting on the fluid and, therefore

$$(\frac{4\pi R_p^3}{3}\rho_0 + M_{\text{add}})\frac{\partial \vec{u}}{\partial t} = f \quad , \tag{3.50}$$

where we have added a bouyancy term. Now combining (3.49) and (3.50) we get (see Appendix C for details)

$$v_i = \frac{3\rho_0}{2\rho_p + \rho_0} u_i \quad . \tag{3.51}$$

This final relation ensures momentum conservation for (3.43), where equal velocities $\vec{u}$ and $\vec{v}$ were assumed. In general, the actual velocity must be the one which is relative to the fluid in order to still satisfy (3.41). Thus

$$\vec{A} = \frac{R_p^3}{2}(\vec{v} - \vec{u}) \quad , \tag{3.52}$$

and with (3.51) the definitive expression for $\vec{A}$ is

$$\vec{A}(t) = \frac{R_p^3}{2} f_2 \quad \text{, with} \quad f_2 = \left(\frac{2(\rho_p - \rho_0)}{2\rho_p + \rho_0}\right)\vec{u} \quad , \tag{3.53}$$

where we introduce the density contrast factor f_2.

The Gor'kov's potential in 3D

With (3.38) and (3.53) it is now possible to write a particular solution for the scattered velocity potential previously defined in terms of $a(t_{\text{ret}})$ and $\vec{A}(t_{\text{ret}})$ (Eq. (3.30)). It becomes

$$\phi_{\text{sc}}(r,t) = -f_1 \frac{R_p^3}{3\rho_0 r}\dot{\rho_{\text{in}}} - f_2 \frac{R_p^3}{2r^2}\nabla \cdot \left(\frac{\vec{u}_{\text{in}}}{r}\right) \quad . \tag{3.54}$$

this potential actually satisfies a non-homogeneous wave equation. By applying the D'Alembert operator, as it is done in (3.29), the following source is gathered

$$\nabla^2 \phi_{\text{sc}} - \frac{1}{c_0^2}\frac{\partial^2 \phi_{\text{sc}}}{\partial t^2} = f_1 \frac{V_p}{\rho_0}\frac{\partial \rho_{\text{in}}}{\partial t}\delta(\vec{r}) + f_2 \frac{3V_p}{2}\nabla \cdot (\vec{u}_{\text{in}}\delta(\vec{r})) \tag{3.55}$$

After plugging in (3.55) into (3.29), we have

$$\begin{aligned}\langle F_i\rangle &= -\rho_0 \int \left\langle f_1 \frac{V_p}{\rho_0}\frac{\partial \rho_{\text{in}}}{\partial t} u^i_{\text{in}}\delta(\vec{r}) + f_2 \frac{3V_p}{2} u^i_{\text{in}}\partial_k(u^k_{\text{in}}\delta(\vec{r}))\right\rangle dV \\ &= -f_1 V_p \int \left\langle \frac{\partial \rho_{\text{in}}}{\partial t} u^i_{\text{in}}\delta(\vec{r})\right\rangle dV - f_2\frac{3\rho_0 V_p}{2}\int \left\langle u^i_{\text{in}}\partial_k(u^k_{\text{in}}\delta(\vec{r}))\right\rangle dV \\ &= -f_1 V_p \left\langle \frac{\partial \rho_{\text{in}}}{\partial t} u^i_{\text{in}}\right\rangle - f_2\frac{3\rho_0 V_p}{2}\left(\oint \left\langle u^i_{\text{in}}u^k_{\text{in}}\delta(\vec{r})\right\rangle dS_k - \int \left\langle (u^k_{\text{in}}\partial_k)u^i_{\text{in}}\delta(\vec{r})\right\rangle dV\right) .\end{aligned} \tag{3.56}$$

Because the Dirac's delta of the second term of does not contain the surface, the whole integrand is identically zero, leading to

$$\langle F_i\rangle = -f_1 V_p \left\langle \frac{\partial \rho_{\text{in}}}{\partial t} u^i_{\text{in}}\right\rangle + f_2\frac{3\rho_0 V_p}{2}\left\langle (u^k_{\text{in}}\partial_k)u^i_{\text{in}}\right\rangle \quad . \tag{3.57}$$

As a final step, we can exchange the time derivative in the first term, because the derivative of the whole product is identically zero (just because the incident field oscillates harmonically); thus

$$\left\langle \frac{\partial \rho_{\text{in}}}{\partial t} u^i_{\text{in}}\right\rangle = -\left\langle \rho_{\text{in}}\frac{\partial u^i_{\text{in}}}{\partial t}\right\rangle = \left\langle \rho_{\text{in}}\frac{\partial_i \rho_{\text{in}}}{\rho_0 c_0^2}\right\rangle = \frac{1}{2\rho_0 c_o^2}\left\langle \partial_i p^2_{\text{in}}\right\rangle \quad . \tag{3.58}$$

where (2.44) was considered. By using (3.5) in the second term of (3.57) and by replacing the previous result, the Gor'kov Force takes its definitive form,

$$\langle F_i\rangle = -\partial_i V_p \left(f_1 \frac{1}{2\rho_0 c_0^2}\langle p^2_{\text{in}}\rangle + f_2\frac{3\rho_0}{4}\langle u^2_{\text{in}}\rangle\right) = -\nabla U \quad . \tag{3.59}$$

The potential U is defined as

$$U = V_p \left(f_1 \frac{1}{2\rho_0 c_0^2}\langle p^2_{\text{in}}\rangle + f_2\frac{3\rho_0}{4}\langle u^2_{\text{in}}\rangle\right) \quad , \tag{3.60}$$

or, bu using (3.38) and (3.53)), as

$$U = V_p \left((\kappa_0 - \kappa_p)\frac{\langle p^2_{\text{in}}\rangle}{2} + \left(\frac{\rho_p - \rho_0}{2\rho_p + \rho_0}\right)\frac{3\rho_0\langle u^2_{\text{in}}\rangle}{2}\right) \quad . \tag{3.61}$$

This is called the *Gor'kov's potential*. This potential is commonly used for acoustic levitation of small objects, even regardless of the shape of the object (or dimension) as soon as (3.16) is satisfied.

In the particular case of incident stationary pressure waves, like

$$p_{\text{in}}(x,t) = p_0 \sin\omega t \cos kx \quad , \tag{3.62}$$

if we take into account (2.44b) to compute the velocity and by assuming that the force is done only along the x-axis, the velocity takes the form

$$v_{\text{in}}^{x}(x,t) = -\frac{p_0}{c_0\rho_0}\cos\omega t \sin kx \quad . \tag{3.63}$$

By plugging it into the Gor'kov potential and solving the time-average integration, this potential for standing waves becomes

$$U = \frac{V_p p_0^2}{4\rho_0 c_0^2}\left(f_1\cos^2 kx + \frac{3}{2}f_2\sin^2 kx\right) \tag{3.64}$$

such that the force can be gathered using (3.59), (3.38) and (3.53) the expression for the force becomes

$$F_x = -\frac{\pi R_p^3 p_0^2 k}{3\rho_0 c_0^2}\Phi(\tilde{\rho},\tilde{\kappa})\sin 2kx \tag{3.65}$$

where $\tilde{\rho} = \rho_p/\rho_0$, $\tilde{\kappa} = \kappa_p/\kappa_0$ and $\Phi(\tilde{\rho},\tilde{\kappa})$ is defined as

$$\Phi(\tilde{\rho},\tilde{\kappa}) = \frac{5\tilde{\rho}-2}{2\tilde{\rho}+1} - \tilde{\kappa} \quad . \tag{3.66}$$

3.4 The radiation force on a disk

In the case of the sphere we showed one of many ways to solve the wave's equation under the premise that this is a scattering problem, which is a reason to split the fields into an incident and a scattered contribution, such that the scattered solution is generated by the particle as a point source due to (3.16), as a small disk may be seen as a point particle in the three-dimensional space. For the two-dimensional case the process is analogous except that the macroscopic quantities will acquire another units. The scattered potential field defined in (3.17) is [37]

$$\phi_{sc} = -a(t_{\text{ret}})\log r - (\vec{A}(t_{\text{ret}})\cdot\nabla)\log r + \dots \tag{3.67}$$

where $t_{\text{ret}} = t - r/c_0$ is the retarded time. Here we shall define the monopolar and dipolar terms for the scattered potential as follows:

$$\phi_{\text{mp}}(\vec{r},t) = -a(t)\log r \tag{3.68a}$$

$$\phi_{\text{dip}}(\vec{r},t) = -\vec{A}(t)\cdot\nabla(\log r) = -\vec{A}(t)\cdot\frac{\vec{r}}{r^2} \quad . \tag{3.68b}$$

Analogous to explained in section 3.3 it is possible to find that the acoustic radiation force will only depend on the scattered contributions but instead considering an integration over the area of the disk and a lower-dimension integration over the loop border of the disk

$$\langle F_i\rangle = -\rho_0\int\left\langle u_{\text{in}}^{i}\left(\nabla^2\phi_{sc} - \frac{1}{c_0^2}\frac{\partial^2\phi_{sc}}{\partial t^2}\right)\right\rangle dA \quad , \tag{3.69}$$

Indeed, this wave equation is not homogeneous as the scattered field comes from the interaction between the particle and the fluid. The scalar field a and vector field $\vec{A}$ are determined in the following section.

Deduction of the constants of the scattered field

The scalar field a(t)

Let us assume that the disk of area A_p is elastic, shrinking or expanding isotropically just by simply enlarging or decreasing its radius R_p in response to the incident pressure p_{in}. In that case, the area change dA_p is related to p_{in} by

$$dp_{in} = -B_p^{2\mathrm{D}} \frac{dA_p}{A_p} \quad , \text{ or } \quad \frac{\partial p_{in}}{\partial t} = -\frac{B_p^{2\mathrm{D}}}{A_p} \frac{dA_p}{dt} \quad , \tag{3.70}$$

with $B_p = c_p^2 \rho_p$ the bi-dimensional equivalent of the particle's bulk modulus defined this time as

$$B_p^{2\mathrm{D}} = -A \frac{dP}{dA} \quad , \tag{3.71}$$

c_p the particle's speed of sound and ρ_p the particle's density. Furthermore, because $p_{in} = \rho_{in} c_0^2$, with c_0 the speed of sound in the fluid,

$$\frac{dA_p}{dt} = -A_p \frac{c_0^2}{\rho_p c_p^2} \frac{\partial \rho_{\mathrm{in}}}{\partial t} \quad . \tag{3.72}$$

Now, let us consider a mathematical spherical region Ω of radius R_Ω concentric to the disk with $\lambda \gg R_\Omega > R_p$. When the disk expands, the mass flux leaving Ω through its circumference $\partial\Omega$ equals the rate at which the disk pushes fluid out of it,

$$\oint_{\partial\Omega} (\rho_0 \vec{u}_1) \cdot \hat{r} dl = \oint_{\partial\Omega} (\rho_0 \vec{\nabla} \phi_{sc}) \cdot \hat{r} dl = \frac{\partial}{\partial t} [(\rho_0 + \rho_{\mathrm{in}}) A_p] \quad , \tag{3.73}$$

with $\hat{r}$ the radial unitary vector.

By replacing the monopolar field (3.68a) and the volume time derivative (3.72) into (3.73), one obtains (See Appendix D for details)

$$a(t) = \frac{R_p^2}{2\rho_0} \frac{\partial \rho_{in}}{\partial t} f_1 \quad , \text{ with } \quad f_1 = 1 - \frac{\kappa_p}{\kappa_0} \quad , \tag{3.74}$$

where $\kappa_0 = 1/(\rho_0 c_0^2)$ and $\kappa_p = 1/(\rho_p c_p^2)$ are the particle and fluid compressibility, respectively.

The vectorial field A(t)

Now let us consider the dipole contribution for the potential. Consider a disk that moves with velocity $\vec{v}$ immersed to the fluid, and let us assume that the potential has the form

$$\phi_{\mathrm{dip}} = -\vec{A} \cdot \nabla (\log r) = -\vec{A} \cdot \frac{\vec{r}}{r^2} \quad . \tag{3.75}$$

where the position vector is measured between an observation point and the center of the disk. The disk is moving with a velocity $\vec{v}$ such that the vector $\vec{r}$ is

$$\vec{r} = \vec{r}_0 - t\vec{v} \quad , \tag{3.76}$$

where $\vec{r}_0$ is the disk's position measured in a static reference frame. A first boundary condition is the fact that during the motion of the disk there is no flow passing through the body, that is the normal velocities matches

$$\vec{u} \cdot \hat{r} = \vec{v} \cdot \hat{r} \quad , \tag{3.77}$$

Now the velocity $\vec{u}$ will be a fluid velocity around the disk due to the disturbance of the disk, but it is measured in reference frame where there is no external flow. Then

$$\vec{u} = \nabla \left(-\vec{A} \cdot \frac{\hat{r}}{r} \right) = -(\vec{A} \cdot \nabla)\frac{\hat{r}}{r} = \frac{2(\vec{A} \cdot \hat{r})\hat{r} - \vec{A}}{r^2} \quad , \tag{3.78}$$

By replacing (3.78) into (3.77), we obtain (see Appendix **??** for details)

$$\vec{A} = R_p^2 \vec{v} \quad . \tag{3.79}$$

The vector $\vec{A}$ is related now to the dipolar moment of a *Doublet* and the fluid velocity written at (3.78) would take the following form:

$$\vec{u} = R_p^2 \frac{2(\vec{v} \cdot \hat{r})\hat{r} - \vec{v}}{r^2} = R_p^2 \left(\frac{2(\vec{v} \cdot \vec{r})\vec{r}}{r^4} - \frac{\vec{v}}{r^2} \right) \tag{3.80}$$

But the motion occurs due to the interaction between the fluid and the object immersed to it, meaning that the momentum must be conserved between them and the considered boundary condition is not enough. In order to take into account this interaction, we shall calculate the **drag** force made by the fluid on the object; but this time, as mentioned earlier, the fluid was assumed incompressible due to the length-scale separation between the wavelength and the radius of the object (3.16) and with this the force made by the fluid is

$$\vec{F}_i^{(\text{drag})} = -\rho_0 \oint \left(-\frac{1}{2}|\nabla \phi_{\text{dip}}|^2 - \frac{\partial \phi_{\text{dip}}}{\partial t} \right) \Bigg|_{r=R_p} \hat{n} dl \quad , \tag{3.81}$$

where the Bernoulli principle has been used [40]. (This expression is basically (3.14) but taking away the squared pressure term due to incompressinility and the dyadic tensor term because only the normal contribution contributes to the drag). Then, by using (3.75) and (3.79) we get (see Appendix **??** for details)

$$\begin{aligned} \vec{F}^{(\text{drag})} &= -\rho_0 \oint \left(-\frac{v^2}{2} + \left(\vec{r} \cdot \frac{\partial \vec{v}}{\partial t} - 2(\hat{r} \cdot \vec{v})^2 + v^2 \right) \right) \hat{n} dl \\ &= -\oint R_p \hat{r} \cdot \frac{\partial \vec{v}}{\partial t} \hat{n} dl - \oint \frac{3v^2}{2} - 2(\hat{r} \cdot \vec{v})^2 \hat{n} dl \quad . \end{aligned} \tag{3.82}$$

Then, by taking θ as the angle between the disk's velocity $\vec{v}$ and its position $\vec{r}$, we have for the second integral, and

$$\hat{r} \cdot \vec{v} = v \cos\theta \tag{3.83}$$

and, after some algebra (see Appendix **??** for details), we obtain

$$\vec{F}^{(\text{drag})} = -\pi R_p^2 \rho_0 \frac{\partial v}{\partial t} \hat{e}_x \equiv -M_{\text{add}} \frac{\partial v}{\partial t} \hat{e}_x \tag{3.84}$$

where we define $M_{\text{add}} = \pi R_p^2 \rho_0$ as the *added mass* due to the motion of the fluid. With that force, the equation of motion for the particle becomes

$$m_p \frac{\partial v}{\partial t} = f - M_{\text{add}} \frac{\partial v}{\partial t} \quad , \tag{3.85}$$

By Newton's Third Law $-\vec{f}$ is the force acting on the fluid and, therefore

$$(\pi R_p^2 \rho_0 + M_{\text{add}}) \frac{\partial \vec{u}}{\partial t} = f \quad . \tag{3.86}$$

where we have added a bouyancy term. Now combining (3.85) and (3.86) we get (see Appendix **??** for details)

$$v_i = \frac{2\rho_0}{\rho_p + \rho_0} u_i \quad . \tag{3.87}$$

This final relation ensures momentum conservation for (3.79), where equal velocities $\vec{u}$ and $\vec{v}$ were assumed. In general, the actual velocity must be the one which is relative to the fluid in order to still satisfy (3.77). Thus

$$\vec{A} = \frac{R_p^3}{2}(\vec{v} - \vec{u}) \quad , \tag{3.88}$$

and with (3.87) the definitive expression for $\vec{A}$ is

$$\vec{A}(t) = \frac{R_p^2}{2} f_2 \quad , \text{ with} \quad f_2 = 2\left(\frac{\rho_0 - \rho_p}{\rho_0 + \rho_p}\right) \quad , \tag{3.89}$$

where we introduce the density contrast factor f_2.

The Gor'kov potential in 2D

With (3.74) and (3.89) it is now possible to write a particular solution for the scattered velocity potential, previously defined in terms of $a(t_{\text{ret}})$ and $\vec{A}(t_{\text{ret}})$, of the form

$$\phi_{\text{sc}}(r,t) = -f_1 \frac{R_p^2}{2\rho_0} \rho_{\text{in}} \log r - f_2 \frac{R_p^2}{2} \nabla \cdot (\vec{u}_{\text{in}} \log r) \quad , \tag{3.90}$$

which actually satisfies a non-homogeneous wave equation, because applying the D'Alembert operator, as it is done in (3.69), the following source is gathered

$$\nabla^2\phi_{\rm sc} - \frac{1}{c_0^2}\frac{\partial^2\phi_{\rm sc}}{\partial t^2} = f_1\frac{A_p}{\rho_0}\frac{\partial\rho_{\rm in}}{\partial t}\delta(\vec{r}) + f_2 A_p\nabla\cdot(\vec{u}_{\rm in}\delta(\vec{r})) \tag{3.91}$$

Considering the fact that the incident fields are harmonical as well as $\phi_{\rm in}$ if we look the incident velocity as its gradient. After plugging in (3.91) into (3.69), and solving the integration, we have

$$\begin{aligned}\langle F_i\rangle &= -\rho_0\int\left\langle f_1\frac{A_p}{\rho_0}\frac{\partial\rho_{\rm in}}{\partial t}u^i_{\rm in}\delta(\vec{r}) + f_2 A_p u^i_{\rm in}\partial_k(u^k_{\rm in}\delta(\vec{r}))\right\rangle dA\\ &= -f_1 A_p\int\left\langle\frac{\partial\rho_{\rm in}}{\partial t}u^i_{\rm in}\delta(\vec{r})\right\rangle dA - f_2\rho_0 A_p\int\left\langle u^i_{\rm in}\partial_k(u^k_{\rm in}\delta(\vec{r}))\right\rangle dA\\ &= -f_1 A_p\left\langle\frac{\partial\rho_{\rm in}}{\partial t}u^i_{\rm in}\right\rangle - f_2\rho_0 A_p\left(\oint\left\langle u^i_{\rm in}u^k_{\rm in}\delta(\vec{r})\right\rangle dS_k - \int\left\langle(u^k_{\rm in}\partial_k)u^i_{\rm in}\delta(\vec{r})\right\rangle dV\right)\ .\end{aligned} \tag{3.92}$$

As the Dirac's delta of the second term of does not contain the surface, the whole integrand is identically zero, leading to

$$\langle F_i\rangle = -f_1 A_p\left\langle\frac{\partial\rho_{\rm in}}{\partial t}u^i_{\rm in}\right\rangle + f_2\rho_0 A_p\left\langle(u^k_{\rm in}\partial_k)u^i_{\rm in}\right\rangle \quad . \tag{3.93}$$

As a final step we can exchange the time derivative in the first term because the derivative of the whole product is identically zero, thus

$$\left\langle\frac{\partial\rho_{\rm in}}{\partial t}u^i_{\rm in}\right\rangle = -\left\langle\rho_{\rm in}\frac{\partial u^i_{\rm in}}{\partial t}\right\rangle = \left\langle\rho_{\rm in}\frac{\partial_i\rho_{\rm in}}{\rho_0 c_0^2}\right\rangle = \frac{1}{2\rho_0 c_o^2}\left\langle\partial_i p^2_{\rm in}\right\rangle \quad , \tag{3.94}$$

after (2.44) was considered and using (3.5) in the second term of (3.93) the Gor'kov Force in its definitive expression is

$$\langle F_i\rangle = -\partial_i A_p\left(f_1\frac{1}{2\rho_0 c_0^2}\langle p^2_{\rm in}\rangle + f_2\frac{\rho_0}{2}\langle u^2_{\rm in}\rangle\right) = -\nabla U \tag{3.95}$$

where a potential U is defined as

$$U = A_p\left(f_1\frac{1}{2\rho_0 c_0^2}\langle p^2_{\rm in}\rangle + f_2\frac{\rho_0}{2}\langle u^2_{\rm in}\rangle\right) \quad , \tag{3.96}$$

or after using (3.74) and (3.89)

$$U = V_p\left((\kappa_0-\kappa_p)\frac{\langle p^2_{\rm in}\rangle}{2} + \left(\frac{\rho_p-\rho_0}{\rho_p+\rho_0}\right)\rho_0\langle u^2_{\rm in}\rangle\right) \quad , \tag{3.97}$$

to be called the Gor'kov potential. This potential is commonly used for acoustic levitation of small objects, even regardless of the shape of the object (or dimension) as soon as (3.16) is satisfied. In the particular case of incident stationary waves in the pressure, like

$$p_{\text{in}}(x,t) = p_0 \sin\omega t \cos kx \quad , \tag{3.98}$$

taking into account (2.44b) to compute the velocity and assuming that the force is done only along the x-axis, the velocity takes the form

$$v_{\text{in}}^x(x,t) = -\frac{p_0}{c_0\rho_0} \cos\omega t \sin kx \quad , \tag{3.99}$$

and plugging into the Gor'kov potential and solving the time-average integration, this potential for standing waves becomes

$$U = \frac{A_p p_0^2}{4\rho_0 c_0^2} \left(f_1 \cos^2 kx + f_2 \sin^2 kx\right) \tag{3.100}$$

such that the force can be gathered using (3.95), (3.74) and (3.89) the expression for the force becomes

$$F_x = -\frac{\pi R_p^2 p_0^2 k}{4\rho_0 c_0^2} \Phi(\tilde{\rho},\tilde{\kappa}) \sin 2kx \tag{3.101}$$

where $\tilde{\rho} = \rho_0/\rho$, $\tilde{\kappa} = \kappa_0/\kappa$ and $\Phi(\tilde{\rho},\tilde{\kappa})$ is defined as

$$\Phi(\tilde{\rho},\tilde{\kappa}) = \frac{3-\tilde{\rho}}{1+\tilde{\rho}} - \tilde{\kappa} \quad . \tag{3.102}$$

This last expression of the force (3.101) coincides with the equation 18 and 22 of the paper of Wei et al. [13, page. 204] and thus validating this shorter deduction as an analogous case of the Gor'kov derivation.

Chapter 4

A Lattice-Boltzmann model for acoustics

4.1 What is a Lattice-Boltzmann method?

A Lattice-Boltzmann Method (or LBM) is a numerical approach to solve a discrete version of the transport Boltzmann equation. This numerical method is basically a cellular automata which evolves a set of population distribution functions representing the probability to find a particle at some position with a given velocity in an instant of time, such that from these distribution functions one can obtain the temporal evolution of macroscopic moments which behave under certain conservation laws, then the LBM solves the partial differential equations (PDE) for the moments in the macroscopic limit, being an alternative to more used numerical methods as finite differences or finite elements, which can solve these PDE's in the time domain.

The main advantages of LBM are two: one, that the solution of the transport Boltzmann equation is made over a discrete space of positions and a discrete set of velocities by developing a quadrature, avoiding to integrate over a continuous velocity space, and two, the fact that the temporal evolution for all distribution functions is independent of the neighbor cells, making this method much easier to paralellize than others. This method solves a density probability function for a system of microscopic particles from which macroscopic quantities are gotten, thus, LBM is considered a mesoscopic method, because it simulates a hypothetical fluid transporting ideal particles between discrete cells colliding themselves in order to combine the information under a evolution rule for the cellular automata. These rules are based on the kinetic theory of gases and will be explained in this chapter. Although LBM is mostly used to solve the Navier Stokes equations fully explained in the second chapter, this method can actually solve any partial differential equation, as soon as it may be written as a conservation law. In this chapter we will explain the theory behind LBM, how does it work, how does it reproduce partial differential equations as the Navier Stoke's equation and then a Lattice-Boltzmann model able to solve the wave's equation will be explained as well.

Given a system of particles described by a number density function $f(\vec{x}, \vec{v}_i, t)$ defined as the probability to find a particle at the position $\vec{x}$ with a given velocity $\vec{v}_i$ at the instant of time t, the transport Boltzmann equation, written in a discrete space and using a discrete set of velocities $\{\vec{v}_i\}$, has the following form:

$$f_i(\vec{x} + \vec{v}_i\delta t, t + \delta t) = f_i(\vec{x}, t) + \Omega_i(\vec{x}, t) \tag{4.1}$$

Where $\Omega_i(\vec{x}, t)$ is the collision operator. For the entire work we will focus on LB models where there exists a solution for the distribution function called *the equilibrium function* f^{eq}, defined as the distribution function of the system when this one is left evolving by itself after a long period of time. In general, the collision operator is a double integral of the total derivative of f where all interactions among particles must be considered [38], but this integration can be avoided assuming that the actual distribution function f is similar to f^{eq} except for a small linear difference, such that f will try to relax to f^{eq} in a time interval τ. This small difference will be the Bhatnagar-Gross-Krook (BGK) collision operator and its definition is the following:

$$\Omega_i(\vec{x}, t) = -\delta t \frac{f_i(\vec{x}, t) - f^{\text{eq}}(\vec{x}, t)}{\tau} \tag{4.2}$$

where τ is known as the relaxation time, then the equation (4.1) becomes

$$f_i(\vec{x} + \vec{v}_i\delta t, t + \delta t) - f_i(\vec{x}, t) = -\delta t \frac{f_i - f^{\text{eq}}}{\tau} \tag{4.3}$$

where f^{eq} is the equilibrium distribution function. When the system relaxes to equilibrium the following macroscopic moments are obtained:

$$\Pi^{\text{eq}} = \sum_i f_i^{\text{eq}} \tag{4.4a}$$

$$\Pi_\alpha^{\text{eq}} = \sum_i v_{i\alpha} f_i^{\text{eq}} \tag{4.4b}$$

$$\Pi_{\alpha\beta}^{\text{eq}} = \sum_i v_{i\alpha} v_{i\beta} f_i^{\text{eq}} \tag{4.4c}$$

$$\Pi_{\alpha\beta\gamma}^{\text{eq}} = \sum_i v_{i\alpha} v_{i\beta} v_{i\gamma} f_i^{\text{eq}} \tag{4.4d}$$

The definition of these moments will be covered later, but the main idea behind the equilibrium function is that this one must be chosen such that summing (4.4) over i, multiplying by the corresponding order of $\vec{v}_i$, the desired moments of the system are gotten. As the space and time are discretized, the velocities set $\{\vec{v}_i\}$ are discretized as well in a defined set in general defined as DdQq where d is the dimension of the lattice and q is the amount of vectors existing per cell. Some examples are D3Q19 or D2Q9.

If the reader wonders why velocity can be discretized in such way, the reader shall consider reading [38, sec. 3.4], but here we will provide the following basic explanation: The macroscopic moments first defined at (4.4) should be written as integrals over the entire velocity space, however, if the equilibrium distribution function is written as a truncated summation of Hermite polynomials, it is possible to make use of orthogonality properties of these polynomials to reduce the integration to a summation over a finite set of velocities, without compromising the macroscopic behavior of the system. This mathematical approach is known as a Gauss quadrature and this is the secret behind the possibility of solving the Boltzmann equation without trying to integrate over an infinite and continuous set of velocities. But this benefit comes with the price of choosing the proper set of velocities and also a proper set of factors $\{\omega_i\}$ called *weigths*. Thus, for each velocities set there is a set of weights associated for each velocity, so that now we define a set of velocities and weights $\{\vec{v}_i, \omega_i\}$ that must satisfy the following conditions:

$$\sum_i \omega_i = 1 \quad , \tag{4.5a}$$

$$\sum_i v_{i\alpha}\omega_i = 0 \quad , \tag{4.5b}$$

$$\sum_i v_{i\alpha}v_{i\beta}\omega_i = c_s^2\delta_{\alpha\beta} \quad , \tag{4.5c}$$

$$\sum_i v_{i\alpha}v_{i\beta}v_{i\gamma}\omega_i = 0 \quad , \tag{4.5d}$$

$$\sum_i v_{i\alpha}v_{i\beta}v_{i\gamma}v_{i\mu}\omega_i = c_s^4(\delta_{\alpha\beta}\delta_{\gamma\mu} + \delta_{\alpha\gamma}\delta_{\beta\mu} + \delta_{\alpha\mu}\delta_{\beta\gamma}) \quad , \tag{4.5e}$$

where c_s^2 is for now a constant that will take an important role later. With the mentioned elements the Boltzmann transport equation is solved for every distribution function $f_i(\vec{x}, t) = f(\vec{x}, \vec{v}_i, t)$, but this evolution only considers a mesoscopic dynamic of a bunch of particles without any physical meaning associated, only the moments are able to provide the physical quantities associated to a system, but these macroscopic moments satisfy a set of PDE's considered conservation laws, like for example the conservation of mass written as

$$\int \Omega(f) d^3v = 0 \quad , \tag{4.6}$$

as soon as all particles share a same value of mass, because $\Omega(f)$ is the total variation of f including interactions between particles, thus (4.6) implies that the total amount of particles for all possible velocities must be kept constant, in other words, that the total variation of the amount of particles for every velocity is zero. In the same manner one can also write a conservation of momentum noticing that the momentum is the particle density times the velocity a particle carries, thus

$$\int \vec{v}\Omega(f) d^3v = 0 \tag{4.7}$$

is the equation of conservation for momentum. Another conservation law is the conservation of the total energy, namely

$$\int v^2 \Omega(f) d^3 v = 0 \tag{4.8}$$

among others [38, sec.1.3.4]. By plugging in (4.1) into the mentioned conservation laws it is possible to get a general form of the PDE's described but in terms of the particle density function f, but in order to ensure that the behavior of the macroscopic moments defined at (4.4) fulfills the PDE's in the macroscopic limit, we need to develop a *Chapman-Enskog analysis* which will be detailed explained in the Appendix F. The Chapman-Enskog expansion is a multiscale expansion of the continious Boltzmann equation and a perturbative expansion of f around the Knusden number $\epsilon = \delta x/x$ as the parameter to determine how close we are to the macroscopic limit, as the discretization of the system is done by dividing the space into small cells of size δx, such that if this quantity is much smaller than a charasteristic length x then this limit has been reached. When this occurs, the partial differential equations satisfied by the scalar and vector moments are

$$\partial_t \Pi + \partial_\alpha \Pi_\alpha = 0 \quad , \tag{4.9}$$

which can be seen as a continuity equation. Another PDE for higher order moments is

$$\partial_\beta \Pi_{\alpha\beta} + \partial_t \Pi_\alpha = -\epsilon^2 \left(1 - \frac{\delta t}{2\tau}\right) \partial_\beta^{(1)} \Pi_{\alpha\beta}^{(1)} \quad , \tag{4.10}$$

Noting that if $\tau = \delta t/2$ the right side of equation (4.10) vanishes, giving a continuity-like equation for the tensors Π_α and $\Pi_{\alpha\beta}$ as

$$\partial_\beta \Pi_{\alpha\beta} + \partial_t \Pi_\alpha = 0 \quad . \tag{4.11}$$

To see these equations as conservation laws (mass conservation or momentum conservation) we shall define the macroscopic moments in terms of fields with physical meaning. For example, as f_i has been interpreted as the probability density function to find a particle at certain position and velocity at any instant of time, it makes sense to define Π as a density field, because it's basically a discrete summation (or an integral in the continuous velocity space) of f_i which accounts for the probability at every possible velocity the particle can take at the position $\vec{x}$ and time t. In the same way it is possible to relate the momentum of this fluid of particles as the summation of velocities weighted by the probability density function f_i, just as it's defined in (4.4b), so that the following physical quantities for the zero and first order tensors shall be defined:

$$\Pi \equiv \rho = \sum_i f_i \quad , \tag{4.12a}$$

$$\Pi_\alpha \equiv \rho u_\alpha = \sum_i v_{i\alpha} f_i \quad , \tag{4.12b}$$

and for higher order tensor as well

$$\Pi_{\alpha\beta} \equiv p\delta_{\alpha\beta} + \rho u_\alpha u_\beta = \sum_i v_{i\alpha} v_{i\beta} f_i \tag{4.13a}$$

$$\Pi_{\alpha\beta\gamma} \equiv p(u_\alpha \delta_{\beta\gamma} + u_\beta \delta_{\alpha\gamma} + u_\gamma \delta_{\alpha\beta}) = \sum_i v_{i\alpha} v_{i\beta} v_{i\gamma} f_i \tag{4.13b}$$

considering the main macroscopic variables for a fluid such as the density ρ, the velocity u_α and the pressure p. Also, the tensor $\Pi_{\alpha\beta}$ has been identified as the **moment flux tensor**. For now these physical macroscopic fields have not been mentioned in the Lattice-Boltzmann model, thus this definition will have nothing to do with the model itself, unless the distribution function at equilibrium f_i^{eq} manages to recover the macroscopic fields from (4.4). This will be shown later on. Using eqn. (4.9) with (4.12a) and (4.12b) the continuity equation is given as

$$\partial_\alpha(\rho u_\alpha) + \partial_t \rho = 0 \quad . \tag{4.14}$$

In the other hand, using eqn. (4.10) with (4.13a) a PDE similar to NSE equation is gotten (see Appendix F for details):

$$\partial_\beta(\rho u_\alpha u_\beta) + \partial_t(\rho u_\alpha) = -\partial_\alpha p + \eta \partial_\beta(\partial_\beta u_\alpha + \partial_\alpha u_\beta) \tag{4.15}$$

with

$$\eta = \rho c_s^2 \left(\tau - \frac{\delta t}{2}\right) \tag{4.16}$$

will be the viscosity. Is possible to see that for $\tau = \delta t/2$ we end up with the Euler equation, however this case will lead to numerical instability as it's a limit case before the distribution functions become negative and the model instantly gets unstable (please see details in [38, sec. 4.4.2]). Although we have associated the moments from f_i to physical quantities to get continuity and NSE equation in (4.12), as mentioned before, this association is not possible if the equilibrium function f_i^{eq} is not properly defined in terms of these physical quantities. The equilibrium function must be written such that is possible to retrieve all the macroscopic moments using (4.4). One way to find the proper f_i^{eq} is by *moment matching*. This consist of writing the equilibrium function as an *ansatz* written as

$$f_i^{\text{eq}} = \omega_i \rho(1 + a_1 v_{i\alpha} u_\alpha + a_2 v_{i\alpha} v_{i\beta} u_\alpha u_\beta - a_3 u_\alpha u_\beta) \tag{4.17}$$

where ω_i are the weights that complement the velocity set. Then the constants a_1, a_2 and a_3 are found such that using the conditions for $v_{i\alpha}$ and ω_i described in (4.5) the macroscopic variables are obtained. For the case of fluids we have

$$a_1 = \frac{1}{c_s^2} \quad ; \quad a_2 = \frac{1}{2c_s^4} \quad ; \quad a_3 = \frac{1}{2c_s^2} \tag{4.18}$$

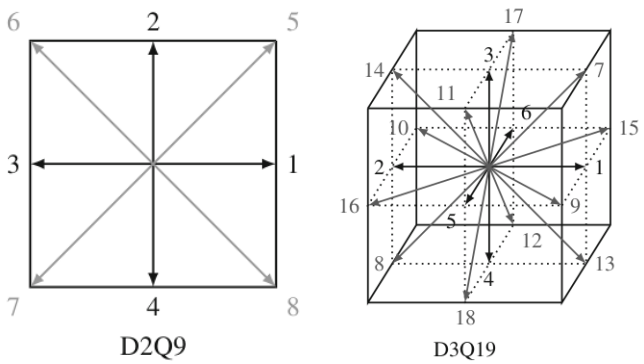

(a) D2Q9 lattice set. **(b)** D3Q19 lattice set.

Fig. 4.1. Examples of different Lattices.

where c_s^2 constant appears once again due to (4.5), but finding the second order tensor, after doing the math we find that this matches the momentum flux tensor

$$\sum_i v_{i\alpha} v_{i\beta} f_i^{\text{eq}} = c_s^2 \rho \delta_{\alpha\beta} + \rho u_{i\alpha} u_{i\beta} = \Pi_{\alpha\beta} \tag{4.19}$$

thus, the constant c_s^2 appearing in (4.5) matches with the c_s^2 of (2.42) and f_i^{eq} is

$$f_i^{\text{eq}} = \omega_i \rho \left(1 + \frac{v_{i\alpha} u_\alpha}{c_s^2} + \frac{v_{i\alpha} v_{i\beta} u_\alpha u_\beta}{2 c_s^4} - \frac{u_\alpha u_\beta}{2 c_s^2} \right) \tag{4.20}$$

The equilibrium function is important to recover the required forms of the moments involved in the partial differential equations to solve, thus, its form is crucial in order to make this method to work. In the following sections we will describe another Lattice-Boltzmann model where the equilibrium function is different such that another kind of moments are obtained and therefor satisfying another set of equations if we introduce some restrictions to the algorithm.

4.2 How to implement a Lattice-Boltzmann method?

We have discussed how this cellular automata is able to reproduce in the macroscopic behavior a series of partial differential equations for a series of tensorial moments, and also, defining properly the equilibrium distribution function these equations become the ones that describe the dynamics of the macroscopic properties of a fluid. Everything by only solving a discrete version of the transport Boltzmann equation. In this short section we will discuss the basic standard implementation of a LBM to solve the dynamics of a fluid in three dimensions using the D3Q19 Lattice.

i	0	1	2	3	4	5	6	7	8	9	10	11	12	13	14	15	16	17	18
ω_i	$\frac{1}{3}$	$\frac{1}{18}$	$\frac{1}{18}$	$\frac{1}{18}$	$\frac{1}{18}$	$\frac{1}{18}$	$\frac{1}{18}$	$\frac{1}{36}$	$\frac{1}{36}$	$\frac{1}{36}$	$\frac{1}{36}$	$\frac{1}{36}$	$\frac{1}{36}$	$\frac{1}{36}$	$\frac{1}{36}$	$\frac{1}{36}$	$\frac{1}{36}$	$\frac{1}{36}$	$\frac{1}{36}$
v_{ix}	0	1	-1	0	0	0	0	1	-1	1	-1	0	0	1	-1	1	-1	0	0
v_{iy}	0	0	0	1	-1	0	0	1	-1	0	0	1	-1	-1	1	0	0	1	-1
v_{iz}	0	0	0	0	0	1	-1	0	0	1	-1	1	-1	0	0	-1	1	-1	1

Chart 4.1. Set of vector components and weights used in D3Q19.

A first basic element is the definition of the computational domain. The space is divided into $L_x \times L_y \times L_z$ cubic cells of side length δx such that the figure 4.2b is a representation of one single cell of the entire domain. Each cell will provide the same set of vector velocities D3Q19 whose components with the respective index are shown in chart 4.1. For each cell will also reside one distribution function for each of the 19 directions of index i, namely f_i, where the information will be contained. An initial configuration for f_i must be established before starting to evolve the cellular automata. For example, in order to set the density field to an initial value $\rho_0(\vec{x})$ for all cells, as well as an initial value for the velocity $\vec{u}_0(\vec{x})$, that is done by calculating the equilibrium distribution function in terms of these initial values for the macroscopic fields for all cells using (4.20). Then at the time $t = t_0$ the distribution functions are set as

$$f_i(\vec{x}, t_0) = f_i^{\text{eq}}(\rho_0(\vec{x}), \vec{u}_0(\vec{x})) \quad . \tag{4.21}$$

As a next step, the Lattice information or distribution functions are combined at each cell following an evolution rule based on the transport Boltzmann equation, such that the new value of f_i at the time $t_1 = t_0 + \delta t$ is

$$f_i(\vec{x}, t_0 + \delta t) = f_i(\vec{x}, t_0)\left(1 - \frac{\delta t}{\tau}\right) + \frac{\delta t}{\tau} f^{\text{eq}}(\rho(\vec{x}, t_0), \vec{u}(\vec{x}, t_0)) \quad . \tag{4.22}$$

This step is called the *Collision* where the system dynamics is actually evolving to the next time iteration, as the current time step after this step will be $t_{n+1} = t_n + \delta t$. After calculating the new values of f_i for all cells, these must be transferred to the neighbor cells in order to spread the information along the Lattice using the D3Q19 vector set. This step is known as the *Streaming* or *Advection* step, where the value of all populations f_i are computed as follows:

$$f_i(\vec{x} + \delta t \vec{v}_i, t_{n+1}) = f_i(\vec{x}, t_n) \quad , \tag{4.23}$$

ensuring to be developed for all $i = 1, \ldots, 19$. The reader may wonder what must be done at the boundary or edge cells of the domain, in other words, which will be boundary condition of the system as these edge cells have no neighbor to transfer its information with. There are plenty of boundary conditions shown in detail in [38, sec. 5.3], like the periodic boundary condition, where the cell to be following the ending one $\vec{x}_n$ will be the one at the opposite edge $\vec{x}_0 = \vec{x}_n - \vec{L}$. That is

$$f_i(\vec{x}_n, t_{n+1}) = f_i(\vec{x}_n - \vec{L}, t_n) \quad , \tag{4.24}$$

where $\vec{L} = (L_x, L_y, L_z)$ is a vector containing the number of cells per dimension. At the same time, the cell behind the first edge cell $\vec{x}_0$ will be the last cell of the Lattice at one direction $\vec{x}_n$, that is

$$f_i(\vec{x}_0, t_{n+1}) = f_i(\vec{x}_0 + \vec{L}, t_n) \quad . \tag{4.25}$$

Another kind of boundary conditions are the *bounce-back* conditions with different ways to implement it. This boundary condition consist of reflecting the information back to the inner region of the fluid, including a small attenuation factor $\Phi \in [0, 1]$. One way to implement it is by exchanging the velocity vectors at any edge cell

$$f_i(\vec{x}_n, t_{n+1}) = \Phi f_j(\vec{x}_n, t_n) \quad \text{and} \tag{4.26a}$$

$$f_i(\vec{x}_0, t_{n+1}) = \Phi f_j(\vec{x}_0, t_n) \quad , \tag{4.26b}$$

where j is an index of the velocities set which satisfies

$$\vec{v}_j = -\vec{v}_i \quad . \tag{4.27}$$

Notice that here we are evolving the state of the system at the next time iteration, then the next step in order to evolve to the next time iteration would be to repeat first the Streaming step written at (4.23) and then the collision step (4.22) for each time iteration, until the end of the simulation. As the last updated value of f_i in t_{n+1} depends on the current value of f_i at t_n as shown in (4.22), there must be knowledge of the previous value $f_i(t_n)$. This may be done in two ways: One is storing the value of f_i in a temporal variable to exchange it with the new value, and the other one is allocating an entire copy of f_i which will store the old values of the system, one step behind, also exchanging between them during the Advection step. As a last remark, in order to set a fixed value for the macroscopic fields $\rho_\Omega(\vec{x}_\Omega, t)$ and $\vec{u}_\Omega(\vec{x}_\Omega, t)$ over a region Ω of the domain containing a set of cells, like a way to impose a Dirichlet boundary condition for the relevant physical quantities, one way to do it is by fixing the populations f_i for all cells $\vec{x}_\Omega \in \Omega$ as the equilibrium function evaluated with $\rho_\Omega(t)$ and $\vec{u}_\Omega(t)$. This technique works even for time-dependent fields so that sources are possible to implement, as the change or presence of these fixed fields will produce a propagation over the surroundings of Ω and eventually, the rest of the domain. This step is usually called *Impose* fields over a region and it's executed after the Collision step and just before the Advection step. After the first iteration of the system the macroscopic fields must also be updated as well, meaning that from now on these must be computed as in (4.12) with the new values of f_i previously treated. Finally, after each step one can print or dump any information of the system as the macroscopic fields in an output file in order to analyze the desired results of the simulation. In summary, the overall steps to perform in a Lattice-Boltzmann simulation is described in the following list:

1. Set the initial macroscopic fields and compute the equilibrium function at each cell in terms of these initial conditions.

2. Compute the macroscopic moments in which the equilibrium distribution depends on, as described in (4.12).

3. Evolve the system by performing a collision using (4.22) storing the new value of f_i in terms of the last one.

4. If there are fields to be imposed, the equilibrium function must be computed whit these fields at the set of cells where the imposed field is desired to impose.

5. Perform the Streaming or Advection process as in (4.23), applying the chosen boundary conditions, whether to be periodic, bounce-back, or something else.

6. Dump all the desired information to an output file in the disk.

7. Repeat from step 2 in order to execute the next time step, until all desired steps are evolved.

This numeric prodcedure not only allows to perform a Lattice-Boltzmann simulation for fluids, but also for another models with different fields and different conservation laws. In the next section a Lattice-Boltzmann model to solve the waves equation is described, taking into account that NSE equations can be linearised under small perturbation regime in order to get instead the waves equation, as it is shown in chapter 2.

4.3 Lattice-Boltzmann for Acoustics

As shown in section 4.1, the Lattice-Boltzmann numerical approach will be able to solve partial differential equations for a set of moments computed as summations over the populations, as soon as the equilibrium distribution function (written in (4.20)) would be able

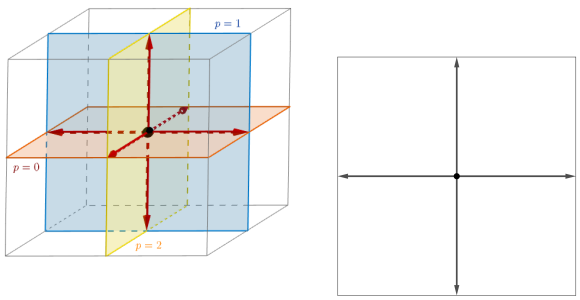

(a) **(b)**

Fig. 4.2. D3Q7 velocity set (a) and D2Q5 velocity set (b).

to reproduce all the involved moments, which in the case of fluids it's enough to reproduce the first four orders of the moments such that the equations (4.14) and (4.15) are automatically obtained. However, in the section 2.2 we learned that if we only consider small variations on macroscopic fields up to first-order perturbations, then higher order terms are neglected and the NSE equation combined with the continuity equation becomes a simple waves equations, as a linearised version of NSE. The following model is based in the original proposal of Chopard, P.O. Luthi and J. Wagen where the waves equation is used with a specific lattice similar to D2Q5 and exclusively for two-dimensional models [33], however it is possible to follow the same procedure to build a similar model with some small differences in order to be able to use another kind of Lattices, like D3Q7, making it possible to simulate three-dimensional systems. As a first remark, we can notice that the macroscopic equation in terms of first and second order tensors (4.10) is simplified to (4.11). In the other hand, if we manage to make the second-order tensor diagonal and isotropic and linear to the zero-order tensor, meaning

$$\Pi_{\alpha\beta} = \kappa \Pi \delta_{\alpha\beta} \quad , \tag{4.28}$$

with κ a constant, the resulting equation is

$$\kappa \partial_\beta \Pi + \partial_t \Pi_\alpha = 0 \quad , \tag{4.29}$$

then applying the operator ∂_β both sides and using (4.9) the last equation becomes

$$\begin{aligned} \kappa \partial_\beta^2 \Pi + \partial_\beta \partial_t \Pi_\alpha &= 0 \\ \kappa \partial_\beta^2 \Pi + \partial_t (\partial_\beta \Pi_\alpha) &= 0 \\ \kappa \partial_\beta^2 \Pi - \partial_t^2 \Pi &= 0 \\ \kappa \partial_\beta^2 \Pi &= \partial_t^2 \Pi \end{aligned} \tag{4.30}$$

Which would be a waves equation if we are able to ensure $\kappa = c^2$ with c some parameter representing a propagation speed. This means that in order to build a LB model which solves the waves equation we need to set $\tau = 1/2$ and write an equilibrium function able to reproduce the following macroscopic moments:

$$\begin{aligned} \rho &= \sum_i f_i \quad , \\ \vec{J} &= \sum_i \vec{v}_i f_i \quad , \end{aligned}$$

as well as the auxiliary field

$$p = c^2 \rho \tag{4.31}$$

and the diagonal tensor

$$\Pi_{\alpha\beta} = p \delta_{\alpha\beta} = \sum_i v_{i\alpha} v_{i\beta} f_i^{eq} \quad . \tag{4.32}$$

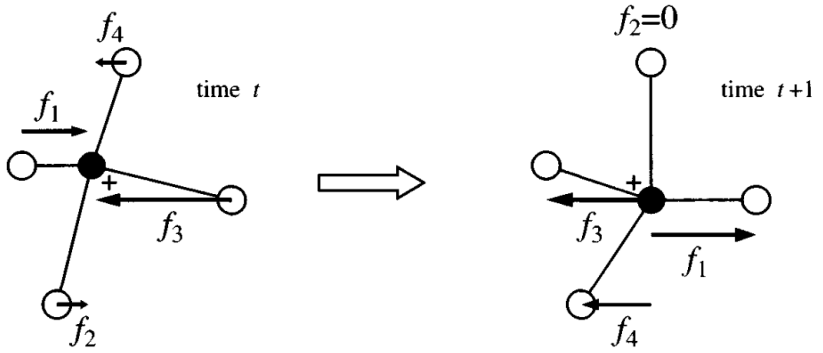

Fig. 4.3. Cellular automata scheme for 2D waves propagation.

One equilibrium function able to recover the mentioned moments after using (4.5) is

$$f_i^{eq} = \begin{cases} \rho(1 + \frac{c^2}{c_s^2}(\omega_0 - 1)) & \text{if} \quad i = 0 \\ \frac{\omega_i}{c_s^2}(c^2\rho + \vec{v}_i \cdot \vec{J}) & \text{if} \quad i \neq 0 \end{cases} \quad , \tag{4.33}$$

where c_s is the constant dependent of the Lattice set, chosen accordingly to the dimension of the domain. The constant c is however an adjustable parameter which takes the role of the speed of propagation of the simulated waves, as suggested in (4.31), which can be even a function of space. This feature provides the possibility of modeling different kind of mediums and materials with different shapes, in order to study the behavior of waves refraction along those. However one must take care of not introducing numerical instability due to sudden changes of this parameter through space, or take values that provokes instabilities like getting negative distribution functions or breaking the Courant-Friedrichs-Lewy criteria. In order to get a proper value for c, we can simply impose that

$$0 < c^2 < \frac{c_s^2}{1 - \omega_0} \quad , \tag{4.34}$$

with $c_s = 1/\sqrt{2}$ for the D2Q5 Lattice set and $c_s = 1/\sqrt{3}$ for the D3Q7 lattice set. Although it has been showed how this model can be built upon the same principles of the LB model for fluids, its origin relies on a proposal of B. Chopard and M. Droz consisting of a cellular automata composed by particles tied with springs between each other forming a two-dimensional square lattice (like a crystal in the classical point of view) [43, ch. 2] where only vertical and horizontal bounds are present according to figure 4.3, for this reason this model was intended to work properly in a D2Q5 Lattice set or a D3Q7 for three-dimensional simulations. The method has been extended to curvilinear coordinates and has been employed to simulate the normal modes in trumpets and even in the human Cochlea by Velasco et.al [34].

Part II

Numerical methodology

Chapter 5

The implementation of the Lattice-Boltzmann method for acoustics in LB3D

LB3D is a software developed by the Helmholtz Institute Erlangen-Nürmberg for Renewable Energy (HI-ERN) focused on performing fluid dynamics simulations in complex systems using the Lattice-Boltzmann method paralellized via MPI. The program is written in FORTRAN90 and it's still under development. One of the main objectives of this project was to implement the Lattice-Boltzmann method for the waves equations in this software in order to develop more general simulations, like acoustics, in any LB3D project inside the HI-ERN. As there were many presets to run specific systems and none of them was designed for waves, modifying parts of the code and making small tests through re-compiling and executing was necessary in order to test the new algorithm, as well as asking to the development team about functionality and logic of the code was needed. The documentation available is not enough to understand the use of it, so it was necessary to directly look at the code and write small modifications, ensuring that the program was still running and analyzing the possible results. The LB3D code has many core features in order to simulate physical systems related to fluid dynamics. The implementation of each feature is written in modules.

The core features include a Lattice-Boltzmann implementation to solve fluid dynamics and using a D3Q19 Lattice set, where more than one fluid may be simulated simultaneously with the purpose of creating interphases between two fluids called *components* in the LB3D context, but for the interest of this project only one component was considered. This is one of the most used modules which consists of several layers of complexity, however many more features have been included during the development as small extensions to enlarge the capabilities of the software. These test include an implementation for the Peskin's Immersed Boundary Method [44] to simulate drops, Ladd particle suspensions [45] and a molecular dynamics engine to implement motion of these objects, among many other features. Modifying some of the features was necessary to get the expected results in the three-dimensional case, however this point will be discussed in the next chapter.

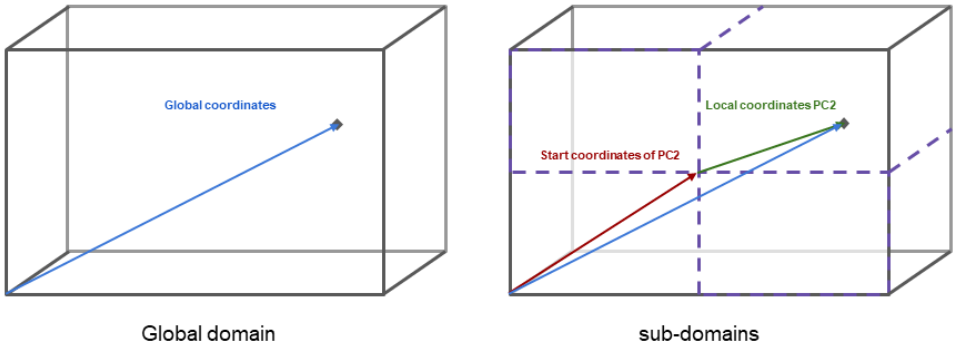

Fig. 5.1. Separation of multiple sub-domains for 4 processors.

5.1 A brief description of the LB3D software

This code have been in a constant process of development where many adaptations have been done. At this moment, the development team is working on a new branch called *rewrite*, where many implementation have been renewed in order to take more advantage on the parallelization, as well as writing more legible lines. Although this branch is completed for all the main features, the documentation is still incomplete, as this one explains the previous branch called *dev*. This particular project was developed under the *rewrite* branch in a separated branch called *WavesImplementationD3Q7*. All features are stored in separated modules defined at the folder `liblb3d`, and the script containing the main loop to run the simulation is stored in a separated folder called `lbe`. There are low-level modules like `core`, `system` in charge of implementing all the basic elements to build the feature modules, the module `parallel` is in charge of the parallelization and the remaining modules are features supported by the program, being the main ones `lb` for the Lattice-Boltzmann method, `offlattice-objects` to simulate a mesh object by Immersed boundary method, related with the module `ibm` and other modules that were not used for this project. Each module contains a class script where the definition of all members, subroutines and functions are written and a set script containing the actual implementation of the sub-routines and functions.

LB3D is written to be easily parallelized for multiple CPU threads, making it easy to run on a Cluster with hundreds of processors allocated by the HI-ERN institute, as it usually runs. How does LB3D handle a simultaneous execution with multiple processors? Basically the program divides the domain box into equal boxes and assigns each piece to each processor as shown in the figure 5.1 for the case of four processors. But something to keep in mind is that these pieces or sub-domains must share information between each other because they make part of a whole system. To solve this problem, the *halo* is introduced as a set of cells at the boundary of the sub-domain (covering the box like a skin) whose role is to exchange the information from the adjacent sub-domains. The important aspect of this is that every subroutine that runs in the main class will consider only one of the sub-domains of the general domain, meaning that the spatial array of cells belongs to a local coordinate

system, meaning that if one needs to simulate a source at a region of the sub-domain, this same region will be imposed at every sub-domain of the box, leading to get four repeated sources and that's not the desired result. This problem becomes important when one wants to simulate a single source on a wall or creating a region with different properties. To solve this problem, one can simply use the global position of the sub-domain, called `start`, to convert the local coordinates to global coordinates. If we only need to simulate the source on a specific sub-domain the conditional statements come in handy to do so.

During the development, the team runs unit tests to ensure that any official modification integrated by pull request does not affect the results of validated simulations. Thus, any proposal to be made must be reviewed by the team before to be integrated into the rewrite branch. But it is not enough by making some test simulations to work, this also requires that this modification follows the same metrics of the overall features in order to avoid compromising future modifications. Although the work done for this project is not forked into the main branch yet, all the tests done with the cases of interest are successfully running inside the branch *WavesImplementationD3Q7*, such as simulating a Gaussian pulse to test initial conditions, a point source of waves and the generation of plane standing waves by imposing fields and bounce-back boundary conditions included already in the module `rocks`, creating interfaces with different speed of sound as a new field of the software, and modifying the immersed boundary method to measure the acoustic radiation force over a sphere. The general workflow involved first analyzing the lines of code written in the scripts of the modules of interest, as `lb`, and run small tests to figure out how does the Lattice-Boltzmann model works in this code. Fortunately the repository contains a numerous set of examples and tests to get a starting point, learning how to compile and run them before jumping to edit the scripts. Once this procedure is understood, the scripts started to be modified by trial and error to reach an expected result during the simulation. As soon as any modification is introduced the code must be recompiled using *CMake* into a separated build folder.

5.2 Input and output files

The very first step was to start familiarizing with the LB3D code, understanding its mechanism in terms of what is necessary to run a simulation and how to read the output information from this execution. In basic terms, the code requires an input file where all parameters, conditions and configuration required to any specific simulation in order to run. The list of possible parameters is huge, but basically all information regarding the size of the domain, the initial conditions, boundary conditions, the amount of iterations, among others, is written in the input file. This kind of file uses the *namelists* Fortran feature to read the parameter which are assigned to global variables and local variables depending on the module to be used. Then, the run command is called using *mpirun*, specifying the executable located in the build folder and the amount of processors to use using the flag `-n`.

During the execution a log information will pop up from the shell, containing information regarding how was the initial configuration set up, how's the progress of the simulation and

also if any errors appear. One of the settings specified by the input file takes into account what physical quantity will be dumped in the output, from what time step and how often will that be dumped. The output files are formatted into the Hierarchical Data Format version 5 (HDF5), which is a file format able to contain large and complex amounts of data. This format must be treated externally to print the desired information. One can either create a Python script using the `h5py` package or use `Paraview`, which is a multi-functional visualization tool to render and analyze data, supporting many file formats.

One example is a Poiseuille flow, which is a basic fluids simulation where a one-directional channel of fluid with parallel walls at the sides has an external force like gravity (see [40, sec. 9.4]). The input file is composed into the following sections: `&system` contains basic information as the L_x, L_y and L_z dimensions in cells of the domain, as well as other parameters like the name of the output files and seeds for random operations. `&lattice_boltzmann` section contains parameters how many fluids (components) are involved in the simulation. `&relax_homogeneous` is a section to be used when the single time relaxation is used instead of the Multiple Time Relaxation approach (explained in [38, ch. 10]).`&variable_input` refers to all the specific conditions of the simulation, including the among of time steps with the `n_iteration` variable, which preset initial condition will be used from `init_cond` organized into labels or numbers corresponding to the defined cases (this aspect will be covered later). `n_sci_start` is the time step where the output dumping will start. The variables starting with `sci_` are flags or booleans indicating wheter a physcal macroscopic field will be dumped or not, as for example for density the variable is `sci_od`, and for velocity `sci_velocities` reffering to the three components of the velocity field vector. `&lbe_input` has to do with troubleshooting and monitorying and many more sections may be added such as `&extforce_constant` to include external forcing and `&rock_boundaries` to specify

Input file:

```
&system
 syst%box = 4 32 32
syst%seed = 1
/

&lattice_boltzmann
lb%ncomponents= 1
/


&variable_input
verbose_timestep = .false.
n_iteration = 10000
n_sci_start = 0
sci_velocities = .true.
n_sci_velocities = 10000
gr_out_file = 'out'
/

&lbe_input
n_sanity_check = 10000
/

&extforce_constant
acc = 0. 0. 1e-4
/
&rock_boundaries
rb%width = 1
rb%add_walls = 'SLIT_Y'
/
```

Result:

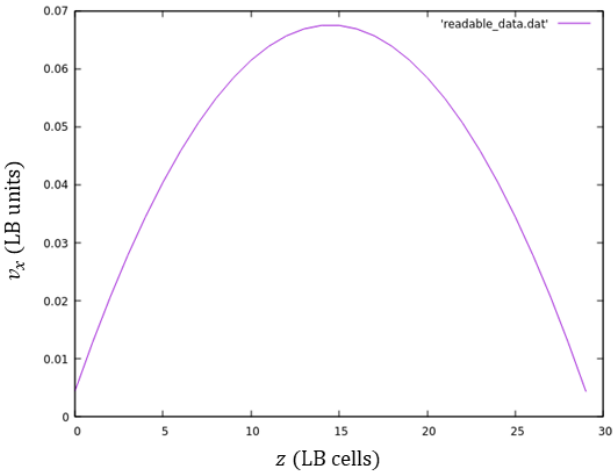

Fig. 5.2. Example of input file and its resulting output.

which rocks configuration from the presets is used in the simulation, for example the value `'SLIT_Y'` mean that in the walls perpendicular to the y-axis there will be walls. The last two sections will produce the required conditions for the Poiseuille flow, where many time steps must be simulated in order to reach an steady state of the velocity. The input file for this case and its result can be seen in the figure 5.2.

5.3 Setting an initial condition

LB3D has some presets to define initial conditions specified by the variable `init_cond` of the input file. These initial conditions are implemented in the script `lbe_init_functions.F90` located in `liblb3d/liblb3d/src/old` and each function is tagged with a string variable name. As explained ins section 4.2, to set an initial condition with specific macroscopic fields one must calculate the distribution functions to be the ones at equilibrium with the desired fields. The subroutine `boltz_bdist` makes this replacement possible by storing the i amount of values of every function f_i, only to set a proper initial condition, but not to evolve the system during the collision step. The figure 5.3 shows the logic representation behind this subroutine, of course with the modified formulae based on the waves equilibrium function (4.33). In order to test the behavior of this function the variable `init_cond_name` must be set to `'INIT_SPIKE'` which makes a uniform density except for a single cell located at one corner of the domain. The value of this cell is hardcoded in the subroutine `lbe_init_spike`, being its default 0.5 for $i = 5$, while the rest of the cells will have the same value defined with the variable `fr` of the input file. A visualization of the resulting initial condition can be seen in figure 5.4 where a single value is different from the rest, generating a disturbance in the following steps. Another kind of initial condition is called `'INIT_CONST'` where the density field is uniform with value `fr`, which will be useful to initialize system

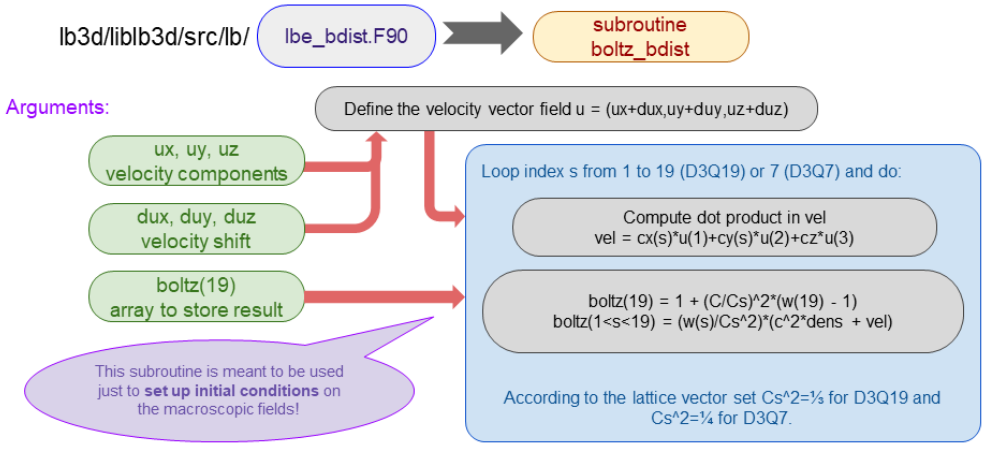

Fig. 5.3. Diagram flow of the `boltz_dist` subroutine.

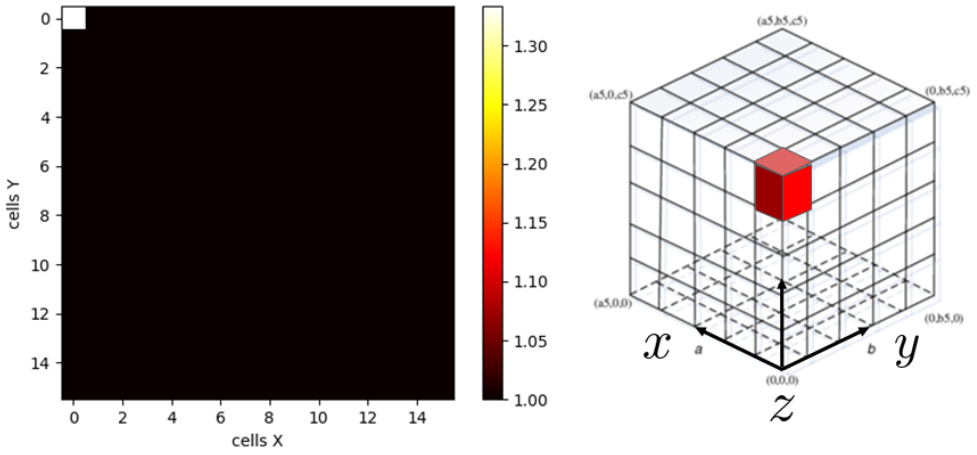

Fig. 5.4. Initial condition with a uniform density except for a single cell.

where sudden changes must be avoided. Although the spike condition does not seem to be useful to simulate as physical system, it is a starting point to make simple test where the LB3D code can be compared with another code by comparing the resulting output under the same conditions. In the next chapter an example of this test will be reported but instead with the implementation of a Gaussian pulse propagating through space.

5.4 Changing the equilibrium function and lattice vectors set

One key difference between the standard Lattice-Botlzmann to simulate fluids and the Chopard's model to solve the wave equation is the equilibrium function, thus, as a first attempt to alter the code of LB3D the objective was to modify this function in order to get the desired behavior. But the LB3D code does not rely on a single subroutine to implement the equilibrium function because each time step must be as optimal as possible, taking the advantage of parallel computing. For this reason, the `boltz_bdist` subroutine is only in charge of initializing the system as discussed previously, but it does not affect the dynamic behavior during the collision step. For this reason, the collision step is studied for this code in order to figure out when and how does the equilibrium function is involved.

The main class of the Lattice-Boltzmann feature, called `lbe_lb_class.F90` contains a member of a sub-class called `lbe_bdist_class.F90` with all the relevant members and elements for the equilibrium distribution function. This class is provided with many kinds of subroutines focused on calculating the equilibrium function with different forcing models (such as Shan-Chen, Guo, Kupershtokh, among others) and the type of forcing is chosen in the subroutine `compute_bdist`. As Forcing is not part of the focus of this project, the

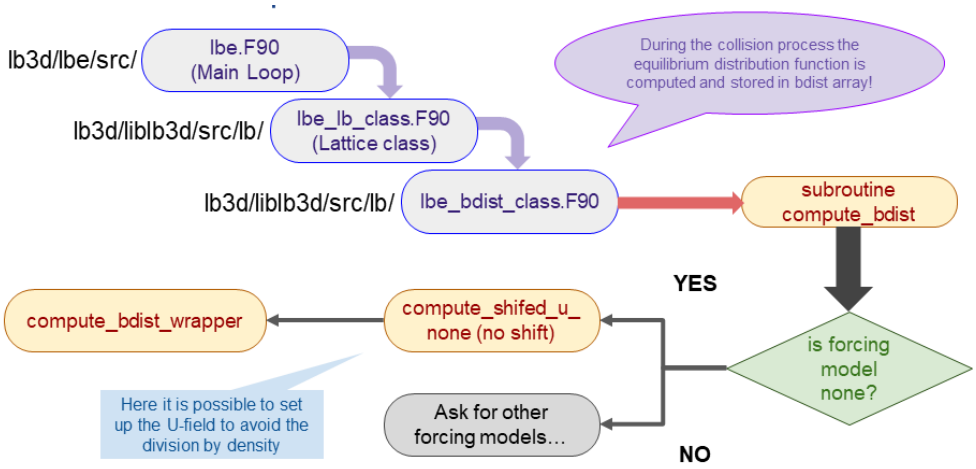

Fig. 5.5. Diagram flow of the calls from the collision step to the distribution function wrapper.

chosen alternative is `compute_shifted_u_none`, calling another subroutine inside the bdist class called `compute_bdist_wrapper`. This subroutine has the job of deciding wether the collision model is a simple BGK operator, which is the case, or if MRT is being used, leading to the subroutine `compute_bdist8`, where the actual implementation of the equilibrium distribution function is written. This process is summarized in the figure 5.5 reaching to the final function to directly decide to call the `bdist8` subroutine. The code has more kind of equilibrium functions implemented, but those were not considered in this project, as this code aims to be as multi-functional as possible, covering special models and cases to simulate

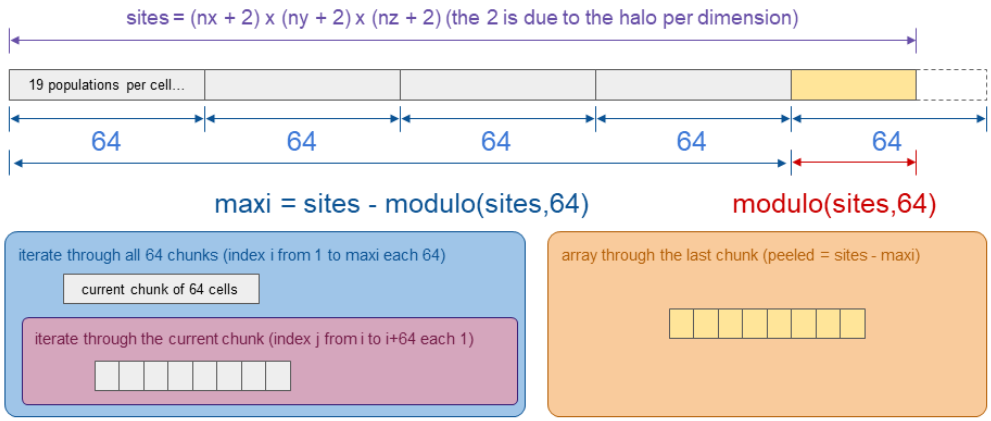

Fig. 5.6. A scheme of how does the information is allocated in LB3D to handle multiple processors.

many physical systems.

The computation of the equilibrium function looks anti-intuitive at first, as the iteration is not made explicitly in a single line, but instead it does the job for every direction, jumping 64 elements at each computation in order to afford computational cost. In the figure 5.6 we can appreciate the structure of a flattened array storing the information of a sub-domain belonging to one processor, separated into several chunks of 64 cells of length, and the total length of the array includes a couple of cells per dimension which accounts for the boundary cells of each sub-domain which are in charge of exchanging information between the adjacent sub-domains. More information about these cells will be explained later. The algorithm to calculate the equilibrium function iterates over each chunk of 64 cells, which is at the same time jumping to the next chunk until the last complete chunk (whose number is stored in the variable `maxi`). Then, the remaining cells are iterated afterwards. Each iteration computes the equilibrium function from the null index - assigned to $i = 19$ for LB3D - to the rest of them line by line, recycling auxiliary variables to calculate the dot product between the vector field and the i^{th} velocity. Following the same logic of the sequential lines, the `bdist8` was modified eliminating additional second-order terms of the equilibrium function for fluids, written in eq. (4.20) and creating a special case for $i = 19$ as the null vector, according to (4.33). As a final remark, the Chopard's model was designed to work with a velocities set where no diagonal vectors are included like D3Q19, meaning that it is necessary to change the lattice set to a three-dimensional lattice with only vectors parallel to the orthogonal Cartesian axes, like D3Q7 (see fig. 5.7). However, changing this lattice will break most of the functionalities of LB3D, because every velocity vector and weight is hard-coded and LB3D was written thinking of using D3Q19 as a unique lattice set, but

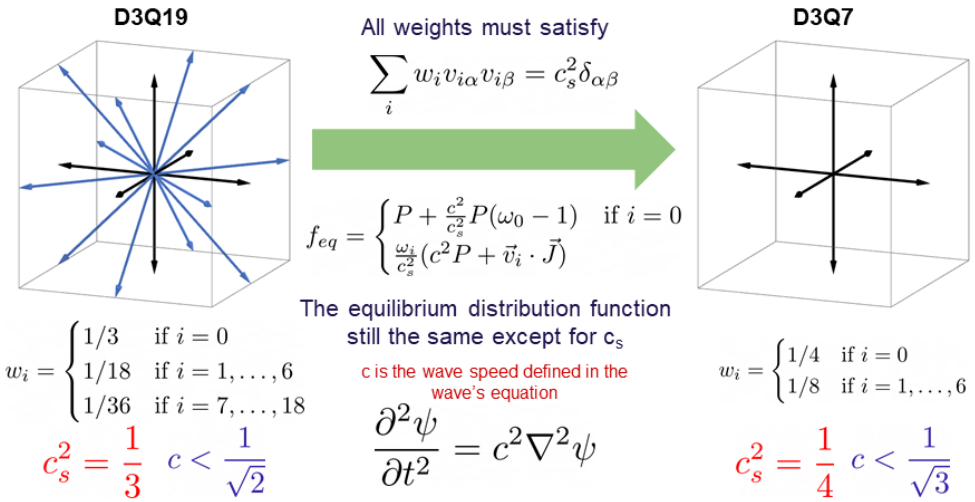

Fig. 5.7. A representative diagram of the simplification of the lattice to change the velocities set that LB3D uses to D3Q7.

fortunately the D3Q19 lattice set contains all the vectors comforming the D3Q7 lattice, thus, the strategy to make this modification possible shall be not elegant but rather simple: Impose at every time step of the simulation that all distribution functions from $i = 7$ to $i = 18$ to be zero. This of course will lead to non-existing functions beyond $i = 7$, where all the lattice vectors of D3Q19 which do not belong to D3Q7 are nonexistent, but the computation of the physical quantities will add unnecessary zeros along the way, making this fact the optimization downside. Despite introducing this inefficiency all the simulations done were not compromised with huge amounts of computation and the development team showed not opposition to this decision. The definition of these vectors as well as the weights are in the script `lbe_globals.F90` inside the feature `globals`.

The implementation of the Lattice-Boltzmann model for waves in LB3D would be completed with the illustrated procedures, but these modifications must be validated with numerical tests. In the next chapter we will report the description and results of all the numerical tests made during the development process, also showing what additional implementation needed to be done on order to simulate phenomena like a Gaussian pulse, a point source of waves, standing waves and planar interfaces between two media with different speeds of sound.

Chapter 6

Benchmarks to validate the implementation

In order to evaluate if the Lattice-Boltzmann model for waves, some numerical tests must be done. The implementation of the Lattice-Boltzmann method for waves was developed in two ways: One to simulate two-dimensional systems by developing a standard code in C++, and another implementation was done in the software LB3D in order to perform simulations in three dimensions. In this chapter we will focus on explaining all the benchmarks done in both implementations relying on the fact that basic methodologies were explained in the previous chapter. As a first test, a point source of waves is produced by imposing a time-variable field in the middle of the domain. then, using the same principle of the first test, standing waves were simulated by extending the source from a single point to one of the bound walls of the domain and adding bounce-back boundary conditions in order to get a steady and one-directional resonator. This test is actually part of the desired system to be simulated and we must ensure that the conditions are matching the analytical solution of a standing plane wave. In order to simulate the proper boundary conditions over the surface of the sphere, this works propose the following: Produce an interphase between the fluid medium and the sphere medium, where the speed of sound is different in both media such that the continuity boundary conditions are properly satisfied as the LB method will try to satisfy the conservation laws nearby the region where the change in the speed of sound occurs. In order to verify if the desired boundary conditions are satisfied, a plane interphase will be simulated as a benchmark. This will make possible to measure the reflected and transmitted waves easier to make a comparison with the theoretical results.

The very first test done was to rewrite the equilibrium function from (4.20) to (4.33) and change the set of velocities and weights from lattice D3Q19 to D3Q7, as the D3Q19 lattice contains all the D3Q7 vectors. During this implementation the very first benchmark was to simulate a Gaussian pulse propagated in space by imposing an initial condition. The idea was to compare the output of two codes, one for a well tested simple code written in C++ and the other for LB3D, such that if the output information differentiates only due numerical precision limit, then the LB3D implementation is validated.

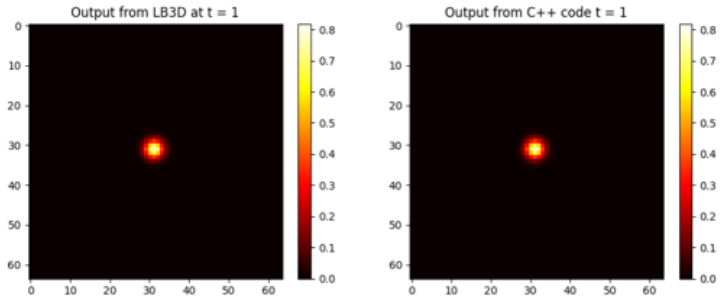

(a) Gaussian pulse at the instant $t = 0$.

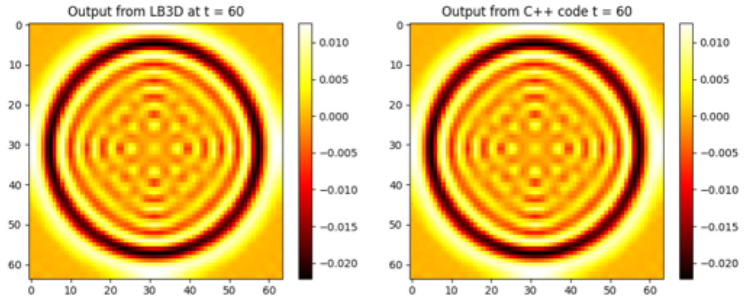

(b) Gaussian pulse at the instant $t = 60$.

Fig. 6.1. A Gaussian pulse.

6.1 A gaussian pulse propagation as an initial condition

In order to compare two outputs from two different programs which implements the same simulation, the best option is to try a simple simulation: A small localized perturbation which propagated through space. This test consist of setting an initial perturbed field by only initializing the density to be uniform except at some region, then this difference will propagate as a pulse isotropically, forming a single pulse with spherical wavefront. This test has the issue of introducing a small numerical instability as the change of the density in space is huge (a spike in the middle of null values) meaning that the algoritm will get harder to relax to the actual equilibrium state. The objective here is to ensure that LB3D is able to reproduce the same output of a generic implementation written in C++. This simple simulation was done in a simulation box of $64 \times 64 \times 64$ cells. Then, the following initial density field at $t = 0$ is set:

$$\rho(x, y, z, 0) = \rho_0 \exp\left(\frac{(x - N/2)^2 + (y - N/2)^2 + (z - N/2)^2}{2\sigma^2}\right) \quad , \tag{6.1}$$

where $\sigma = 5$ in automation units is a constant regarding the width of the pulse.

In order to perform this kind of simulation in LB3D, the subroutine `lbe_init_spike` was modified in order to instead modify the value of the distribution functions of a single cell, to set the density to have the form of a gaussian pulse, as the subroutine lets the access of coordinates x, y and z of the domain and the distribution functions on it by an array, as seen in figure 6.2. With this modified subroutine it was possible to perform this first numerical test to validate the modifications with the C++ code. This required re-compiling the LB3D code and run a test with a single processor as the domain size is small enough to be executed with a single processor.

This test has a purpose of testing only the initial condition for the specific case of LB3D. 60 time steps were simulated in both programs. After numerous executions to check the similarity of both implementations, figure 6.1 shows a similar output for both programs at least qualitatively, also we can see that inside the wavefront there is numerical noise due to the sudden change of imposing a non-zero value in a single value. These figures are basically a 2D plot of a matrix where the density at each cell is dumped, then the difference of each value for both outputs was made and every cell was giving an order of magnitude of 10^{-9}, which is considered a numerical rounding issue because both matrices were printed with numbers of 8 decimal places, meaning that the test is considered a success and the basic implementation of the equilibrium function and the lattice set D3Q7 in LB3D was done.

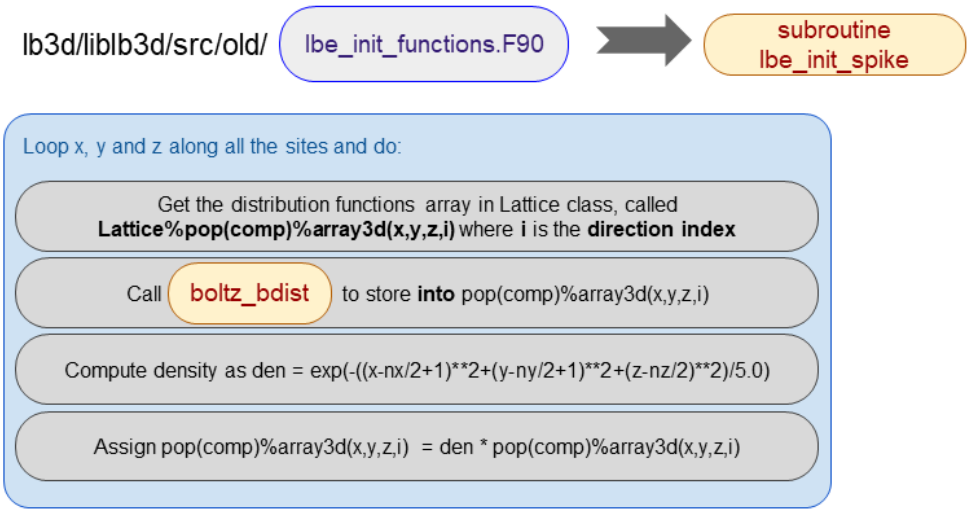

Fig. 6.2. Structure of the modified `lbe_init_spike` to set a density with the form of a gaussian pulse.

6.2 Imposing fields: The point source and standing waves

Setting initial conditions will propagate pulses through space, but plane waves or resonators will require the implementation of localized sources, as any traveling wave is propagated from a time changing vibration, as an oscillating pulse or a vibrating wall membrane. In this section we will explain briefly how to simulate sources by imposing the value of the distribution functions to the equilibrium functions with the desired fields over a certain region.

As discussed in section 4.3, for a time varying scalar field $\rho_\Omega(t)$ or vector field $\vec{J}_\Omega(t)$ at a set of cells Ω, the distribution function evaluated at $\vec{x}_\Omega \in \Omega$ is fixed to

$$f(\vec{x},t)\Big|_\Omega = f_i^{\text{eq}}(\rho_\Omega(t), \vec{J}_\Omega(t)) \tag{6.2}$$

after the collision step and before the advection step. Let's take as a first example a point source at the position $\vec{x}'$ inside the domain. Theoretically one has the following inhomogeneous waves equation:

$$\nabla^2\rho - \frac{1}{c^2}\frac{\partial^2\rho}{\partial t^2} = \delta(\vec{x}-\vec{x}')\rho_0\sin(\omega t) \quad , \tag{6.3}$$

with ω a free parameter for angular frequency. The solution is found through Green functions [42, sec. 6.4] and takes the form

$$\rho(\vec{x},t) = \frac{\rho_0}{4\pi}\int \frac{\delta(\vec{r}-\vec{r}')\sin(k|\vec{r}-\vec{r}'|-\omega t)}{k|\vec{r}-\vec{r}'|}d^3r' = \frac{\rho_0\sin(\omega t)}{4\pi kr} \quad . \tag{6.4}$$

where $r = |\vec{x}-\vec{x}'|$ is the distance from the source position to the measurement point $\vec{x}$. In this particular case the spatial dependence of the source is given as a Dirac's delta as shown in (6.3), but as the domain is composed by discrete finite-sized cells, imposing the temporal component at one cell $\vec{x}'$ is enough and will not provoke any numerical instabilities unlike the Gaussian pulse, because the initial condition in this case is a zero density field in the entire space due to the sine temporal dependence. If there was a cosine instead the initial condition would be similar to the Gaussian pulse, which will lead to numerical undesired noise which may be damped by replacing the Dirac's delta by a Gaussian function. In this sense, for a domain of $N \times N \times N$ cells the source to be imposed at the position $\vec{x}' = (N/2, N/2, N/2)$ take the following form:

$$\rho(\vec{x}',t) = \rho_0\sin(\omega t) \tag{6.5}$$

and the simulation started to evolve the enough amount of steps before the waves reach the boundary of the domain.

Implementing the explained physical system in LB3D was a challenge because LB3D was not designed for simulating sources of waves or fixing the value of a macroscopic field as a physical Dirichlet boundary condition. This means that a new implementation had to be

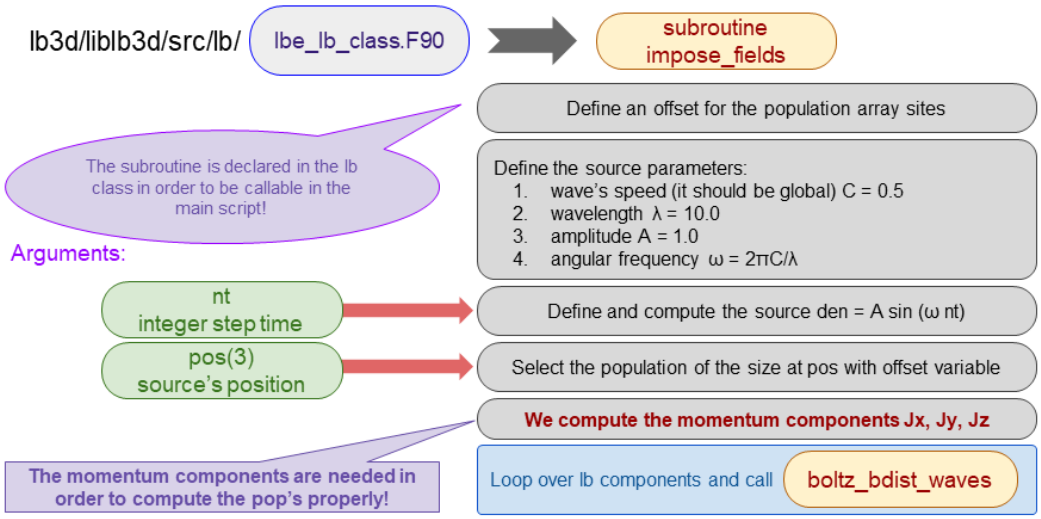

Fig. 6.3. The flow chart of the impose a point source subroutine.

added to fix the value of a field over a region of cells. In section 4.2 the process of fixing a field during all the simulation steps was illustrated in a similar manner of imposing initial conditions: The populations are re-calculated to be the equilibrium function in terms of the fixed fields. This is usually done in a single step between the collision and advection steps.

To implement a new subroutine we need to first write the algorithm in the main class associated to the desired module. In the case of imposing fields, this function must be written in the main class of the Lattice-Boltzmann feature `lbe_lb_class.F90`. The algorithm is summarized in the figure 6.3 where the arguments are the current time step t as an integer and a three-dimensional array with the point position $\vec{x}'$ of the point source. Basically, this subroutine simply compute the expression (6.5) with the given parameters and inserts this value into a location of the domain array of cells, then the equilibrium function is computed using the function `boltz_bdist_waves` which was modified to compute the right equilibrium function, as this process is not part of the collision process. It is worth mentioning that all the not imposed fields must be re calculated to be inserted to the equilibrium function, otherwise we would be imposing those to be null values. Although the function is properly written the code won't be able to use it because its existence is not known by the main program, for this reason the next step is to create a public statement with the declaration of this new subroutine just besides the rest of procedures of the class. Now it is time to call this subroutine between the collision and advection steps, and this is done basically pointing to the module where this function is defined and writing the name of the subroutine with the proper arguments, so that the only needed thing to do is re-compile. As in the first test, both codes were compared between them and with the theoretical solution (6.4). As expected, the figure 6.4 shows that both outputs were identical ignoring numerical rounding and the simulated waves made a good agreement with the theoretical solution.

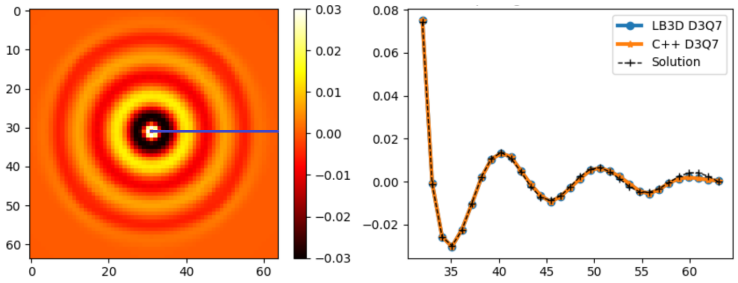

Fig. 6.4. Test of a point source and its comparison with the theoretical solution

6.3 Generating standing waves

Another result reached was the production of standing waves by imposing reflective walls at both sides of the simulation box domain and a source wall at one of the sides. The reflective walls are implemented by using the bounce-back boundary conditions located at two opposing faces perpendicular to x-axis. Thus, for a domian of $L \times N \times N$ where L is the length of the resonator measured in lattice cells and N the amount of cells in the y and z directions, the planes $x = 0$ and $x = L + 2$ will perform the bounce-back evolution rule (4.26), while the remaining planes will be periodic boundaries just as it's expressed in (4.25) and (4.24). In the case of interest it's convenient to get a stationary state where a node is placed in the middle of the box, that is at $x = L/2$, where the spherical object will be placed later on. This is done by simply emitting a plane wave at $x = 1$ cell such that by symmetry the same value must render after reaching a steady state, and setting the size of the channel $L = \lambda/2$, where λ is the wavelength of the emitted waves. The field to be imposed has the form

$$\rho(y, z, t)\Big|_{x=1} = \rho_0 \sin(kr - \omega t) \quad , \tag{6.6}$$

where ω is related with the wavelength via the following relation dispersion:

$$\omega = kc = \frac{2\pi c}{\lambda} \quad . \tag{6.7}$$

It is necessary to run a quantity if steps to wait for the wave to get the opposite side, bounce and return to the side it came from. Once this happens, the next emitted wave will interfere with the previous one such that steady waves with fixed nodes and anti-nodes are produced. It is worth mentioning that bounce-back conditions over the opposite faces of the wall is enough to simulate any kind of resonator as soon as the damping coefficient Φ is less than 1 but close enough. For this test $\Phi = 0.99$ or closer is enough to reach a stable steady state. In the case of LB3D a new subroutine is implemented following the same principle of the `impose_field` subroutine explained in the previous section. This new subroutine iterates manually over the cells along y and z fixed at a position x. The function `boltz_bdist_waves` is used to replace the distribution functions with the equilibrium ones

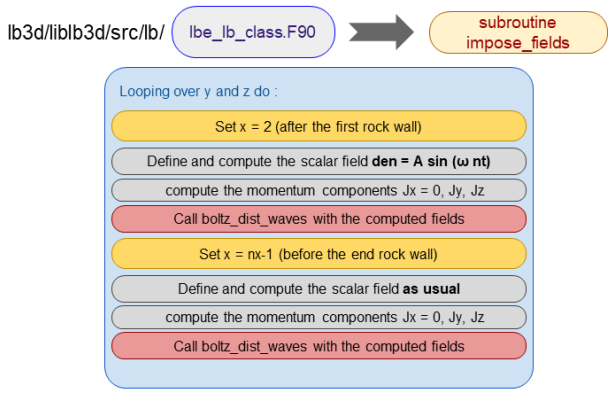

Fig. 6.5. A set of instructions summarizing the standing waves subroutine in LB3D.

with (6.6) and also with $J_x = 0$. The bounce-back boundary conditions are already implemented using the rock boundaries. This is a feature that can be activated from the input file with the `&rock_boundaries` option, setting the width of the rock to one cell via `rb%width = 1` and setting the option `rb%add_walls = 'SLIT_X'` to create the reflecting walls. A set of instructions of the subroutine can be seen in the figure 6.5, written at the same place where the subroutine for the point source was written.

In figure 6.6a shows a time instant where the plane wave just reached the opposite wall. Half period later the amplitude is inverted as in fig. 6.6b and after the complete period the state reaches the maximum inverted amplitude as seen in 6.6c. Although one period is enough to reach the steady state, it is recommended to run at least 10 periods to get an stable standing wave.

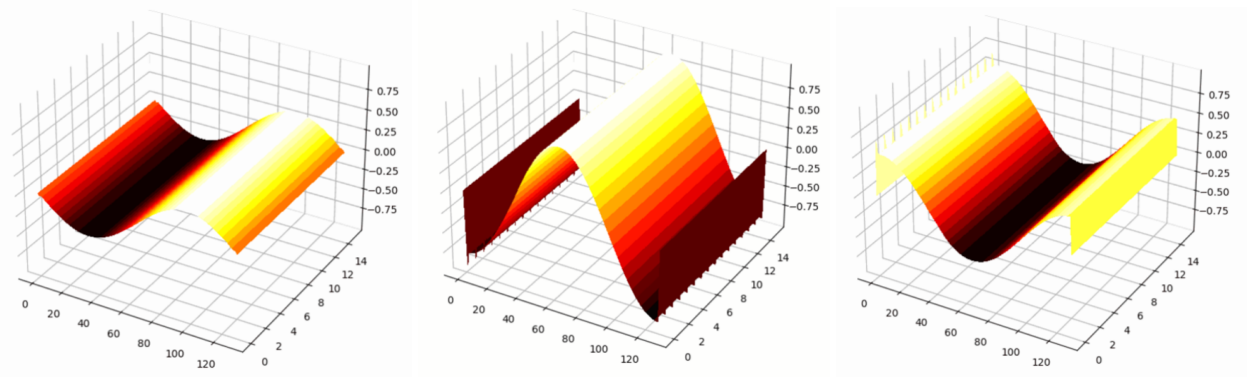

(a) **(b)** **(c)**

Fig. 6.6. Waves before colliding with the opposite wall (a) waves after reflecting back to the origin (b) Steady state reached (c).

6.4 Planar interphase between two media

After being able to produce plane waves and sources, the interaction between the sphere and the ongoing waves relies on two physical boundary conditions: The conservation of mass exchange at the interphase and the conservation of momentum exchange. As the time scale of the motion of the object and the wave's oscillations are quite different, the continuity of pressure and velocity at the interphase is enough to satisfy the first mentioned condition. For this reason, a numerical test to ensure mass conservation when waves interact with an interphase must be done. In order to simulate the boundary conditions for refraction and reflection, another simulation was performed where an plane interphase was placed at the middle of a one-dimensional box. The interphase separates two regions: One with a propagation speed c_1 and the other one of speed c_2, both speeds measured in cells per time steps. The theoretical interphase problem may be solved using the velocity potential for simplicity, thus, the relation between pressure and velocity are (3.12) and (3.13). A normal incident wave comes from the media of sound speed c_1 with an incident wave of potential ϕ_1, once the wave crosses the interphase, a reflected wave with potential ϕ_1' traveling at opposite direction and a transmitted wave of potential ϕ_2 traveling at the other side of the interphase are produced. Those may be written as follows:

$$\phi_1 = A_1 \exp(i\omega(x/c_1 - t)) \quad , \tag{6.8a}$$

$$\phi_1' = A_1' \exp(i\omega(x/c_1 - t)) \quad \text{and} \tag{6.8b}$$

$$\phi_2 = A_2 \exp(i\omega(x/c_2 - t)) \quad , \tag{6.8c}$$

where A_1 is the known amplitude of the incident wave's potential, while A_1' and A_2 are the unknown amplitudes of the reflected and transmitted wave's potentials respectively. The boundary conditions for in the interphase relies that the pressure and the normal velocity must be equal at the left and at the right due to conservation of mass [37, page. 259], thus,

$$p_1 + p_1' = p_2 \quad , \tag{6.9a}$$

$$u_{1x} + u_{1x}' = u_{2x} \quad . \tag{6.9b}$$

These equations provides the information about A_1' and A_2 by using (3.12) and (3.13) and then plugging (6.8) into (6.9) to obtain the following equations:

$$\rho_1(A_1 + A_1') = \rho_2 A_2 \quad , \tag{6.10a}$$

$$\frac{1}{c_1}(A_1 - A_1') = \frac{1}{c_2} A_2 \quad , \tag{6.10b}$$

which leads to the following solutions:

$$A_1' = A_1 \frac{\rho_2 c_2 - \rho_1 c_1}{\rho_2 c_2 + \rho_1 c_1} \quad , \tag{6.11a}$$

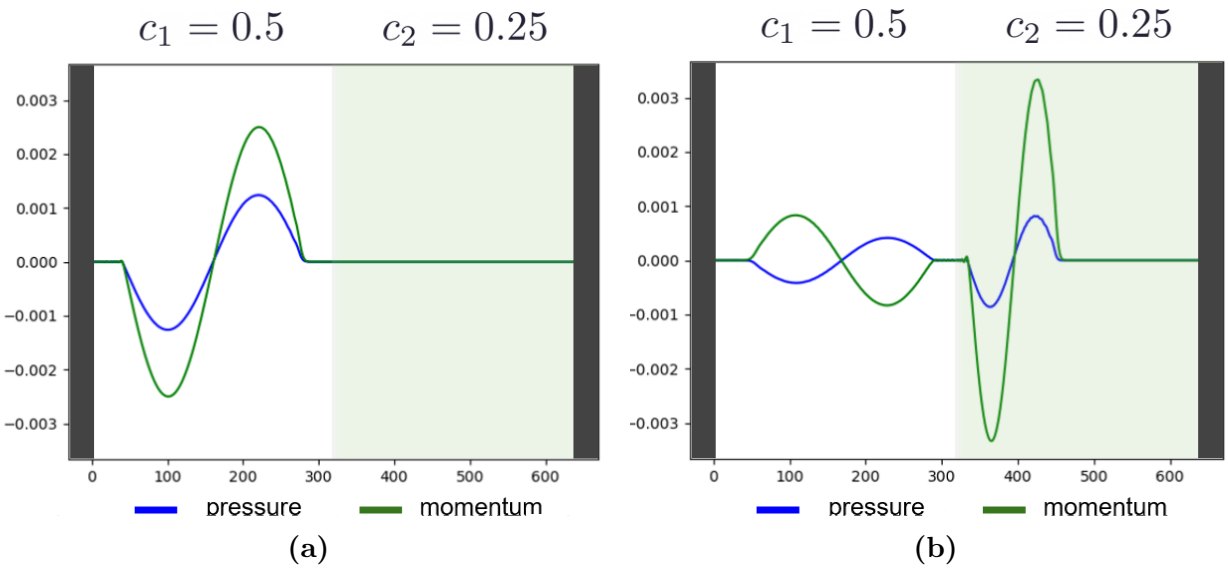

Fig. 6.7. Ongoing incident waves (a) Reflected and Transmitted waves (b).

$$A_2 = A_1 \frac{2\rho_1 c_2}{\rho_2 c_2 + \rho_1 c_1} \quad . \tag{6.11b}$$

Although the reflected and transmitted waves are fully determined with (6.11), we still need to relate theses amplitudes with the actual parameters that the simulation is able to provide in order to make a proper comparison with this analytical solution. First, it's worth keeping in mind that if the amplitude of the ongoing waves density is ρ_i then

$$A_1 = -\frac{c_1^2 \rho_i}{\omega \rho_1} \quad , \tag{6.12}$$

which will be useful to compare with the density and momentum amplitude, however two physical quantities which does not depend on the initial amplitude and are more relevant are the reflection and transmission coefficients, named R and T respectively. These coefficients are defined as the energy flux density ratio of the reflected wave in the case of reflection coefficient or the transmitted wave for transmission coefficient relative to the energy flux density of the incident wave. If the energy flux density has the form

$$E = c\rho u^2 \quad , \tag{6.13}$$

the expressions for the reflection and transmission coefficients are:

$$R = \frac{c_1 \rho_1 (u_1')^2}{c_1 \rho_1 u_1^2} = \frac{|A_1'|^2}{|A_1|^2} = \left(\frac{\rho_2 c_2 - \rho_1 c_1}{\rho_2 c_2 + \rho_1 c_1} \right)^2 \quad \text{and} \tag{6.14a}$$

$$T = \frac{c_2 \rho_2 u_2^2}{c_1 \rho_1 u_1^2} = \frac{c_1 \rho_2 |A_2|^2}{c_2 \rho_1 |A_1|^2} = \frac{4 c_1 \rho_1 c_2 \rho_2}{(\rho_2 c_2 + \rho_1 c_1)^2} \quad , \tag{6.14b}$$

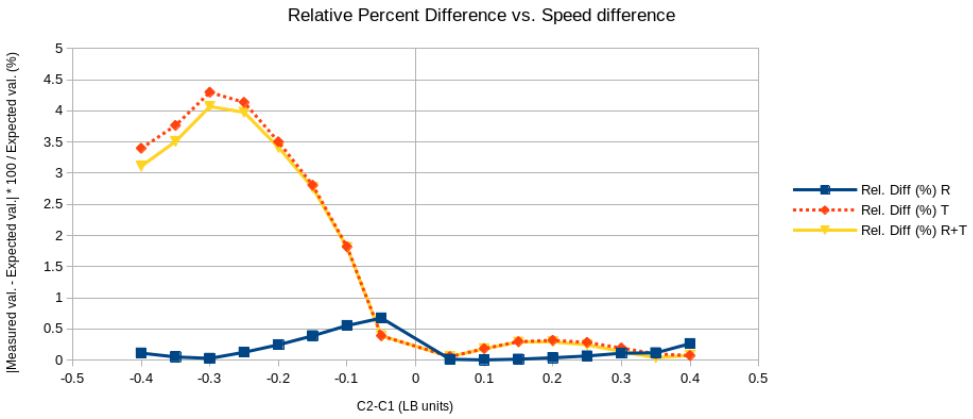

Fig. 6.8. Relative discrepancy between the expected and measured values of R and T for the difference between c_1 and c_2.

where it can be seen with no difficulty that $R + T = 1$. As the numerical method does not contain information regarding the bulk steady density of the media, it is necessary to limit this solution to the particular case where the bulk densities for both sides are the same. Meaning that R and T take the form

$$R = \left(\frac{c_2 - c_1}{c_2 + c_1} \right)^2 \tag{6.15a}$$

$$T = \frac{4c_1c_2}{(c_2 + c_1)^2} \quad , \tag{6.15b}$$

which will be the expected coefficients to be measured in the simulation by computing this quantities at the end of the simulation

$$R_{\text{msr}} = \frac{c_1(u_1')^2}{c_1u_1^2} \quad , \tag{6.16a}$$

$$T_{\text{msr}} = \frac{c_2(u_2)^2}{c_1u_1^2} \quad . \tag{6.16b}$$

A snapshot of this can be seen in figure 4.2 where two moments in time show the ongoing wave before entering the interphase and then after entering the interphase a reflected and transmitted pulse was propagated. The speed of sound c is the parameter to be different in two regions and to change it without introducing numerical instabilities the following expression for this constant is used:

$$c(x) = \frac{c_2 - c_1}{2} \tanh\left(\frac{x - L_x/2}{w} \right) + \frac{c_2 + c_1}{2} \quad , \tag{6.17}$$

where L_x is the size of the one-dimensional domain in lattice cells and w is a number of cells where the factor transitions from c_1 to c_2. For the test, $L = 2000$ cells was used. The measured coefficients calculated with (6.16) were compared with (6.15) for different values of $c_1 - c_2$, showing a difference inferior to 5% when $c_1 < c_2$ and below 1% when $c_2 < c_1$ only for transmission coefficient, according to figure 6.8. It is curious to note that the behavior of this discrepancy is not the same for the reflection coefficient

This simulation was totally necessary in order to be sure that the boundary conditions are satisfied properly. This will produce a scattered field contributing to the acoustic force in the time average. In the LB3D code there is a possibility to modify this constant from the equilibrium distribution function to be a function in space. This implementation was not easy to do and it did cost an entire month of development and assistance with the development team. Finally the results were obtained in a satisfactory way. All the computational benchmarks explained here were chosen to build a setup with the required elements to simulate the sphere immersed in standing waves and to measure its force. In the following chapter, all details regarding how to measure the second order acoustic radiation force is explained in order to reach an accurate result.

Chapter 7

Calculating the acoustic radiation force

The main objective of this present work is to simulate the interaction between an immersed object (which may be an infinite cylinder in 2D and a sphere in 3D) and an acoustic medium where waves are affected by the presence of the object and the object is affected by waves. The action made to the waves due to the presence of the object will be handled by creating a region with different sound speed representing the circular object, based on the interphase tests done and explained in section 6.4. The action made to the object due to waves will be implemented by creating a mesh covering the surface interphase of the circular object, so that an interpolation of the macroscopic fields is done at each vertex of the mesh in order to calculate the acoustic radiation force as written in (3.11). The standing waves benchmark explained in sec. 6.2 will be the starting point of this simulation where the circular object is included in the mentioned ways. The implementation will be explained for the two-dimensional and three-dimensional case, then the results and discussion will be reported.

7.1 Fluid-object interaction

Although there must be a mass exchange and a momentum exchange to simulate the interaction between the object and the fluid, the time scale of the motion of the body is so large that the displacement of the object at every oscillation will not be larger than a single lattice cell. This means that during an amount of time steps corresponding to T the object will be static and no momentum exchange is needed at all. Of course this approach sacrifices some accuracy but in change it will afford more computational cost as the forcing at each cell (following the Immersed boundary method [44]) nearby the surface of the body is not necessary. Thus, simulating the sphere as an interphase separating two regions of different sound speeds will be enough to satisfy the required scattered field because the distribution functions will try to reach a condition where the mass conservation equation is satisfied close

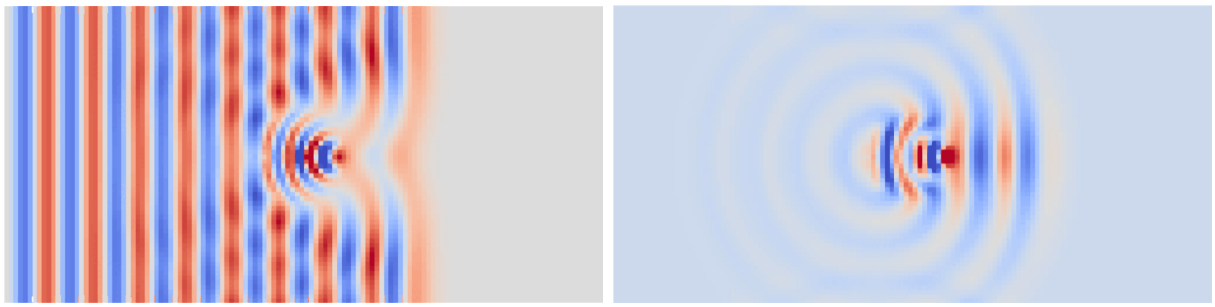

(a) **(b)**

Fig. 7.1. Visualization of the pressure field scattered by the object (a) and visualizing only the scattered contribution (b).

to the boundary, as it was proven in section 6.4, where reflected field are produced generating a perturbation over the outer fluid. The reason behind this approach is not only in the seek of simplicity, but also due to the absence of an adjustable bulk density parameter, known as ρ_0 in chapter 2, in the Lattice-Boltzmann scheme, as in the case of c. As a consequence, the proposed methodology is for now limited to cases where the bulk density is overall a hidden uniform parameter throughout the domain and the bulk density will be considered the same for both the object and the fluid, in the terms of section 3.3 $\rho_p = \rho_0$. The sound speed is therefor a function of Cartesian coordinates mapping each cell and it's built to produce a smooth change from c_0 to c_p with the help of hyperbolic tangents. For the case of a circular two-dimensional object of radius R_p whose center is located at the cell (x_0, y_0), the function

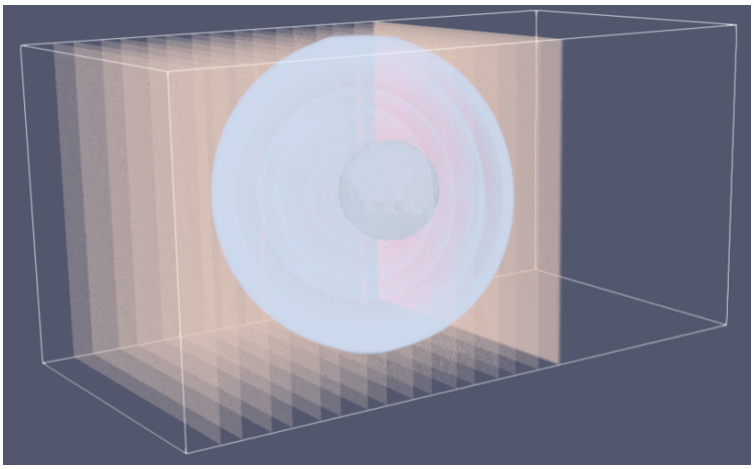

Fig. 7.2. Scattering field in the three-dimemnsional setup.

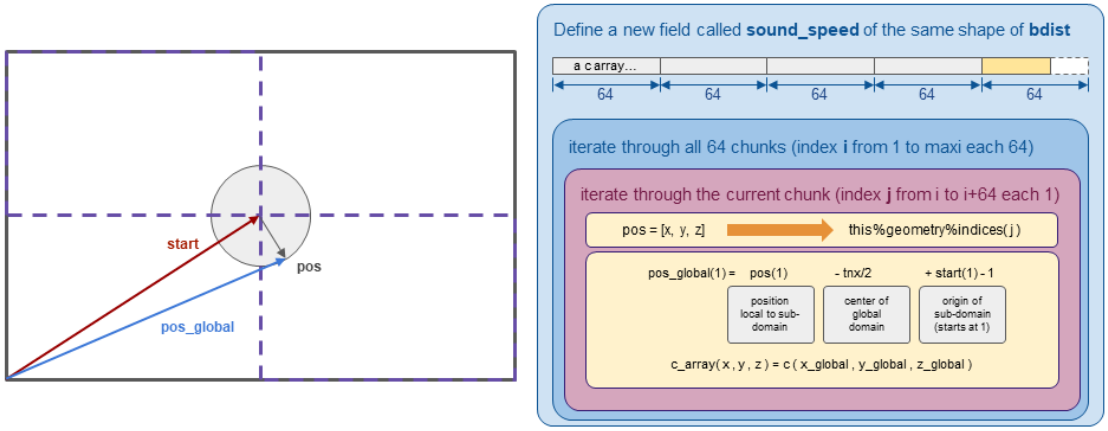

Fig. 7.3. The function is calculated with the global coordinates and is stored with the local coordinates.

of the sound speed is written as follows:

$$c(x,y) = c_0 - \frac{c_0 - c_p}{2}\left(1 - \tanh\left(\frac{(x-x_0)^2 + (y-y_0)^2 - R_p^2}{d}\right)\right) \quad , \tag{7.1}$$

and for the case of a three-dimensional sphere the function is

$$c(x,y,z) = c_0 - \frac{c_0 - c_p}{2}\left(1 - \tanh\left(\frac{(x-x_0)^2 + (y-y_0)^2 + (z-z_0)^2 - R_p^2}{d}\right)\right) \quad , \tag{7.2}$$

where d is a "square thickness" or parameter to adjust the amount of cells where the transition between c_p and c_0 occurs, measured in squared cells and its used value was of at least 4 for a thickness of two cells. This function is calculated in the equilibrium function in order to produce the scattered field as explained in sec. 6.4.

For the three-dimensional case the LB3D code was modified to include the function (7.2) into the same implementation of the equilibrium function. As explained in section 5.3 the code divides the domain into multiple sub-domains for each processor and every subroutine called at the main loop will be called simultaneously by all the sub-domains. As the object does not distinguish between the present sub-domains, the easiest way to avoid a replication of this object at the wrong position is calculating the function (7.2) at each processor in the global coordinates of the general domain but making this calculation at each processor, so that each processor will calculate the segment of the sphere that belongs to its corresponding sub-domain. The figure 7.3 illustrates how is the coordinates transformation done. The speed of sound is a changing parameter that will modify directly the equilibrium function, thus, it is worth allocating the speed of sound as an separated field, which is done just as the equilibrium distribution function is allocated: A one-dimensional array is separated into

chunks of 64 cells, where at each line the computation of (7.2) is made and then used by the `bdist8` function. As a result, the possibility to dump this field from the execution of LB3D is possible not only for visualization convenience, as shown in figure 7.2, but also for debugging purposes.

7.2 Measuring the acoustic radiation force

The equation (3.11) is a surface integral of an expression in terms if the pressure and the velocity of a fluid, but in the Lattice-Boltzmann model the macroscopic fields are the density and a momentum which correspond to $\rho = p_1/c^2$ and $\vec{J} = \rho_0 \vec{u}_1$ respectively, following the notation of section 3.3. However, the macroscopic fields only exist at a discrete cubic lattice cell of position $\vec{R}^{\mathrm{LB}} = (x_l, y_l, z_l)$, but the surface of the sphere is diffuse and it is unclear to determine which cells conform the boundary of the object and which don't, meaning that we need to define what's considered actually the boundary of the object by clothing the inner region of sound speed c_p with a mesh composed by a set of M points in continuous space and coordinates $\vec{R}_k = (x_k, y_k, z_k)$, for the k^{th} point, and calculating the actual fields over these points using an interpolation based on the work of Favier et. al in [46]. Interpolation consist on evaluating the macroscopic field at the continuous point $\vec{R}_k$ making a summation of the field at nearby cells weighted by a Kernel function. This kernel function $\delta(r)$ used to perform the interpolation is introduced as the following piece-wise function:

$$\delta(r) = \begin{cases} \frac{1}{6}\left(5 - 3|r| - \sqrt{1 - 3(1-|r|)^2}\right) & \frac{1}{2} \leq |r| \leq \frac{3}{2} \\ \frac{1}{3}\left(1 + \sqrt{1 - 3r^2}\right) & |r| \leq \frac{1}{2} \\ 0 & \text{elsewhere} \end{cases} \tag{7.3}$$

where $r = |\vec{R}_l^{\mathrm{LB}} - \vec{R}_k|$ is the distance between the continuous point k of the mesh and the discrete lattice cell, of index l, inside a set defined as all the cells contained in a cubic box of side $3\delta x$, centered at $\vec{R}_k$. The evaluation of the density ρ_{I} interpolated at $\vec{R}_k$ is then

$$\rho_{\mathrm{I}}(\vec{R}_k) = \sum_l \rho(\vec{R}_l^{\mathrm{LB}}) \delta(|\vec{R}_l^{\mathrm{LB}} - \vec{R}_k|) \quad , \tag{7.4}$$

and the interpolated momentum $\vec{J_{\mathrm{I}}}$

$$\vec{J}_{\mathrm{I}}(\vec{R}_k) = \sum_l \vec{J}(\vec{R}_k) \delta(|\vec{R}_l^{\mathrm{LB}} - \vec{R}_k|) \quad . \tag{7.5}$$

The set of M continuous points are the vertices of the mesh, which is also composed by edges and faces. In the two-dimensional case the surface is actually a line path covering the circumference of the region of speed c_p. The placement of each point may be defined in different ways, a simple example is the following: For a circle of radius R_p, the amount of

points is $M = 2\pi R_p$ in order to distribute them uniformly, such that the components of $\vec{R}_k$ are

$$x_k = x_0 + \cos(kR_p) \quad , \tag{7.6a}$$

$$y_k = y_0 + \sin(kR_p) \quad , \tag{7.6b}$$

with $k = 0, \ldots, M-1$, forming a circumference when adjacent vertices are tied by an edge. Edges between vertices are segments defined as $\vec{R}_{k+1 \mod M} - \vec{R}_{k \mod M}$, its relevant element is a perpendicular unitary vector to the segment $\hat{n}_k$ which can be computed in two dimensions as follows:

$$\vec{n}_k = \frac{(\vec{R}_{k+1 \mod M} - \vec{R}_{k \mod M}) \times \hat{k}}{|\vec{R}_{k+1 \mod M} - \vec{R}_{k \mod M}|} \tag{7.7}$$

where $\hat{k} = (0, 0, 1)$ is a unit vector pointing out of the page. The normal vector is useful to calculate the surface integral properly and obtain a number with less numerical noise due to the mesh, and naturally the accuracy will depend on M. All elements are now defined to calculate the acoustic radiation force as defined in (3.11), as a summation over all normal vectors

$$\vec{F}(t) = -\sum_{k=0}^{M-1} \left(-\frac{|\vec{J}_{\mathrm{I}}|^2(\vec{R}_{k/2})}{2\rho_0} + \frac{\rho_{\mathrm{I}}^2(\vec{R}_{k/2})c^2}{2\rho_0} \right) \hat{n}_k \Delta s + \frac{\vec{J}_{\mathrm{I}}(\vec{R}_{k/2}) \cdot \hat{n}_k}{\rho_0} \vec{J}_{\mathrm{I}}(\vec{R}_{k/2}) \Delta s \quad , \tag{7.8}$$

evaluating the fields at the middle point $\vec{R}_{k/2}$ of the form

$$\vec{R}_{k/2} = \frac{\vec{R}_{k+1 \mod M} + \vec{R}_{k \mod M}}{2} \quad . \tag{7.9}$$

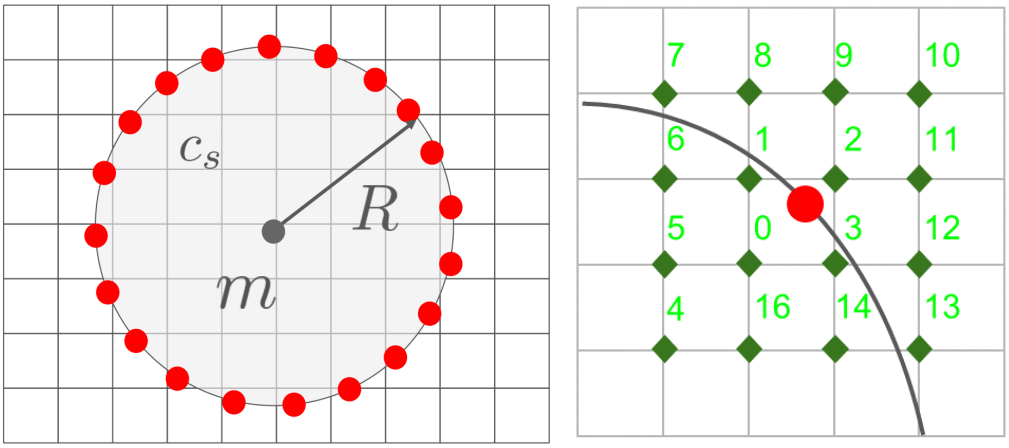

(a) **(b)**

Fig. 7.4. Mesh representation in two-dimensional circular object (a) Neighbor cells set used to calculate the interpolation(b).

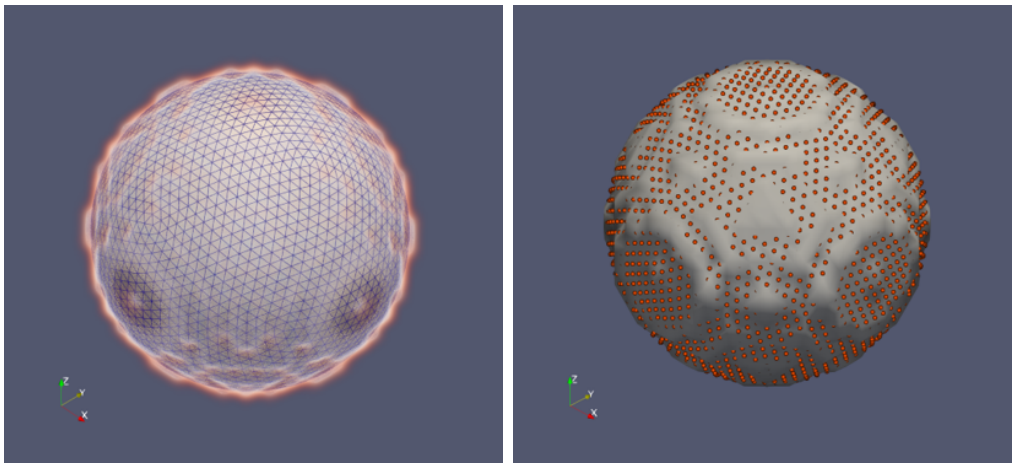

(a) **(b)**

Fig. 7.5. Diffuse interphase of object media covered by mesh (a) Vertices location of the mesh (b).

This is a discrete and numerical version of (3.11) for a two-dimensional mesh, where the length of each segment Δs is the same regardless of the end vertices and ρ_0 takes the unique role of a scale factor, meaning that the real calculated expression is $\rho_0 \vec{F}_(t)$ because there is not any chance to get information regarding the value of ρ_0. In the three-dimensional case the mesh is composed by polygon faces too defined by three vertices connected to each other by segments, thus, the implementation may be hard to accomplish from scratch. Fortunately, LB3D includes a set of modules where the Immersed Boundary method (IBM) is implemented for three-dimensional closed membranes and the interpolation part of this procedure has been used modifying the code to avoid the forcement done towards the fluid (as this is a matter of IBM).

The implementation to create the spherical mesh and compute normal vectors, surface integration, as well as interpolating momentum, was already done inside the LB3D code without any modification, all that was needed to complete was the interpolation of the density and a way to compute (7.8). The feature `offlattice_objects` includes elements like mesh implementation, Lagrangian markers as IBM components, interpolation kernels and more. Each of this modules was written in a class script with the definition of its members, subroutines and functions and a set script with the actual implementation. The module `lagrangian_object` performs the interpolation over the vertices of the mesh, and the interpolation of the pressure was included as a required field in (7.8). The sub-module `force` was a series of different implementation for many kind of forces that were not convered in this project, but some functions were useful to read in order to create the function to compute the acoustic radiation force. All the parameters needed were the three vertices comforming the polygon and its normal vector. As indicated in figure 7.6a these variables are already

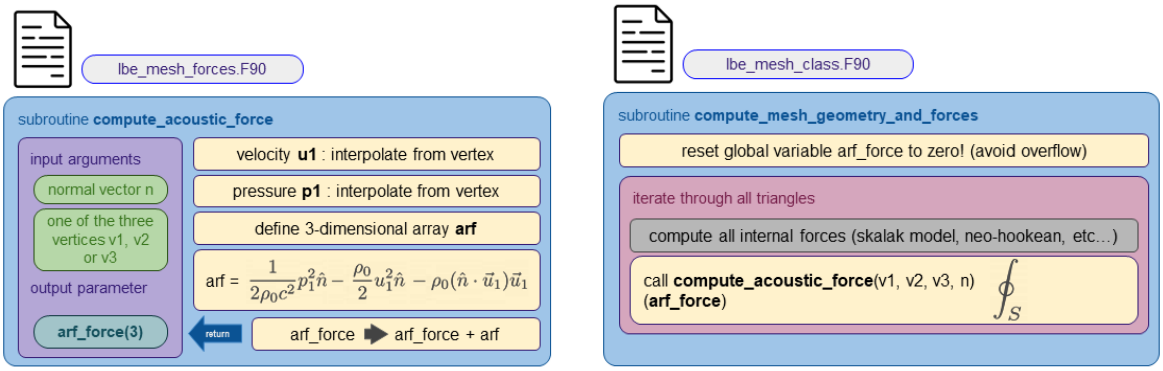

(a) **(b)**

Fig. 7.6. Structure of subroutine to calculate the force at one mesh polygon (a) Structure of a subroutine that adds all the contributions computed with the previous subroutine (b).

computed into the mesh module. Then, the integrand of (3.11) was calculated by extracting the information of p and u at each vertex. To combine these three values, an average was made. This is a rough approximation that would lead into problems, but at this point it was the only available solution. In figure 7.6b a subroutine is explained where the summation of all contributions is made for each polygon, based on other subroutines found from the same code. After working with the HI-ERN development team, the implementation was tested to perform the three-dimensional case and compare with (3.65).

7.3 General setup of the simulation

The domain of the simulation will be as similar as in the tests about standing waves of wavelength λ and period T including the immersed spherical or circular object as seen in fig. 7.7. A rectangular box of $L = \lambda/2$ cells of width and N cells of length and height, depending on the dimension. This means that there will be bounce-back boundary conditions at $x = 0$ and $x = L$ and a wall source at $x = 1$ just as same as the standing waves test of section 6.2, and additionally the immersed object will be placed at any position x along the x-axis so that, by default, its position will be exactly at the pressure node of the standing wave $x = \lambda/4$. The boundary condition along the laterals will be periodic in order to produce a single-directed incident plane wave during the entire simulation. In the first T steps the plane wave will travel to reach the opposite reflective wall and then return, so no standing wave is occurring yet until a static ode is produced at the middle of the domain. Despite this time is in principle enough to reach a steady state, at least 10 oscillations (or $10T$ time steps) will occur before measuring the acoustic radiation force as a way to ensure that the steady state has been reached. After these oscillations, the system will be evolving only

perturbed by the scattered field produced by the presence of the object and the acoustic radiation force starts to be measured at every time step. This will provide a function $F(t)$ of the temporal behavior of this force, where a time average can be gathered processing the output data or simultaneously adding all the force's values of the last period and dividing by T, however a more optimized way to measure this is by only adding the peak and valley values of $F(t)$ and taking the half at the exact moment where one oscillation is completed, because the contribution of this force to the motion of the object will only be relevant from period to period and not each time step.

7.4 Discussion of the results

From the measurements of the time average of the acoustic radiation force, computed with (7.8), it is now possible to contrast the resulting expression with the Gor'kov for the case of the sphere and the Wei solutions for the circular disk, both expressions previously deducted in chapter 3. Because along the entire numerical methodology there is no distinction between the static density of the fluid and the static density of the object, being both ρ_0, the comparison with the theoretical expressions (3.65) and (3.101) is only valid for the particular case where the static densities are the same, that is $\rho_p = \rho_0$, meaning that the mentioned equations become

$$\langle F_x \rangle_{3\mathrm{D}} = -\frac{\pi R_p^3 p_0^2 k}{3\rho_0} \Psi(c_0, c_p) \sin 2kx \quad , \quad \langle F_x \rangle_{2\mathrm{D}} = -\frac{\pi R_p^2 p_0^2 k}{4\rho_0} \Psi(c_0, c_p) \sin 2kx \tag{7.10}$$

where the following extra factor $\Psi(c_0, c_p)$ is introduced as the contrast factor that the numerical approach will be able to reproduce for now, defined as

$$\Psi(c_0, c_p) = \frac{1}{c_0^2} - \frac{1}{c_p^2} \quad , \tag{7.11}$$

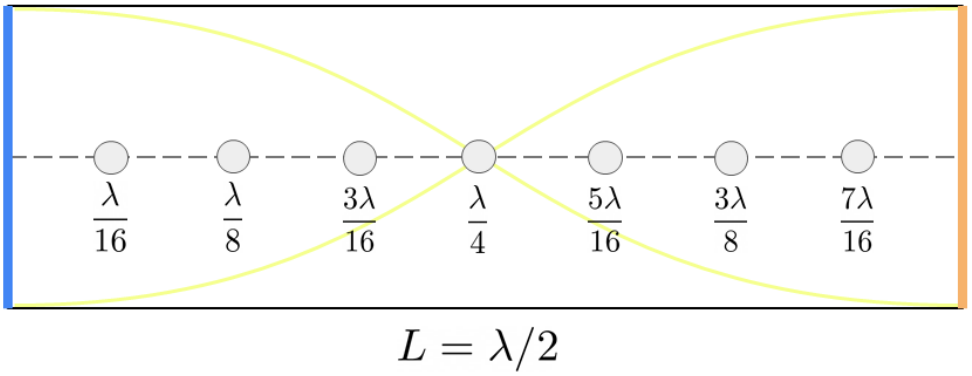

Fig. 7.7. The position of the object will only vary along the x-axis.

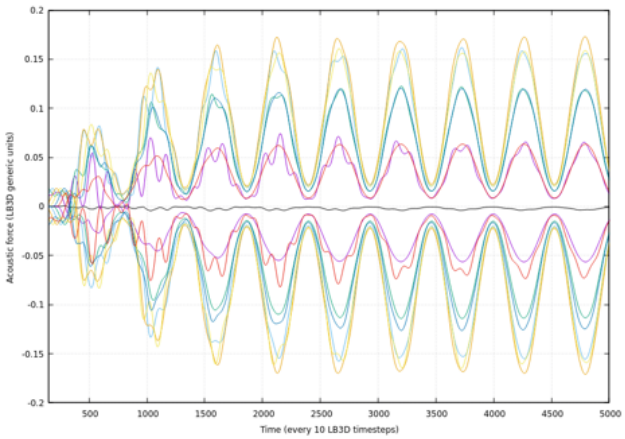

Fig. 7.8. Different Force vs. time curves for different positions of the object along the x-axis.

and it's defined in seek of comparison as the only factor dependent on the sound speeds of both materials. This factor also tells if the particle will move towards a node or towards an anti-node depending on which speed is greater than the other, for example, if $c_p > c_0$ the particle will try to reach the node of the standing wave, as both expressions shares the factor $\sin 2kx$, the only factor which depends on the position of the particle and indicating that the force must be null at $x = \lambda/4$ and its magnitude will be maximum at $x = \lambda/8$ and $x = 3\lambda/8$. Reproducing this facts is crucial to evaluate the results of the simulation and its agreement with the theory, where the position of the object along the x-axis is changed as seen in figure 7.7 and the acoustic radiation force is measured giving a series of graphs as seen in figure 7.8, while the rest of the relevant parameters are kept constant. Then, the speed of sound of the fluid will change while the other one will be fixed (and viceversa) in order to change Ψ linearly. The remaining variables of (7.10) to be changed are the pressure amplitude p_0 of the acoustic waves, the wave number k which will be changed by adjusting the wavelength and the radius of the object R_p, ensuring that the condition $R_p \ll \lambda$ must be satisfied.

Parameter	**Value**
c_p	0.25
c_0	0.24
p_0	1.00
λ	500
R_p	10

Chart 7.1. Default fixed values for the relevant quantities of the acoustic radiation force.

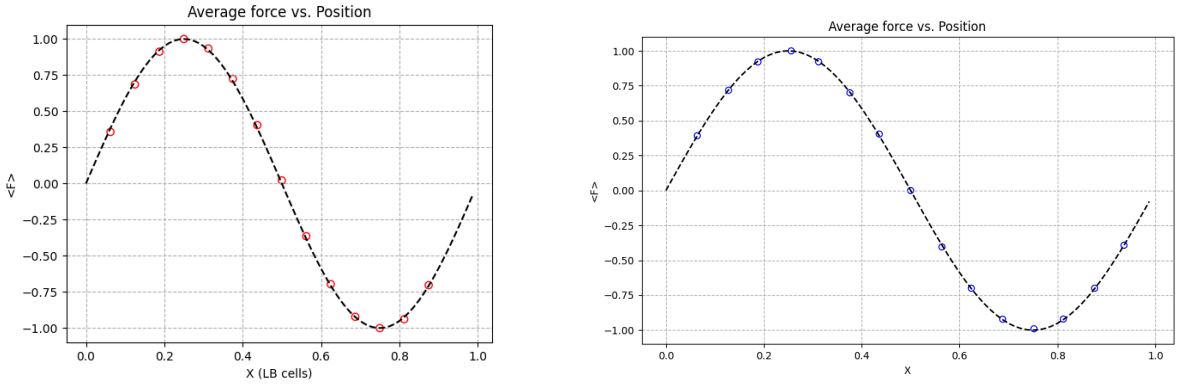

(a) **(b)**

Fig. 7.9. Measurements of the acoustic radiation force (registered by the dots) and the theoretical behavior $\sin 2kx$ as the dashed black curve for the three-dimensional case (a) and the two-dimensional case (b).

A set of default values for the mentioned parameters were chosen so that the time average of the measured acoustic radiation force gives a number close to the unity at the maximum positional amplitude $x = \lambda/8$. These values can be appreciated in the table 7.1. In the figure 7.9 is shown how the force is dependent of position, such that in the pressure node this force will be zero and the object will be confined in the node, thus, the effect of acoustic levitation was simulated successfully. This results shows that it have been possible to reproduce a simulation with the acoustic radiation force in a general way, where an acoustic field is able to affect this object in the time average.

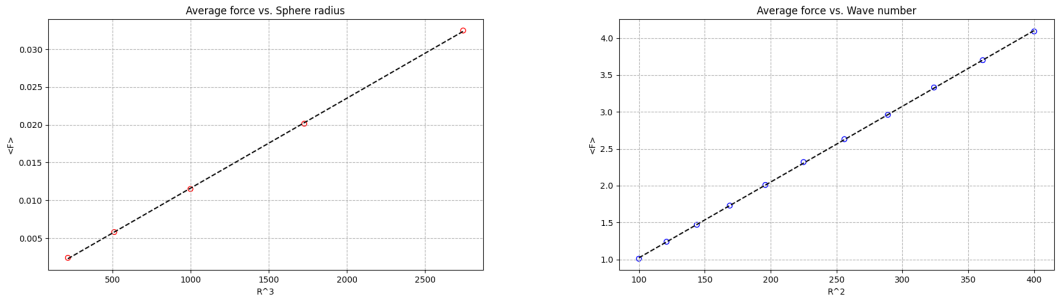

(a) **(b)**

Fig. 7.10. Measurements of the acoustic radiation force (registered by the dots) for values of the radius, fitted with a powers law.

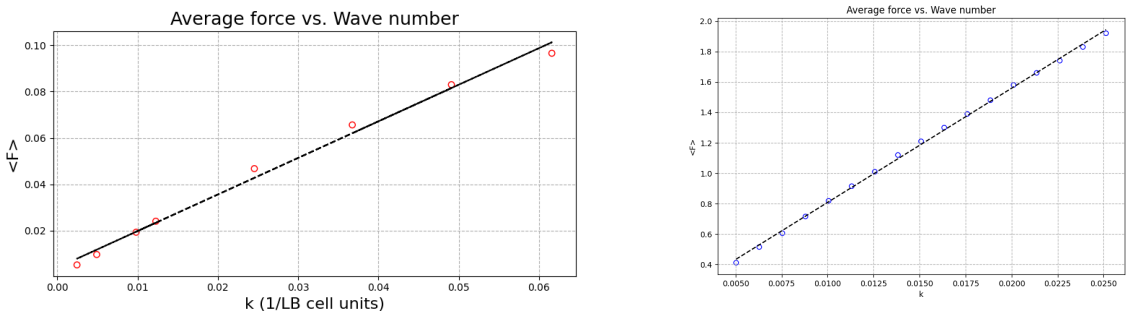

(a) **(b)**

Fig. 7.11. Measurements of the acoustic radiation force (registered by the dots) for values of the wave number fitted with a simple linear relationship.

The force is related to the size of the particle, being linear to either the volume in the case of the sphere or the area in the case of the cylinder. Here we studied the radius as a common parameter and related through a power law, expecting to see a cubic relation with the force of the sphere and a quadratic relation with the force on the cylinder. The measurements varying the radius are shown in the figure 7.10 and the power law is verified by fitting the data with a linear relationship in the logarithmic scale, such that the slope will correspond to the exponent of the power law. The expected values are 2 for the two-dimensional case and 3 for the three-dimensional case, as clearly seen in (7.10), obtaining a discrepancy of 0.47% for the disk and 2.71% for the sphere. A higher result from the sphere is expected due to the amount of measurements. Something to remark is that the approximation $R_p \ll \lambda$

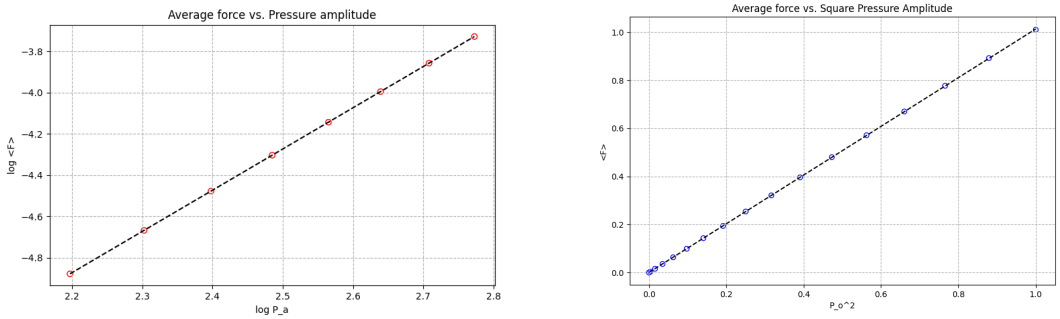

(a) **(b)**

Fig. 7.12. Measurements of the acoustic radiation force (registered by the dots) for values of the pressure amplitude p_0 of acoustic standing waves, fitted with a simple linear relationship.

must be present to make a proper comparison with the theory, then all the measurements were taken for radius that never overcome one tenth of the wavelength.

The acoustic radiation force must expected to be also dependent of the wavelength because the waves are the actors of the production of this force, as explained along the entire theoretical part of this document. The simplest comparison is though made with the wave number which is a single factor of $\langle F_x \rangle$, implying that one linear fit to the measurements of this force for different values of k is more than enough. As seen in figure 7.11 the fit was successful for both cases giving a Pearson correlation coefficient of $R^2 = 0.9987$ for the disk and $R^2 = 0.9923$ for the sphere. Another clear dependent parameter is the amplitude of the standing waves, which must be quadratic in both cases because $\langle F_x \rangle$ was calculated with the squared values of the macroscopic quantities. As expected, in figure 7.12 the pressure follows a power law with exponents 2, resenting discrepancies of $10^{-8}\%$ in both cases.

One important test is the relationship with the contrast factor defined in (7.11). It is important to note that the whole factor is linear with the force for a position different from the node. This implies that measuring the time average of the acoustic radiation force at $x = \lambda/8$ will result in a linear relationship which crosses the origin, as the force would be non-existent if $c_p = c_0$. For this test the speed of sound of the fluid was set to $c_0 = 0.25$ and c_p was adjusted to values that let the factor Ψ to scale linearly. According to the result registered in the figure 7.13 the behavior is the expected at least for the two-dimensional case, made by a well-known generic implementation in C++, appreciating in the figure 7.13a how the linear fit is successful and the force gives zero for $\Psi = 0$. However it is not possible to say the same for the three-dimensional case, as the behavior tends to get apart from the linear trend and there is no match with the origin, but the force is minimum when $\Psi = 0$ and the behavior is proportional, meaning that the force will go to the node if $\Psi > 0$ and

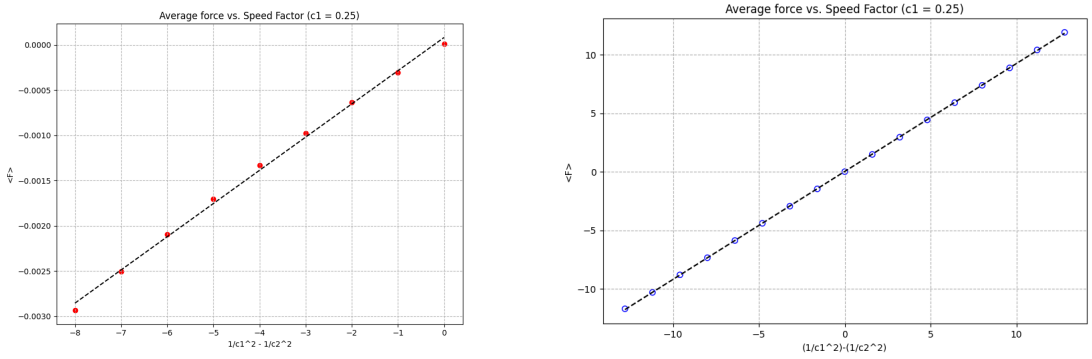

(a) **(b)**

Fig. 7.13. Measurements of the acoustic radiation force (registered by the dots) versus the contrast factor Ψ and a fitted line according to (7.10).

to the anti-node in the opposite case. The reason behind this unexpected result has to do with the implementation in the LB3D code, because this implementation is still not solid enough and leave questions even to the developers of the team. One hypothesis behind this issue relies on the interpolation over the pressure as imitation of the interpolation of the momentum.

7.5 Including motion to the object

The main objective of the present work, which is calculating the acoustic radiation force of a sphere and a disk, is already accomplished, and with this result, the possibility to implement the motion on the object is possible. The motion was included in the C++ code with the Omelyan integrator [47]. This integration method solves the Newton's laws by updating the position $\vec{r}(t)$ and velocity $\vec{v}(t)$ of the particle with the following procedure:

$$\begin{aligned}
\vec{r}_1 &= \vec{r}(t) + \zeta h\vec{u}(t) \quad , \\
\vec{v}_1 &= \vec{v}(t) + (1-2\lambda)\frac{h\vec{F}(\vec{r}_1)}{2m} \quad , \\
\vec{r}_2 &= \vec{r}_1 + \xi h\vec{v}_1 \quad , \\
\vec{v}_2 &= \vec{v}_1 + \lambda\frac{h\vec{F}(\vec{r}_2)}{m} \quad , \\
\vec{r}_3 &= \vec{r}_2 + (1-2(\xi+\zeta))h\vec{v}_2 \quad , \\
\vec{v}_3 &= \vec{v}_2 + \lambda\frac{h\vec{F}(\vec{r}_3)}{m} \quad , \\
\vec{r}_4 &= \vec{r}_3 + \xi h\vec{v}_3 \quad , \\
\vec{v}(t+h) &= \vec{v}_3 + (1-2\lambda)\frac{h\vec{F}(\vec{r}_4)}{2m} \quad , \\
\vec{r}(t+h) &= \vec{r}_4 + \zeta h\vec{u}(t+h) \quad ,
\end{aligned} \tag{7.12}$$

where h is the size of the time step, which is independent from the time step of the Lattice-Boltzmann solver. The auxiliary vectors $\vec{r}_1$, $\vec{r}_2$, $\vec{r}_3$, $\vec{r}_4$, $\vec{v}_1$, $\vec{v}_2$, $\vec{v}_3$ and $\vec{v}_4$ take the role of storing temporal values during the integration, and the constants ζ, ξ and λ are set to the following values:

$$\begin{aligned}
\zeta &= 0.1786178958448091 \quad , \\
\xi &= 0.2123418310626054 \quad , \\
\lambda &= 0.06626458266981849 \quad .
\end{aligned} \tag{7.13}$$

The total force $\vec{F}(t)$ includes the acoustic radiation force $\langle\vec{F}_x\rangle$ of (7.10) and a drag additional force, being proportional and opposite to the object's velocity. This force has the form

$$\vec{F}^{\text{drag}} = -6\pi\eta R_p\vec{v} \quad , \tag{7.14}$$

thus, the total force of the particle is

$$\vec{F}(t) = \langle \vec{F}_x \rangle + \vec{F}^{\text{drag}} \quad . \tag{7.15}$$

As we have already emphasized, as soon as the time scale of the motion of the sphere is so large respect to the time scale of the acoustic oscillations in the fluid, during one period of these oscillations the object will produce a displacement smaller than one single cell of the lattice, meaning that the position of the disk will not be updated at each step time of the Lattice-Boltzmann solver, but every oscillation of the acoustic waves, taking T time steps. This avoids the necessity to implement an additional coupling method as Immersed boundary method to ensure momentum conservation, as the system will try to relax to its steady state when the position of the disk is updated, also, because of the differences in the time scale we are measuring the time average of the acoustic radiation force which is actually affecting the object every oscillation. In the figure 7.14 we can see some frames of the recorded disk under the influence of the standing waves, where after some amounts of time steps the disk is attracted to the node.

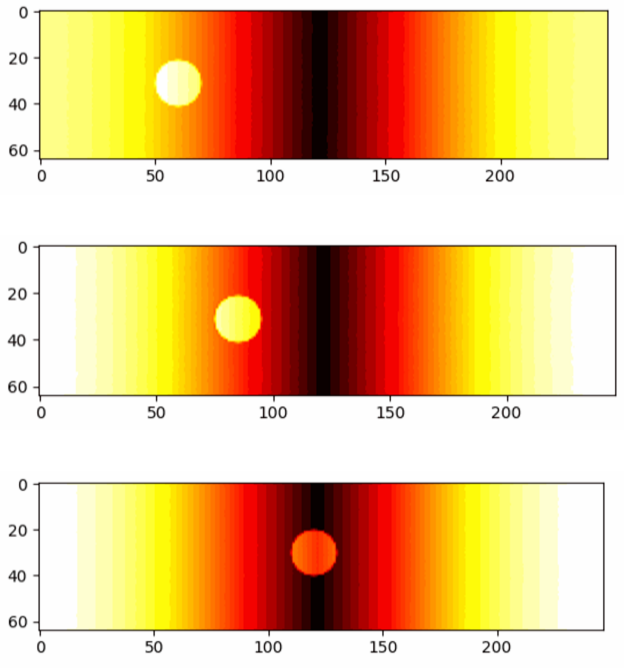

Fig. 7.14. Frames of the motion of the disk approaching towards the node.

Conclusions

This work introduces a numerical methodology to compute the acoustic radiation force produced by standing waves on a compressible object immersed in an inviscid fluid. The proposal combines a Lattice Boltzmann model (LBM) that simulates the wave equation together with a kernel interpolation scheme to compute the first order perturbations p_1 and $\vec{u}_1$ of the pressure and velocity fields just on each surface element $d\vec{S}$ on a discretized version of the object's boundary. Next, it replaces those first order fields into the general expression for the acoustic radiation force on $d\vec{S}$, averaging on a oscillation period,

$$d\langle F_i \rangle = -\left\langle \left(-\rho_0 \frac{u_1^2}{2} + \frac{p_1^2}{2\rho_0 c_0^2} \right) \delta_{ij} + \rho_0 v_i v_j \right\rangle dS_j \quad . \tag{7.16}$$

The total force on the immersed object is obtained by adding the forces on all discrete surface elements on the boundary. This total force can be later used to integrate the immersed object's motion via a molecular dynamics scheme.

By simulating the wave equation to compute p_1 and $\vec{u}_1$ and replacing into (7.16) to compute the forces, the method avoids to simulate the more complex Euler and mass conservation equations. Moreover, many numerical methods to simulate those fluid mechanics equations compute with second-order accuracy the zero order density and velocity fields, and with only first-order accuracy the perturbative fields p_1 and $\vec{u}_1$. In contrast, the LBM for waves we used here computes p_1 and $\vec{u}_1$ with second-order accuracy; therefore, one can use lattices with a relative small number of cells to compute with good accuracy the acoustic radiation force in both 2D and 3D.

The proposed numerical methodology was tested by computing the acoustic radiation force on a disk (in 2D) and on a sphere (in 3D). The 2D simulation was implemented with a self-developed C++ code, and the 3D one, with the LB3D software (a very powerful LBM code developed by J. Harting and collaborators in the HI-ERN, Erlangen, Germany). Because LB3D was originally developed to simulate fluids, it was necessary to extend first LB3D to simulate waves. To perform this task we needed to understand the code architecture and to identify the subroutines to be added or modified to simulate waves. This task was completed with the support of the LB3D developers during a four months research stay at HI-ERN. The 3D simulations were also implemented and performed during that research stay. The implementation was tested by running some benchmarks, like the free propagation of a Gaussian pulse, the waves generated by a point source and the generation of standing

waves inside a box. The last one was also used as starting point for the simulation of the acoustic waves around the sphere.

The simulation results were compared with the theoretical expressions for the sphere and the disks developed by Gor'kov [11] and Wei et. al [13]. Reproducing and understanding those analytical results was a challenging task that took around six months, because many of the original articles and reviews on the subject does not include detailed deductions. Fruit of this work we include here detailed deductions of those results that are presented in the main text and in the appendices that can be useful for the interested reader. The numerical results matches with excellent accuracy the theoretical predictions by Gor'kov and Wei et. al. in all simulated cases. Those cases include to vary parameters like the axial position of the object, its size, the wavelength and the amplitude of the standing waves, and the speed of sound of both the object and the fluid. Finally, the LBM simulation scheme in 2D and the calculus of the acoustic radiation force was coupled to a PEFRL [47] molecular dynamics algorithm to integrate the motion of a stiff disk towards the node of the standing acoustic wave. This movement is the operating principle of the acoustic tweezers, and being able to reproduce this phenomenon illustrates the possibilities of the proposed numerical scheme.

As it was mentioned in the introduction, one recent application of the acoustic radiation force is to form a virtual wall for the rolling of self-assembled magnetic microswimmers. In was shown that the displacement of that microswimmers is the consequence of an oscillation in the distance between the mass and magnetic centers in the object, but the source of that oscillation remains unknown. The numerical scheme developed in the present work may be useful to explore and explain the phenomenon.

The Lattice Boltzmann model for waves we used in the present work has only one parameter for each media: the speed of sound, whereas the theory of acoustic radiation force has two: the density and the bulk modulus. The simulations performed here assume that the immersed object has the same density as the fluid, and that the bulk modulus are different. From conversations with M. Mendoza at Zurich, it seems to be possible to develop a LBM for waves with two parameters, and to use it to compute the acoustic radiation force with the same procedure we developed. This may be an interest subject for future work.

The numerical methodology developed in this work is suitable to compute the acoustic radiation force on any immersed object, as far as it moves much slower than the oscillations. That difference of time scales is present in most today's applications, including the use of acoustic tweezers to manipulate objects [7] or to build virtual walls for the rolling motion of self-assembled microswimmers [21]. The method could be used to compute the acoustic radiation force on particles with complex shapes, and the interactions among immersed objects via the acoustic field. Those future applications are beyond the theoretical solutions by Gor'kov and Wei, and can further extend the use of acoustic waves in medicine and engineering.

This work achieves for the first time the computation of the acoustic radiation force on an object immersed in an inviscid fluid by solving the wave equation around the object with a Lattice-Boltzmann method. The procedure obtain accurate results at moderate computational costs. The proposed procedure shows to be a promising tool for the study of the

many phenomena where the acoustic radiation force plays a relevant role, with applications in medicine and engineering.

Bibliography

(1) Andrade, M. A. B.; Pérez, N.; Adamowski, J. C. *Brazilian Journal of Physics* **2018**, *48*, 190–213.

(2) Mohanty, S.; Khalil, I. S. M.; Sarthak Misra1, 2. *The royal society* **2020**, *476*, DOI: 10.1098/rspa.2020.0621.

(3) Ahmed, D.; Sukhov, A.; Hauri, D.; Rodrigue, D.; Maranta, G.; Harting, J.; Nelson, B. J. *Nat Mach Intell* **2021**, *3*, 116–124.

(4) Shi, J.; Ahmed, D.; Mao, X.; Lin, S.-C. S.; Lawit, A.; Huang, T. J. *Lab Chip* **2009**, *9*, 2890–2895.

(5) Marzo, A.; Seah, S. A.; et. al., B. W. D. *NATURE COMMUNICATIONS* **2015**, *6*, DOI: 10.1038/ncomms9661.

(6) Ozcelik, A.; Rufo, J.; et. al., F. G. *Nature Methods* **2018**, *15*, 1021–1028.

(7) Ghanem, M. A.; Maxwell, A. D.; Wang, Y.-N.; Cunitz, B. W.; Khokhlova, V. A.; Sapozhnikov, O. A.; Bailey, M. R. *Proceedings of the National Academy of Sciences* **2020**, *117*, 16848–16855.

(8) Ashkin, A. *Phys. Rev. Lett.* **1970**, *24*, 156–159.

(9) King, L. V. *Proc. R. Soc. Lond. A* **1934**, *147*, 212–240.

(10) King, L. V. *Proc. R. Soc. Lond. A* **1935**, *153*, 1–16.

(11) Gor'kov, L. P. *SOVIET PHYSICS- DOKLADY* **1962**, *6*, 773–776.

(12) Wu, J.; Du, G. *J. Acoust. Soc. Am.* **1990**, *87*, 997–1003.

(13) Wei Wei, D. B. T.; Marston, P. L. *The Journal of the Acoustical Society of America* **2004**, *116*, 201–208.

(14) Bruus, H., *Theoretical microfuidics*, 3rd ed.; Lecture notes from Department of Micro and Nanotechnology, Technical University of Denmark: 2006; Vol. 6.

(15) Bruus, H. *Lab Chip* **2011**, *11*, 3742–3751.

(16) Bruus, H. *Lab Chip* **2012**, *12*, 20–28.

(17) Bruus, H. *Lab Chip* **2012**, *12*, 1014–1021.

(18) Medina-Sánchez, M.; Schmidt, O. G. *Nature* **2017**, *545*, 406–408.

(19) Purcell, E. M. *Am. J. Phys* **1977**, *45*, DOI: 10.1119/1.10903.

(20) Lauga, E. *The Royal Society of Chemistry* **2011**, *7*, 3060–3065.

(21) Zhang, Z.; Sukhov, A.; Harting, J.; Malgaretti, P.; Ahmed, D. *nature communications* **2022**, *13*, DOI: 10.1038/s41467-022-35078-8.

(22) Prasianakis, N. I.; Karlin, I. V. *Phys. Rev. E* **2008**, *78*, 016704.

(23) Wei, S.; Scott, L.; Haihu, L.; Lei, W. *Phys. Rev. E* **2017**, *96*, 023309.

(24) X., S.; G., D. *Journal of Statistical Physics* **1995**, *81*, 379–393.

(25) H., L.; Q., K.; et al, L. C. *Computational Geosciences* **2016**, *20*, 777–805.

(26) Chai, Z.; Shi, B.; Guo, Z.; Rong, F. *Journal of Non-Newtonian Fluid Mechanics* **2011**, *166*, 332–342.

(27) Karlin, I. V.; Ansumali, S.; Angelis, E. D.; Öttinger, H. C.; Succi, S. **2003**.

(28) Frapolli, N.; Chikatamarla, S. S.; Karlin, I. V. *Phys. Rev. E* **2015**, *92*, 061301.

(29) Mendoza, M.; Muñoz, J. D. *PRE* **2010**, *82*, 056708.

(30) Et al., M. M. *Journal of Physics: Conference Series* **2015**, *640*, DOI: 10.1088/1742-6596/640/1/012018.

(31) Ilseven, E.; Mendoza, M. *Physical Review E* **2016**, *93*, DOI: 10.1103/physreve.93.023303.

(32) J.A. Cosgrove, e. *Ultrasonics* **2004**, *43*, 21–25.

(33) B. Chopard, P. L.; Wagen, J. *IEE Proceedings - Microwaves, Antennas and Propagation* **1997**, *144*, 251–255.

(34) Velasco, A.; Muñoz, J.; Mendoza, M. *Journal of Computational Physics* **2019**, *376*, 76–97.

(35) Dynamics of Complex Fluids and Interfaces, https://www.hi-ern.de/en/research/dynamics-of-complex-fluids-and-interfaces-1, Accessed: 2024-26-01.

(36) Mühlenstädt, T.; Kuhnt, S. *Computational Statistics and Data Analysis* **2011**, *55*, 2962–2974.

(37) Landau, L. D.; Lifshitz, E. M., *FLUID MECHANICS*, 2nd ed.; Pergamon Press: Great Britain: England, 1987; Vol. 6.

(38) Krüger, T. e. a., *The Lattice Boltzmann Method: Principles and Practice*; Springer: Switzerland, 2017.

(39) Manneberg, O. Multidimensional ultrasonic standing wave manipulation in microfluidic chips, Doctoral dissertation, KTH, Universidad Nacional de Colombia, 2018.

(40) Pijush K. Kundu, I. M. C., *Fluid Mechanics, Second edition*, 2nd ed.; Academic Press, an Imprint of Elsevier Science: 1990; Vol. 1.

(41) Elmore, W. C.; Heald, M. A., *Physics of waves*, 1st ed.; McGraw-Hill, Inc: New York: United States of America, 1969.

(42) Jackson, J. D., *Classical Electrodynamics Third edition*, 3rd ed.; John Wiley & Sons, Inc.: 1999; Vol. 1.

(43) Chopard B., D. M., *Cellular Automata Modeling of Physical Systems*, 1st ed.; Cambridge University Press: 1998; Vol. 1.

(44) Peskin, C. S. *Acta Numerica* **2002**, 479–517.

(45) Ladd, A. J. C. *Journal of Fluid Mechanics* **1994**, *271*, 285–309.

(46) Favier, J.; Revell, A.; Pinelli, A. *Journal of Computational Physics* **2014**, *261*, 145–161.

(47) Omelyan, I.; Mryglod, I.; Folk, R. *Computer Physics Communications* **2002**, *146*, 188–202.

Appendix A

Appendix I: The second order contribution of the incident wave to the acoustic radiation force

Let us verify that for an incident plane wave.

$$\phi_{\text{in}} = \phi_0 \cos\Big(\vec{k}\cdot\vec{r} - \omega t\Big) \quad , \tag{A.1}$$

with ϕ_0 a constant amplitude, the time-averaged second order contribution to the acoustic force

$$\langle F_i \rangle = -\oint \left\langle \left(-\frac{\rho_0}{2}|\nabla\phi|^2 + \frac{\rho_0}{2c_0^2}\left[\frac{\partial\phi}{\partial t}\right]^2 \right)\delta_{ij} + \rho_0 \partial_i\phi\partial_j\phi \right\rangle dS_j \quad , \tag{A.2}$$

is zero.

Starting from (A.1),

$$\nabla\phi_{\text{in}} = -\vec{k}\phi_0 \sin\Big(\vec{k}\cdot\vec{r} - \omega t\Big) \quad , \tag{A.3a}$$

$$\frac{\partial\phi_{\text{in}}}{\partial t} = \omega\phi_0 \sin\Big(\vec{k}\cdot\vec{r} - \omega t\Big) \quad , \tag{A.3b}$$

Now, by plugging them into **??** and writing $dS_i = \hat{n}_i dS$, we get

$$\begin{aligned}\langle F_{i,\text{IN}} \rangle &= -\oint \left\langle \left(-\frac{\rho_0}{2}|-i\vec{k}\phi_{\text{in}}|^2 + \frac{\rho_0}{2c_0^2}(-i\omega\phi_{\text{in}})^2 \right)\hat{n}_j + \rho_0(-ik_i\phi_{\text{in}})(-ik_j\phi_{\text{in}})\hat{n}_i \right\rangle dS \\ &= -\oint \left(\frac{\rho_0 k^2}{2} - \frac{\rho_0\omega^2}{2c_0^2} \right)\phi_0^2\langle\sin^2(\vec{k}\cdot\vec{r} - \omega t)\rangle\hat{n}_j - \rho_0 k_i k_j \hat{n}_i \phi_0^2 \langle\cos^2(\vec{k}\cdot\vec{r} - \omega t)\rangle dS\end{aligned} \tag{A.4}$$

Because $\vec{k}$ is uniform on the whole space, with $k = \omega/c_0$, and the time averages $\langle cos^2(\omega t - \beta)\rangle = \langle sin^2(\omega t - \beta)\rangle = \frac{1}{2}$, Eq. (A.4) becomes

$$-\oint \left(\frac{\rho_0 k^2}{2} - \frac{\rho_0 k^2}{2} \right)\frac{\phi_0^2}{2}\hat{n}_j dS - \rho_0 k_i k_j \frac{\phi_0^2}{2}\oint \hat{n}_i dS = 0 \quad , \tag{A.5}$$

where we have used the fact that $\hat{n}$ integrated on the spherical surface is zero.

Appendix B

Appendix II: Detailed computation of the scalar field $a(t)$ for a sphere

Let us assume that the sphere is elastic, shrinking or expanding isotropically just by simply enlarging or decreasing its radius R_p. Now, let us consider a mathematical spherical region Ω of radius R_Ω concentric to the sphere with $\lambda \gg R_\Omega > R_p$. When the sphere expands, the mass flux leaving Ω through its surface $\partial\omega$ is, at first order,

$$\dot{m} = \oint_{\partial\Omega} (\rho_0 \vec{u}_1) \cdot \hat{r} dS = \oint_{\partial\Omega} (\rho_0 \vec{\nabla}\phi_{sc}) \cdot \hat{r} dS \quad , \tag{B.1}$$

with $\hat{r}$ the radial unitary vector. Since we are interested just in the case where the sphere vibrates without displacing, only the monopolar contribution (3.33a) will be relevant for this computation [37, p.282], [39, p.70] Thus,

$$\oint_{\partial\Omega} (\rho_0 \nabla\phi_{\text{mp}}) \cdot \hat{r} dS = -a(t)\rho_0 \oint_{\partial\Omega} \nabla\left(\frac{1}{r}\right) \cdot \hat{r} dS = a(t)\rho_0 \oint_{\partial\Omega} \frac{1}{r^2}\hat{r} \cdot \hat{r} dS \tag{B.2}$$

$$= \frac{a(t)\rho_0}{R_\Omega^2} \oint_{\partial\Omega} dS = \frac{a(t)\rho_0}{R_\Omega^2} 4\pi R_\Omega^2 = 4\pi a(t)\rho_0 \quad , \tag{B.3}$$

Because mass is conserved, the mass flux through the surface $\partial\Omega$ equals the rate the fluid is displaced by the growing volume V_p of the particle,

$$\dot{m} = \frac{\partial}{\partial t}[(\rho_0 + \rho_{\text{in}})V_p] = (\rho_0 + \rho_{\text{in}})\frac{dV_p}{dt} + \frac{\partial \rho_{\text{in}}}{\partial t} V_p \quad . \tag{B.4}$$

The particle's volume V_p changes because it is compressed by the incident field pressure p_{in}. According to Hooke's Law (Eq. (2.24)),

$$dp_{in} = -B_p \frac{dV_p}{V_p} \quad \text{, or} \quad \frac{\partial p_{in}}{\partial t} = -\frac{B}{V_p}\frac{dV_p}{dt} \quad , \tag{B.5}$$

with $B_p = c_p^2 \rho_p$ the particle's bulk modulus, c_p the particle's speed of sound and ρ_p the particle's density. Furthermore, because $p_{in} = \rho_{in} c_0^2$, with c_0 the speed of sound in the fluid,

$$\frac{dV_p}{dt} = -V_p \frac{c_0^2}{\rho_p c_p^2} \frac{\partial \rho_{\text{in}}}{\partial t} \quad , \tag{B.6}$$

and the expression (B.4) becomes

$$\begin{aligned} \dot{m} &= \rho_0 \frac{\partial V_p}{\partial t} + \rho_{\text{in}} \frac{\partial V_p}{\partial t} + V_p \frac{\partial \rho_{\text{in}}}{\partial t} \\ &= -V_p \frac{\rho_0 c_0^2}{\rho_p c_p^2} \frac{\partial \rho_{\text{in}}}{\partial t} - V_p \frac{c_0^2}{\rho_p c_p^2} \rho_{\text{in}} \frac{\partial \rho_{\text{in}}}{\partial t} + V_p \frac{\partial \rho_{\text{in}}}{\partial t} \\ &= -V_p \frac{\rho_0 c_0^2}{\rho_p c_p^2} \frac{\partial \rho_{\text{in}}}{\partial t} - V_p \frac{c_0^2}{\rho_p c_p^2} \frac{1}{2} \frac{\partial (\rho_{\text{in}}^2)}{\partial t} + V_p \frac{\partial \rho_{\text{in}}}{\partial t} \\ &= -V_p \frac{c_0^2}{\rho_p c_p^2} \frac{\partial}{\partial t} \left(\rho_0 \rho_{\text{in}} + \frac{1}{2} \rho_{\text{in}}^2 \right) + V_p \frac{\partial \rho_{\text{in}}}{\partial t} \quad . \end{aligned} \tag{B.7}$$

As mentioned before, the incident density is a perturbation of the total density of the fluid, i.e. $\rho_0 \gg \rho_{\text{in}}$ and the term $\frac{1}{2}\rho_{\text{in}}^2$ is much smaller than $\rho_0 \rho_{in}$ and can be vanished. Therefore,

$$\dot{m}_{\text{in}} = 4\pi a(t) \rho_0 = V_p \frac{\partial \rho_{\text{in}}}{\partial t} \left(1 - \frac{\rho_0 c_0^2}{\rho_p c_p^2} \right) \quad , \tag{B.8}$$

and

$$a(t) = \frac{R_p^3}{3\rho_0} \frac{\partial \rho_{in}}{\partial t} \left(1 - \frac{\rho_0 c_0^2}{\rho_p c_p^2} \right) \quad , \tag{B.9}$$

where we used $V_p = \frac{4}{3}\pi R_p^3$. Notice that $a(t)$ is proportional to the cube of the radius and the non-dimensional contrast factor

$$f_1 = 1 - \frac{\rho_0 c_0^2}{\rho_p c_p^2} = 1 - \frac{\kappa_p}{\kappa_0} \quad , \tag{B.10}$$

which has been expressed in terms of the fluid's compressibility $\kappa_0 = 1/(\rho_0 c_0^2)$ and the particle's compressibility $\kappa_p = 1/(\rho_p c_p^2)$. When $\kappa_0 = \kappa_1$, $f_1 = 0$ and the monopole term of (3.30) does not contribute to the force.

Appendix C

Appendix III: Detailed computation of the vector field $A(t)$ for a sphere

Consider a sphere that moves with velocity $\vec{v}$ immersed to the fluid, and let us assume that the potential has the form

$$\phi_{\text{dip}} = \vec{A} \cdot \nabla \left(\frac{1}{r} \right) = -\vec{A} \cdot \frac{\vec{r}}{r^3} \quad , \tag{C.1}$$

where the position vector is measured between an observation point and the center of the sphere. The sphere is moving with a velocity $\vec{v}$ such that the vector $\vec{r}$ is related with

$$\vec{r} = \vec{r}_0 - t\vec{v} \quad , \tag{C.2}$$

where $\vec{r}_0$ is a position measured in a static reference frame. A first boundary condition is the fact that during the motion of the sphere there is no flow passing through the body, the normal velocities matches

$$\vec{u} \cdot \hat{r} = \vec{v} \cdot \hat{r} \quad , \tag{C.3}$$

Now the velocity $\vec{u}$ will be a fluid velocity around the sphere due to the disturbance of the sphere, but it is measured in a reference frame where there is no external flow. Then

$$\vec{u} = \nabla \left(-\vec{A} \cdot \frac{\hat{r}}{r^2} \right) = -(\vec{A} \cdot \nabla) \frac{\hat{r}}{r^2} = \frac{3(\vec{A} \cdot \hat{r})\hat{r} - \vec{A}}{r^3} \quad , \tag{C.4}$$

which leads to

$$\begin{aligned}\frac{3(\vec{A}\cdot\hat{r})\hat{r}-\vec{A}}{R_p^3}\cdot\hat{r} &= \vec{v}\cdot\hat{r}\\ \frac{2(\vec{A}\cdot\hat{r})}{R_p^3} &= \vec{v}\cdot\hat{r}\\ \vec{A}\cdot\hat{r} &= \frac{R_p^3}{2}(\vec{v}\cdot\hat{r})\\ \vec{A} &= \frac{R_p^3}{2}\vec{v} \quad .\end{aligned} \tag{C.5}$$

The vector $\vec{A}$ is related now to the dipolar moment of a *Doublet* and the fluid velocity written at (C.4) would take the following form:

$$\vec{u} = \frac{R_p^3}{2}\frac{3(\vec{v}\cdot\hat{r})\hat{r}-\vec{v}}{r^3} = \frac{R_p^3}{2}\left(\frac{3(\vec{v}\cdot\vec{r})\vec{r}}{r^5}-\frac{\vec{v}}{r^3}\right) \tag{C.6}$$

But the motion occurs due to the interaction between the fluid and the object immersed to it, meaning that the momentum must be conserved between them and the considered boundary condition is not enough. In order to take into account this interaction, we shall calculate the **drag** force made by the fluid on the object but this time, as mentioned earlier, the fluid was assumed incompressible due to the length-scale separation between the wavelength and the radius of the object (3.16) and with this the force made by the fluid is

$$\vec{F}_i^{(\text{drag})} = -\oint\left(-\frac{\rho_0}{2}|\nabla\phi_{\text{dip}}|^2-\frac{\partial\phi_{\text{dip}}}{\partial t}\right)\Bigg|_{r=R_p}\hat{n}dS \quad , \tag{C.7}$$

where the Bernoulli principle has been used [40]. (This expression is basically (A.2) but taking away the squared pressure term du to incompressinility and the dyadic tensor term because only the normal contribution contributes to the drag). Then, using (C.1) and (C.5) we can get the time derivative as

$$\frac{\partial\phi_{\text{dip}}}{\partial t} = -\frac{\partial\vec{v}}{\partial t}\cdot\left(\frac{R_p^3}{2}\frac{\vec{r}}{r^3}\right)-\vec{v}\cdot\left(\frac{R_p^3}{2}\frac{\partial}{\partial t}\left(\frac{\vec{r}}{r^3}\right)\right) \tag{C.8}$$

By using the chain rule it's possible to rewrite for the second term of (C.13) as

$$v_i\frac{\partial}{\partial t}\left(\frac{R_p^3}{2}\frac{r_i}{r^3}\right) = v_i\frac{\partial}{\partial r_j}\left(\frac{R_p^3}{2}\frac{r_i}{r^3}\right)\frac{\partial r_j}{\partial t} = \nabla\left(\frac{R_p^3}{2}\frac{v_i r_i}{r^3}\right)\cdot\frac{\partial\vec{r}}{\partial t} = -\nabla\phi_{\text{dip}}\cdot\frac{\partial\vec{r}}{\partial t} \tag{C.9}$$

since $\vec{v}$ is not dependent of the space coordinates as mentioned earlier. The time derivative of the vector position is related to the motion of the object because of the reference frame described in (C.2), leading to

$$\frac{\partial\vec{r}}{\partial t} = -\vec{v} \quad , \tag{C.10}$$

and (C.9) becomes

$$v_i \frac{\partial}{\partial t}\left(\frac{r_i}{r^3}\right) = -\nabla\phi_{\text{dip}} \cdot \frac{\partial \vec{r}}{\partial t} = \nabla\phi_{\text{dip}} \cdot \vec{v} \tag{C.11}$$

and the time derivative of ϕ_{dip} is written according to (C.8) as

$$\frac{\partial \phi_{\text{dip}}}{\partial t} = -\frac{\partial \vec{v}}{\partial t} \cdot \left(\frac{R_p^3}{2}\frac{\vec{r}}{r^3}\right) - \nabla\phi_{\text{dip}} \cdot \vec{v} \quad , \tag{C.12}$$

and using (C.6) we get finally

$$\begin{aligned}
\frac{\partial \phi_{\text{dip}}}{\partial t} &= -\frac{R_p^3}{2}\left(\frac{\partial v}{\partial t} \cdot \left(\frac{\vec{r}}{r^3}\right) - 3\frac{(\vec{r}\cdot\vec{v})^2}{r^5} + \frac{v^2}{r^3}\right) \\
\frac{\partial \phi_{\text{dip}}}{\partial t} &= -\frac{R_p^3}{2r^3}\left(\vec{r}\cdot\frac{\partial \vec{v}}{\partial t} + 3\frac{(\vec{r}\cdot\vec{v})^2}{r^2} - v^2\right) \quad .
\end{aligned} \tag{C.13}$$

The square of the gradient is, using (C.6) and (C.5),

$$|\nabla\phi|^2 = \left(\frac{R_p^3}{2}\right)^2 \left|\frac{3(\vec{v}\cdot\vec{r})}{r^5}\vec{r} - \frac{\vec{v}}{r^3}\right|^2 \quad , \tag{C.14}$$

which written as an expanded double dot product takes the following form

$$\begin{aligned}
|\nabla\phi|^2 &= \left(\frac{R_p^3}{2}\right)^2 \left(\frac{3(\vec{v}\cdot\vec{r})\vec{r}}{r^5} - \frac{\vec{v}}{r^3}\right) \cdot \left(\frac{3(\vec{v}\cdot\vec{r})\vec{r}}{r^5} - \frac{\vec{v}}{r^3}\right) \\
|\nabla\phi|^2 &= \left(\frac{R_p^3}{2}\right)^2 \left(\frac{9(\vec{v}\cdot\vec{r})^2}{r^8} + \frac{v^2}{r^6} - \frac{6(\vec{v}\cdot\vec{r})^2}{r^8}\right) \\
|\nabla\phi|^2 &= \left(\frac{R_p^3}{2}\right)^2 \left(\frac{3(\vec{v}\cdot\vec{r})^2}{r^8} + \frac{v^2}{r^6}\right) \\
|\nabla\phi|^2 &= \left(\frac{R_p^3}{2r^3}\right)^2 \left(3\frac{(\vec{r}\cdot\vec{v})^2}{r^2} + v^2\right) \quad .
\end{aligned} \tag{C.15}$$

Now plugging both expressions (C.13) and (C.15) into (C.7) we get

$$\begin{aligned}
\vec{F}^{(\text{drag})} &= -\rho_0 \oint \left(\frac{1}{2}\left(R_p\hat{r}\cdot\frac{\partial \vec{v}}{\partial t} + 3(\hat{r}\cdot\vec{v})^2 - v^2\right) - \frac{1}{8}\left(3(\hat{r}\cdot\vec{v})^2 + v^2\right)\right)\hat{n}dS \\
&= -\oint \frac{R_p}{2}\hat{r}\cdot\frac{\partial \vec{v}}{\partial t}\hat{n}dS - \oint \frac{v^2}{2}\left(\frac{9}{4}\frac{(\hat{r}\cdot\vec{v})^2}{v^2} - \frac{5}{4}\right)\hat{n}dS \quad .
\end{aligned} \tag{C.16}$$

Then using the fact that θ is the angle between the motion of the sphere v and r we have for the second integral, and

$$\hat{r}\cdot\vec{v} = v\cos\theta \tag{C.17}$$

we can write

$$\rho_0 \int_0^{2\pi} \int_0^{\pi} \frac{v^2}{2} \left(1 - \frac{9}{4}\sin^2\theta\right) \hat{n}(R_p^2 \sin\theta d\phi d\theta) \quad , \tag{C.18}$$

as the surface is a sphere and $\vec{r}$ points at the center of the sphere then $\hat{n} = \hat{r}$, then

$$\begin{aligned} &\rho_0 \int_0^{2\pi} \int_0^{\pi} \frac{v^2}{2} \left(1 - \frac{9}{4}\sin^2\theta\right) (\cos\phi\sin\theta, \sin\phi\sin\theta, \cos\theta)(R_p^2 \sin\theta d\phi d\theta) \\ = &\frac{\rho_0 v^2 R_p^2}{2} \int_0^{2\pi} \int_0^{\pi} \Bigg[\cos\phi \left(\sin^2\theta - \frac{9}{4}\sin^4\theta\right), \\ &\sin\phi \left(\sin^2\theta - \frac{9}{4}\sin^4\theta\right), \\ &\cos\theta \left(\sin\theta - \frac{9}{4}\sin^3\theta\right) \Bigg] d\phi d\theta \quad , \end{aligned} \tag{C.19}$$

the integration over ϕ vanishes the first two components, while the third one becomes

$$\begin{aligned} &\pi\rho_0 v^2 R_p^2 \int_0^{\pi} \cos\theta\sin\theta - \frac{9}{4}\cos\theta\sin^3\theta d\theta \\ &\pi\rho_0 v^2 R_p^2 \left[\frac{1}{2}\sin^2\theta - \frac{9}{16}\sin^4\theta\right]_0^{\pi} = 0 \end{aligned} \tag{C.20}$$

Now the first integral includes the acceleration of the sphere and it gives

$$\frac{\partial v}{\partial t}\frac{R_p^3\rho_0}{2}(2\pi)\int_0^{\pi}(\hat{r}\cdot\hat{e}_z)\cos\theta\hat{e}_z\sin\theta d\theta = \frac{\partial v}{\partial t}\pi R_p^3\hat{e}_z\rho_0\int_0^{\pi}\cos^2\theta\sin\theta d\theta \tag{C.21}$$

taking into account that θ is an angle measured from the direction of $\vec{v}$ and $\vec{r}$, meaning that this term will get the same direction of $\vec{v}$. While the integral may be solved in the following way:

$$\int_0^{\pi}\cos^2\theta\sin\theta d\theta = -\frac{1}{3}\cos^3\theta\Big|_0^{\pi} = -\frac{(-1)^3 - (1)^3}{3} = \frac{2}{3} \tag{C.22}$$

resulting in the following expression for (C.21):

$$\pi R_p^3\rho_0\int_0^{\pi}\cos^2\theta\sin\theta d\theta = \frac{2\pi R_p^3\rho_0}{3} \quad . \tag{C.23}$$

This means that the drag force exerted is

$$\vec{F}^{(\text{drag})} = -\frac{2\pi R_p^3\rho_0}{3}\frac{\partial v}{\partial t}\hat{e}_z \equiv -M_{\text{add}}\frac{\partial v}{\partial t}\hat{e}_z \tag{C.24}$$

defining the *added mass* M_{add} factor due to the motion of the fluid. Now if we want to set a motion equation for the fluid, we can see the force exerted by the fluid as an external one $\vec{f}$ such that the total force is

$$m_p\frac{\partial v}{\partial t} = f - M_{\text{add}}\frac{\partial v}{\partial t} \quad , \tag{C.25}$$

now f would be at the same time the opposing force that the piece of fluid around receives to the ball. This implies an equation of motion for that surrounding fluid, as the buyonant force plus the added mass force, but instead made to the fluid. That is

$$(\frac{4\pi R_p^3}{3}\rho_0 + M_{\text{add}})\frac{\partial \vec{u}}{\partial t} = f \quad . \tag{C.26}$$

Now combining (C.25) and (C.26) we get

$$\begin{aligned}
\left(\rho_p V_p + \frac{2\pi\rho_0 R_p^3}{3}\right) v_i &= \left(\rho_0 V_p + \frac{2\pi\rho_0 R_p^3}{3}\right) u_i \\
\left(\frac{4\pi\rho_p R_p^3}{3} + \frac{2\pi\rho_0 R_p^3}{3}\right) v_i &= \left(\frac{4\pi\rho_0 R_p^3}{3} + \frac{2\pi\rho_0 R_p^3}{3}\right) u_i \\
\left(\rho_p + \frac{\rho_0}{2}\right) v_i &= \left(\rho_0 + \frac{\rho_0}{2}\right) u_i \\
v_i &= \frac{3\rho_0}{2\rho_p + \rho_0} u_i \quad .
\end{aligned} \tag{C.27}$$

This final relation will ensure momentum conservation for (C.5), where equal velocities $\vec{u}$ and $\vec{v}$ were assumed. In general, the actual velocity must be the one which is relative to the fluid in order to still satisfy (C.3). Thus

$$\vec{A} = \frac{R_p^3}{2}(\vec{v} - \vec{u}) \quad , \tag{C.28}$$

and with (C.27) the definitive expression for $\vec{A}$ is

$$\vec{A}(t) = \frac{R_p^3}{2}\left(\frac{2(\rho_p - \rho_0)}{2\rho_p + \rho_0}\right)\vec{u} \quad , \tag{C.29}$$

introducing the density contrast factor f_2 defined as

$$f_2 = \frac{2(\rho_p - \rho_0)}{2\rho_p + \rho_0} \tag{C.30}$$

where we can see that for the particular case where both densities matches this factor is zero, meaning that no dipolar contribution is added.

Appendix D

Appendix VI: Detailed computation of the scalar field $a(t)$ for a disk

Assuming the disk to be a compressible one such that it shrinks or expands isotropically by simply enlarging or decreasing its radius, a mathematical circular region Ω of radius R_Ω concentric to the disk with radius R_p which fulfills $\lambda \gg R_\Omega \gg R_p$ is considered, such that there is an excess of fluid around the disk, thus, its outgoing mass flux would be computed as the following integral:

$$\dot{m} = \frac{\partial}{\partial t}\int_\Omega dA\rho_1 = -\int_\Omega dA\nabla\cdot(\rho_0\vec{u}_1) = -\oint_{\partial\Omega} dl(\rho_0\vec{u}_1)\cdot\hat{n} \quad , \tag{D.1}$$

In which we have kept only terms up to first order, as according to (3.17) the macroscopic first-order fields are deducted from both the incident and scattered fields and we are interested in those. This mass flux which comes from the outside of the boundary of radius R_Ω is

$$\dot{m}_{\text{out}} = -\oint_{\partial\Omega} dl(\rho_0\nabla\phi_{\text{mp}})\cdot\hat{n} \tag{D.2}$$

where $\hat{n}$ is a vector normal to $\partial\Omega$. As we are interested in the case where the disk only vibrates maintaining its center of mass motionless [37, p.282], [39, p.70] only the monopolar contribution (3.68a) will be relevant for this computation. Thus,

$$\oint_{\partial\Omega} dl(\rho_0\nabla\phi_{\text{mp}})\cdot\hat{n} = -a(t)\rho_0\oint_{\partial\Omega} dl\nabla\left(\log r\right)\cdot\hat{n} = -a(t)\oint_{\partial\Omega} dl\frac{\vec{r}}{r^2}\cdot\hat{n} \quad , \tag{D.3}$$

then applying the gradient and evaluating in the circular surface where $r = R_\Omega$, with $\hat{n} = \hat{r}$ due to be $\vec{r}$ a position measured from the center of the disk, the integral is reduced to

$$\dot{m}_{\text{out}} = a(t)\rho_0\int_0^{2\pi}\frac{\hat{r}\cdot\hat{r}}{R_\Omega}R_\Omega d\phi = \frac{a(t)\rho_0}{R_\Omega}(2\pi R_\Omega) = 2\pi a\rho_0 \quad . \tag{D.4}$$

Now we can compute the flow of mass going out of the circular surface of radius R_Ω. This mass flux is basically the rate of change of the incoming fluid density times the area of the

particle, because the presence of the particle exerts an amount of fluid occupied now by the object. Then,

$$\dot{m}_{\text{in}} = \frac{\partial}{\partial t}[(\rho_0 + \rho_{\text{in}})A_p] \quad . \tag{D.5}$$

The variation of the particle's area A_p will be due to the compression of the incident field, thus, the time derivative is strictly related with the two-dimensional equivalent of the Bulk's modulus

Then we can write the following thanks to the chain rule:

$$\frac{\partial A_p}{\partial t} = -A_p \frac{c_0^2}{\rho_p c_p^2} \frac{\partial \rho_{\text{in}}}{\partial t} \quad , \tag{D.6}$$

and using this expression (D.5) becomes

$$\begin{aligned} \dot{m}_{\text{in}} &= -A_p \frac{\rho_0 c_0^2}{\rho_p c_p^2} \frac{\partial \rho_{\text{in}}}{\partial t} - A_p \frac{c_0^2}{\rho_p c_p^2} \rho_{\text{in}} \frac{\partial \rho_{\text{in}}}{\partial t} + A_p \frac{\partial \rho_{\text{in}}}{\partial t} \\ &= -A_p \frac{c_0^2}{\rho_p c_p^2} \frac{\partial}{\partial t} \left(\rho_0 \rho_{\text{in}} + \frac{1}{2} \rho_{\text{in}}^2 \right) + A_p \frac{\partial \rho_{\text{in}}}{\partial t} \quad . \end{aligned} \tag{D.7}$$

As mentioned before, the incident density is a perturbation of the total density of the fluid and this implies that the bulk density ρ_0 is much larger than the incident field ρ_{in}, thus the term proportional to ρ_{in}^2 shall be vanished as well, ending up with

$$\dot{m}_{\text{in}} = A_p \frac{\partial \rho_{\text{in}}}{\partial t} \left(1 - \frac{\rho_0 c_0^2}{\rho_p c_p^2} \right) \quad . \tag{D.8}$$

Such that $a(t)$ may be gotten by only equaling (D.4) and (D.8) as the incoming mass must be equal to the outgoing mass exchanged at the boundary $\partial\Omega$ (the mass is conserved). Thus

$$a(t) = \frac{A_p}{2\pi\rho_0} \frac{\partial \rho_{in}}{\partial t} \left(1 - \frac{\rho_0 c_0^2}{\rho_p c_p^2} \right) \quad , \tag{D.9}$$

or in terms of the particle's radius

$$a(t) = \frac{R_p^2}{2\rho_0} \frac{\partial \rho_{in}}{\partial t} \left(1 - \frac{\rho_0 c_0^2}{\rho_p c_p^2} \right) \quad , \tag{D.10}$$

noting the proportionality with the square of the radius and a definition of the non-dimensional contrast factor f_1 as

$$f_1 = 1 - \frac{\rho_0 c_0^2}{\rho_p c_p^2} = 1 - \frac{\kappa_p}{\kappa_0} \tag{D.11}$$

in terms of the compressibility of the fluid $\kappa_0 = 1/(\rho_0 c_0^2)$ and the compressibility of the particle $\kappa_p = 1/(\rho_p c_p^2)$, indicating according to (D.11) that if both compressibilities match for both media, the particle and the fluid, the monopole term of (3.30) does not contribute to the force.

Appendix E

Appendix V: Detailed computation of the vector field $A(t)$ for a disk

Now let's consider the dipole contribution for the potential. First, the solution to consider for a disk moving with velocity $\vec{v}$ and immersed to the fluid has the form

$$\phi_{\text{dip}} = -\vec{A} \cdot \nabla (\log r) = -\vec{A} \cdot \frac{\vec{r}}{r^2} \quad . \tag{E.1}$$

A first boundary condition is the fact that during the motion of the disk there is no flow passing through it, the normal velocities matches

$$\vec{u} \cdot \hat{r} = \vec{v} \cdot \hat{r} \quad , \tag{E.2}$$

Now the velocity $\vec{u}$ will be a fluid velocity around the disk due to the disturbance of the disk, but it is measured in a reference frame where there is no external flow. Then

$$\vec{u} = \nabla \left(-\vec{A} \cdot \frac{\hat{r}}{r} \right) = -(\vec{A} \cdot \nabla) \frac{\hat{r}}{r} = \frac{2(\vec{A} \cdot \hat{r})\hat{r} - \vec{A}}{r^2} \quad , \tag{E.3}$$

which leads to

$$\begin{aligned} \frac{2(\vec{A} \cdot \hat{r})\hat{r} - \vec{A}}{R_p^2} \cdot \hat{r} &= \vec{v} \cdot \hat{r} \\ \frac{(\vec{A} \cdot \hat{r})}{R_p^2} &= \vec{v} \cdot \hat{r} \\ \vec{A} \cdot \hat{r} &= R_p^2 (\vec{v} \cdot \hat{r}) \\ \vec{A} &= R_p^2 \vec{v} \quad . \end{aligned} \tag{E.4}$$

The vector $\vec{A}$ is related now to the dipolar moment of a *Doublet* and the fluid velocity written at (E.3) would take the following form:

$$\vec{u} = R_p^2 \frac{2(\vec{v} \cdot \hat{r})\hat{r} - \vec{v}}{r^2} = R_p^2 \left(\frac{2(\vec{v} \cdot \vec{r})\vec{r}}{r^4} - \frac{\vec{v}}{r^2} \right) \tag{E.5}$$

But the motion occurs due to the interaction between the fluid and the object immersed to it, meaning that the momentum must be conserved between them and the considered boundary condition is not enough. In order to take into account this interaction, we shall calculate the **drag** force made by the fluid on the object but this time, as mentioned earlier, the fluid was assumed incompressible due to the length-scale separation between the wavelength and the radius of the object (3.16) and with this the force made by the fluid is

$$\vec{F}_i^{(\text{drag})} = -\rho_0 \oint \left(-\frac{1}{2}|\nabla\phi_{\text{dip}}|^2 - \frac{\partial\phi_{\text{dip}}}{\partial t} \right) \Big|_{r=R_p} \hat{n} dl \quad , \tag{E.6}$$

where the Bernoulli principle has been used [40]. (This expression is basically (A.2) but taking away the squared pressure term du to incompressinility and the dyadic tensor term because only the normal contribution contributes to the drag). Then, using (E.1) and (E.4) we can get the time derivative as

$$\frac{\partial\phi_{\text{dip}}}{\partial t} = -\frac{\partial\vec{v}}{\partial t} \cdot \left(R_p^2 \frac{\vec{r}}{r^2} \right) - \vec{v} \cdot \left(R_p^2 \frac{\partial}{\partial t} \left(\frac{\vec{r}}{r^2} \right) \right) \tag{E.7}$$

By using the chain rule it's possible to rewrite for the second term of (E.13) as

$$v_i \frac{\partial}{\partial t} \left(R_p^2 \frac{r_i}{r^2} \right) = v_i \frac{\partial}{\partial r_j} \left(R_p^2 \frac{r_i}{r^2} \right) \frac{\partial r_j}{\partial t} = \nabla \left(R_p^2 \frac{v_i r_i}{r^2} \right) \cdot \frac{\partial\vec{r}}{\partial t} = -\nabla\phi_{\text{dip}} \cdot \frac{\partial\vec{r}}{\partial t} \tag{E.8}$$

since $\vec{v}$ is not dependent of the space coordinates as mentioned earlier. The time derivative of the vector position is related to the motion of the object. The position vector must be relative to the center of the disk, thus $\vec{r}$ actually becomes

$$\vec{r} = \vec{r}_0 - t\vec{v} \quad , \tag{E.9}$$

where $\vec{r}_0$ is a position measured in a static reference frame, thus, its time derivative yields to zero and (E.9) becomes

$$\frac{\partial\vec{r}}{\partial t} = -\vec{v} \quad , \tag{E.10}$$

meaning that (E.8) becomes

$$v_i \frac{\partial}{\partial t} \left(\frac{r_i}{r^2} \right) = -\nabla\phi_{\text{dip}} \cdot \frac{\partial\vec{r}}{\partial t} = \nabla\phi_{\text{dip}} \cdot \vec{v} \tag{E.11}$$

and the time derivative of ϕ_{dip} is written according to (E.7) as

$$\frac{\partial\phi_{\text{dip}}}{\partial t} = -\frac{\partial\vec{v}}{\partial t} \cdot \left(R_p^2 \frac{\vec{r}}{r^2} \right) - \nabla\phi_{\text{dip}} \cdot \vec{v} \quad , \tag{E.12}$$

and using (E.5) we get finally

$$\begin{aligned} \frac{\partial\phi_{\text{dip}}}{\partial t} &= -R_p^2 \left(\frac{\partial v}{\partial t} \cdot \left(\frac{\vec{r}}{r^2} \right) - 2\frac{(\vec{r}\cdot\vec{v})^2}{r^4} + \frac{v^2}{r^2} \right) \\ \frac{\partial\phi_{\text{dip}}}{\partial t} &= -\frac{R_p^2}{r^2} \left(\vec{r} \cdot \frac{\partial\vec{v}}{\partial t} - 2\frac{(\vec{r}\cdot\vec{v})^2}{r^2} + v^2 \right) \quad . \end{aligned} \tag{E.13}$$

The square of the gradient is, using (E.5) and (E.4),

$$|\nabla\phi|^2 = R_p^4 \left| \frac{2(\vec{v}\cdot\vec{r})}{r^4}\vec{r} - \frac{\vec{v}}{r^2} \right|^2 \quad , \tag{E.14}$$

which written as an expanded double dot product takes the following form

$$\begin{aligned} |\nabla\phi|^2 &= R_p^4 \left(\frac{4(\vec{v}\cdot\vec{r})^2}{r^6} + \frac{v^2}{r^4} - \frac{4(\vec{v}\cdot\vec{r})^2}{r^6} \right) \\ |\nabla\phi|^2 &= R_p^4 \frac{v^2}{r^4} \quad . \end{aligned} \tag{E.15}$$

Now plugging both expressions (E.13) and (E.15) into we get

$$\begin{aligned} \vec{F}^{(\text{drag})} &= -\rho_0 \oint \left(-\frac{v^2}{2} + \left(\vec{r}\cdot\frac{\partial\vec{v}}{\partial t} - 2(\hat{r}\cdot\vec{v})^2 + v^2 \right) \right) \hat{n} dl \\ &= -\oint R_p \hat{r}\cdot\frac{\partial\vec{v}}{\partial t}\hat{n} dl - \oint \frac{3v^2}{2} - 2(\hat{r}\cdot\vec{v})^2 \hat{n} dl \quad . \end{aligned} \tag{E.16}$$

Then using the fact that θ is the angle between the motion of the disk v and r we have for the second integral, and

$$\hat{r}\cdot\vec{v} = v\cos\phi \tag{E.17}$$

we can write

$$\rho_0 \int_0^{2\pi} \frac{v^2}{2}\left(3 - 4\cos^2\phi\right)\hat{n}(R_p d\phi) \quad , \tag{E.18}$$

as the surface is a disk and $\vec{r}$ points at the center of the disk then $\hat{n} = \hat{r}$, then

$$\begin{aligned} &\rho_0 \int_0^{2\pi} \frac{v^2}{2}\left(3 - 4\cos^2\phi\right)(\cos\phi, \sin\phi)(R_p d\phi) \\ &= \frac{\rho_0 v^2 R_p}{2} \int_0^{2\pi} \Big[3\cos\phi - 4\cos^3\phi, \\ &\qquad\qquad 3\sin\phi - 4\cos^2\phi\sin\phi \Big] d\phi = 0 \quad , \end{aligned} \tag{E.19}$$

Now the first integral includes the acceleration of the disk and it gives

$$\frac{\partial v}{\partial t} R_p^2 \rho_0 \int_0^{2\pi} (\hat{r}\cdot\hat{e}_z)\cos\phi d\phi \hat{e}_x = \frac{\partial v}{\partial t} R_p^2 \hat{e}_x \rho_0 \int_0^{2\pi} \cos^2\phi d\phi \tag{E.20}$$

taking into account that θ is an angle measured from the direction of $\vec{v}$ and $\vec{r}$, meaning that this term will get the same direction of $\vec{v}$.The resulting expression for (E.20) is:

$$R_p^2 \rho_0 \int_0^{2\pi} \cos^2\phi d\phi = \pi R_p^2 \rho_0 \quad . \tag{E.21}$$

This means that the drag force exerted is

$$\vec{F}^{(\text{drag})} = -\pi R_p^2 \rho_0 \frac{\partial v}{\partial t}\hat{e}_x \equiv -M_{\text{add}}\frac{\partial v}{\partial t}\hat{e}_x \tag{E.22}$$

defining the *added mass* M_{add} factor due to the motion of the fluid. Now if we want to set a motion equation for the fluid, we can see the force exerted by the fluid as an external one $\vec{f}$ such that the total force is

$$m_p \frac{\partial v}{\partial t} = f - M_{\text{add}}\frac{\partial v}{\partial t} \quad , \tag{E.23}$$

now f would be at the same time the opposing force that the piece of fluid around receives to the ball. This implies an equation of motion for that surrounding fluid, as the buyonant force plus the added mass force, but instead made to the fluid. That is

$$(\pi R_p^2 \rho_0 + M_{\text{add}})\frac{\partial \vec{u}}{\partial t} = f \quad . \tag{E.24}$$

Now combining (E.23) and (E.24) we get

$$\begin{aligned} \left(\rho_p A_p + \pi\rho_0 R_p^2\right) v_i &= \left(\rho_0 A_p + \pi\rho_0 R_p^2\right) u_i \\ \left(\rho_p + \rho_0\right) v_i &= 2\rho_0 u_i \\ v_i &= \frac{2\rho_0}{\rho_p + \rho_0} u_i \quad . \end{aligned} \tag{E.25}$$

This final relation will ensure momentum conservation for (E.4), where equal velocities $\vec{u}$ and $\vec{v}$ were assumed. In general, the actual velocity must be the one which is relative to the fluid in order to still satisfy (E.2). Thus

$$\vec{A} = R_p^2(\vec{v} - \vec{u}) \quad , \tag{E.26}$$

and with (E.25) the definitive expression for $\vec{A}$ is

$$\vec{A}(t) = R_p^2 \left(\frac{\rho_0 - \rho_p}{\rho_p + \rho_0}\right)\vec{u} = \frac{R_p^2}{2} f_2 \vec{u} \quad , \tag{E.27}$$

introducing the density contrast factor f_2 defined as

$$f_2 = 2\left(\frac{\rho_0 - \rho_p}{\rho_p + \rho_0}\right) \tag{E.28}$$

where we can see that for the particular case where both densities matches this factor is zero, meaning that no dipolar contribution is added.

Appendix F

Appendix IV: The Chapman-Enskog analysis

This analysis consist of developing a multiscale Taylor expansion of (4.3) written in its continuous version

$$\left(\partial_t + v_{i\alpha}\partial_\alpha\right) f_i = -\frac{\delta t}{\tau}(f_i - f^{\mathrm{eq}}) \quad , \tag{F.1}$$

where $\partial_t = \partial/\partial t$ and $\partial_\alpha = \partial/\partial x_\alpha$, and then developing a perturbative expansion of f around the Knusden number, as this is a suitable parameter to determine if the macroscopic limit has been reached (see sec. 2.1). First, the Taylor expansion is done up to second order for the total temporal differential operator as follows:

$$\delta t\left(\partial_t + v_{i\alpha}\partial_\alpha\right) f_i + \frac{\delta t^2}{2!}\left(\partial_t + v_{i\alpha}\partial_\alpha\right)^2 f_i + \mathcal{O}(\delta t^3) = -\frac{\delta t}{\tau}(f_i - f^{\mathrm{eq}}) \quad , \tag{F.2}$$

in this case the temporal derivative was expanded up to second order of δt and the chain rule has been used, while the distribution function is written as an expansion in response of a small perturbation proportional to the Knusden number $\epsilon = \delta x/x$, with x the characteristic size of the system and δx the size of a lattice cell. Although this is an expansion done through space, the Chapman Enskog expansion must ensure that this expansion must be done at multiple time-scales, for this reason it is also necessary to perform this expansion for the differential operators in the following manner:

$$f_i = f_i^{(0)} + \epsilon f_i^{(1)} + \epsilon^2 f_i^{(2)} + \dots \tag{F.3a}$$

$$\partial_t = \epsilon\partial_t^{(1)} + \epsilon^2\partial_t^{(2)} + \dots \tag{F.3b}$$

$$\partial_\alpha = \epsilon\partial_\alpha^{(1)} + \dots \tag{F.3c}$$

where the components of ∂_t by themselves does not form a time derivative but the total summation of those, while $\partial_t^{(n)}$ are only terms for the n-th order of ϵ [38, Sec. 4.1.2]. As the macroscopic moments must not be affected by the size of the lattice cells δx due to be

macsrocopic, these moments must only contribute at order zero of ϵ instead of depend on them. For this reason it is possible to write

$$\sum_i f_i^{(n)} = 0 \quad , \quad \sum_i v_{i\alpha} f_i^{(n)} = 0 \quad \text{if} \quad n > 0 \quad . \tag{F.4}$$

Then, replacing (F.3) in (F.2) and neglecting the terms of higher orders of ϵ we have

$$\begin{aligned} &\epsilon^2 \left\{ \partial_t^{(2)} f_i^{(0)} + \left(\partial_t^{(1)} + v_{i\alpha} \partial_\alpha^{(1)} \right) f_i^{(1)} + \frac{\delta t}{2} \left(\partial_t^{(1)} + v_{i\alpha} \partial_\alpha^{(1)} \right)^2 f_i^{(0)} \right\} + \dots \\ &\cdots + \epsilon \left(\partial_t^{(1)} + v_{i\alpha} \partial_\alpha^{(1)} \right) f_i^{(0)} = -\frac{1}{\tau} \left(f_i^{(0)} - f_i^{\text{eq}} + \epsilon f_i^{(1)} + \epsilon^2 f_i^{(2)} \right) \quad . \end{aligned} \tag{F.5}$$

So that equaling terms of the same order of ϵ gives the following relations:

$$f_i^{(0)} = f_i^{\text{eq}} \quad , \tag{F.6a}$$

$$\left(\partial_t^{(1)} + v_{i\alpha} \partial_\alpha^{(1)} \right) f_i^{(0)} = -\frac{1}{\tau} f_i^{(1)} \quad \text{and} \tag{F.6b}$$

$$\partial_t^{(2)} f_i^{(0)} + \left(\partial_t^{(1)} + v_{i\alpha} \partial_\alpha^{(1)} \right) f_i^{(1)} + \frac{\delta t}{2} \left(\partial_t^{(1)} + v_{i\alpha} \partial_\alpha^{(1)} \right)^2 f_i^{(0)} = -\frac{1}{\tau} f_i^{(2)} \quad . \tag{F.6c}$$

The third term of equation (F.6c) may be rewritten using (F.6b) in the following way:

$$\begin{aligned} \frac{\delta t}{2} \left(\partial_t^{(1)} + v_{i\alpha} \partial_\alpha^{(1)} \right)^2 f_i^{(0)} &= \frac{\delta t}{2} \left(\partial_t^{(1)} + v_{i\alpha} \partial_\alpha^{(1)} \right) \left(\partial_t^{(1)} + v_{i\alpha} \partial_\alpha^{(1)} \right) f_i^{(0)} \\ &= -\frac{\delta t}{2\tau} \left(\partial_t^{(1)} + v_{i\alpha} \partial_\alpha^{(1)} \right) f_i^{(1)} \end{aligned} \tag{F.7}$$

so that it is possible to rewrite (F.6) as

$$f_i^{(0)} = f_i^{\text{eq}} \quad , \tag{F.8a}$$

$$\left(\partial_t^{(1)} + v_{i\alpha} \partial_\alpha^{(1)} \right) f_i^{(0)} = -\frac{1}{\tau} f_i^{(1)} \quad \text{and} \tag{F.8b}$$

$$\partial_t^{(2)} f_i^{(0)} + \left(1 - \frac{\delta t}{2\tau} \right) \left(\partial_t^{(1)} + v_{i\alpha} \partial_\alpha^{(1)} \right) f_i^{(1)} = -\frac{1}{\tau} f_i^{(2)} \quad . \tag{F.8c}$$

Separating every order of ϵ is actually a way to obtain the macroscopic equations easier, as there will be only one equation for each of the moments, which is built by multiplying by the velocity vectors a number of times corresponding the tensor order of the moment. Let's deduct the conservation equation for the zero-order tensor Π by simply performing a summation over i in all relations of (F.8), but relation must be multiplied by the corresponding order of ϵ in order to recover the complete differential operators, as mentioned before, (F.8) is just a separation of (F.5) by every order of ϵ. Thus, one add over all i on (F.8), (F.8b) is

multiplied by ϵ and (F.8c) multiplied by ϵ^2, then both equations are added. For (F.8b) we have

$$\epsilon \sum_i \left(\partial_t^{(1)} + v_{i\alpha} \partial_\alpha^{(1)} \right) f_i^{\text{eq}} = -\epsilon \frac{1}{\tau} \sum_i f_i^{(1)} \tag{F.9}$$

and taking into account (F.4) and the fact that $v_{i\alpha}$ does not depend on x_α as it's an homogeneous set in space, the eq. (F.9) becomes

$$\begin{aligned} \epsilon \partial_t^{(1)} \sum_i f_i^{\text{eq}} + \epsilon \partial_\alpha^{(1)} \sum_i v_{i\alpha} f_i^{\text{eq}} = 0 \\ \epsilon \partial_t^{(1)} \Pi + \epsilon \partial_\alpha^{(1)} \Pi_\alpha = 0 \quad . \end{aligned} \tag{F.10}$$

For (F.8c) also taking into account (F.4) we have

$$\begin{aligned} \epsilon^2 \left(1 - \frac{\delta t}{2\tau} \right) \sum_i \left(\partial_t^{(1)} + v_{i\alpha} \partial_\alpha^{(1)} \right) f_i^{(1)} + \epsilon^2 \sum_i \partial_t^{(2)} f_i^{\text{eq}} = -\epsilon \frac{1}{\tau} \sum_i f_i^{(2)} \\ \epsilon^2 \left(1 - \frac{\delta t}{2\tau} \right) \left(\partial_t^{(1)} \sum_i f_i^{(1)} + \partial_\alpha^{(1)} \sum_i v_{i\alpha} f_i^{(1)} \right) + \epsilon^2 \partial_t^{(2)} \sum_i f_i^{\text{eq}} = 0 \\ \epsilon^2 \partial_t^{(2)} \Pi = 0 \end{aligned} \tag{F.11}$$

Therefor adding (F.10) and (F.11) the following equation is obtained for the zero-order and first-order moments taking into account (F.3):

$$\begin{aligned} \left(\epsilon \partial_t^{(1)} + \epsilon^2 \partial_t^{(2)} \right) \Pi + \epsilon \partial_\alpha^{(1)} \Pi_\alpha = 0 \\ \partial_t \Pi + \partial_\alpha \Pi_\alpha = 0 \quad , \end{aligned} \tag{F.12}$$

which may be seen as a continuity equation just as (F.12), because the temporal derivative of a scalar field Π is the divergence of a vectorial field Π_α. Now, noticing how are moments defined in (4.4) one can notice that the tensor order of each momentum is given by the amount of times in which f_i has been multiplied by components of the velocities $v_{i\alpha}$, such that in order to get more conservation laws for higher tensor order moments the same process showed earlier must be done but multiplying (F.8) by $\vec{v}_i$ and adding over i. Doing this with (F.8b) and (F.8c) we have:

$$\begin{aligned} \epsilon \partial_t^{(1)} \sum_i v_{i\alpha} f_i^{\text{eq}} + \epsilon \partial_\beta^{(1)} \sum_i v_{i\alpha} v_{i\beta} f_i^{\text{eq}} = 0 \\ \epsilon \partial_t^{(1)} \Pi_\alpha + \epsilon \partial_\beta^{(1)} \Pi_{\alpha\beta} = 0 \end{aligned} \tag{F.13}$$

and

$$\epsilon^2 \left(1 - \frac{\delta t}{2\tau} \right) \left(\partial_t^{(1)} \sum_i v_{i\alpha} f_i^{(1)} + \partial_\beta^{(1)} \sum_i v_{i\alpha} v_{i\beta} f_i^{(1)} \right) + \epsilon^2 \partial_t^{(2)} \sum_i v_{i\alpha} f_i^{\text{eq}} = 0 \quad , \tag{F.14}$$

although the leftmost term of (F.14) is vanished due to (F.4), the second one is a second order tensor in terms of the first order contribution $f_i^{(1)}$. This is an unknown moment defined naturally from the last equation as

$$\Pi_{\alpha\beta}^{(1)} = \sum_i v_{i\alpha} v_{i\beta} f_i^{(1)} \quad , \tag{F.15}$$

such that the following PDE equation is obtained:

$$\epsilon^2 \left(1 - \frac{\delta t}{2\tau}\right) \partial_\beta^{(1)} \left(\Pi_{\alpha\beta}^{(1)}\right) + \epsilon^2 \partial_t^{(2)} \Pi_\alpha = 0 \quad , \tag{F.16}$$

another way to relate this tensor with the macroscopic moments at equilibrium is found by multiplying the equation (F.8b) by $v_{i\alpha} v_{i\beta}$ and adding it over i. That would give us the second tensor order conservation equation

$$\partial_t^{(1)} \Pi_{\alpha\beta} + \partial_\gamma^{(1)} \Pi_{\alpha\beta\gamma} = -\frac{1}{\tau} \Pi_{\alpha\beta}^{(1)} \tag{F.17}$$

then adding (F.13) and (F.16) the resulting PDE

$$\partial_\beta \Pi_{\alpha\beta} + \partial_t \Pi_\alpha = -\epsilon^2 \left(1 - \frac{\delta t}{2\tau}\right) \partial_\beta^{(1)} \Pi_{\alpha\beta}^{(1)} \quad . \tag{F.18}$$

Note that if $\tau = \delta t/2$ the right side of equation (F.18) vanishes, giving a continuity-like equation for the tensors Π_α and $\Pi_{\alpha\beta}$ as

$$\partial_\beta \Pi_{\alpha\beta} + \partial_t \Pi_\alpha = 0 \quad . \tag{F.19}$$

To see these equations as conservation laws (mass conservation or momentum conservation) we shall define the macroscopic moments in terms of fields with physical meaning. For example, as f_i has been interpreted as the probability density function to find a particle at certain position and velocity at any instant of time, it makes sense to define Π as a density field, because it's basically a discrete summation (or an integral in the continuous velocity space) of f_i which accounts for the probability at every possible velocity the particle can take at the position $\vec{x}$ and time t. In the same way it is possible to relate the momentum of this fluid of particles as the summation of velocities weighted by the probability density function f_i, just as it's defined in (4.4b), so that the following physical quantities for the zero and first order tensors shall be defined:

$$\Pi \equiv \rho = \sum_i f_i \quad , \tag{F.20a}$$

$$\Pi_\alpha \equiv \rho u_\alpha = \sum_i v_{i\alpha} f_i \quad , \tag{F.20b}$$

and for higher order tensor as well

$$\Pi_{\alpha\beta} \equiv p\delta_{\alpha\beta} + \rho u_\alpha u_\beta = \sum_i v_{i\alpha} v_{i\beta} f_i \tag{F.21a}$$

$$\Pi_{\alpha\beta\gamma} \equiv p(u_\alpha \delta_{\beta\gamma} + u_\beta \delta_{\alpha\gamma} + u_\gamma \delta_{\alpha\beta}) = \sum_i v_{i\alpha} v_{i\beta} v_{i\gamma} f_i \tag{F.21b}$$

considering the main macroscopic variables for a fluid such as the density ρ, the velocity u_α and the pressure p. Also, the tensor $\Pi_{\alpha\beta}$ has been identified as the **moment flux tensor**. For now these physical macroscopic fields have not been mentioned in the Lattice-Boltzmann model, thus this definition will have nothing to do with the model itself, unless the distribution function at equilibrium f_i^{eq} manages to recover the macroscopic fields from (4.4). This will be shown later on. Using eqn. (F.12) with (F.20a) and (F.20b) the continuity equation is given as

$$\partial_\alpha(\rho u_\alpha) + \partial_t \rho = 0 \quad . \tag{F.22}$$

In the other hand, using eqn. (F.18) with (F.21a) a PDE similar to NSE equation is gotten:

$$\partial_\alpha p + \partial_\beta(\rho u_\alpha u_\beta) + \partial_t(\rho u_\alpha) = -\left(1 - \frac{\delta t}{2\tau}\right)\left(\epsilon \partial_\beta^{(1)}\right)\left(\epsilon \Pi_{\alpha\beta}^{(1)}\right) \quad , \tag{F.23}$$

except for the tensor $\Pi_{\alpha\beta}^{(1)}$. This tensor will be determined by (F.17) using (F.21). Taking into account that for any variable x that

$$\partial_x(abc) = a\partial_x(bc) + b\partial_x(ac) - ab\partial_x c \tag{F.24}$$

and doing some algebra detailed in [38, Sec. A.2.2] it is proven that

$$\Pi_{\alpha\beta}^{(1)} = -\tau\left(p(\partial_\beta^{(1)} u_\alpha + \partial_\alpha^{(1)} u_\beta) - \partial_\gamma^{(1)}(\rho u_\alpha u_\beta u_\gamma)\right) \tag{F.25}$$

And finally it is necessary to use an equation of state in order to relate the density and the pressure. In this case the ideal gas law will be used in the sense of establishing a linear relationship between ρ and p just as it was written in (2.32) with c_s^2, previously appearing in (4.5c), the proportion ratio. As this pressure field is recovered from the second order tensor $\Pi_{\alpha\beta}$, the equilibrium distribution function must contain this generic c_s^2 constant. In the other hand, note that the last term of equation (F.25) is cubic in the velocity and appears as a consequence of defining $\Pi_{\alpha\beta\gamma}$ with quadratic terms of u, however it may be neglected as soon as $u^2 \ll c_s^2$ is fulfilled. However this term will naturally lead to affect the accuracy of the model as it will not be able to simulate strongly compressible phenomena. Using the expression obtained by (F.25) without the cubic term and replacing it into (F.18) is possible to get

$$\partial_\beta(\rho u_\alpha u_\beta) + \partial_t(\rho u_\alpha) = -\partial_\alpha p + \eta \partial_\beta(\partial_\beta u_\alpha + \partial_\alpha u_\beta) \tag{F.26}$$

with

$$\eta = \rho c_s^2 \left(\tau - \frac{\delta t}{2} \right) \tag{F.27}$$

will be the viscosity. Is possible to see that for $\tau = \delta t/2$ we end up with the Euler equation, however this case will lead to numerical instability as it's a limit case before the distribution functions become negative and the model instantly gets unstable (please see details in [38, sec. 4.4.2]). Although we have associated the moments from f_i to physical quantities to get continuity and NSE equation in (F.20), as mentioned before, this association is not possible if the equilibrium function f_i^{eq} is not properly defined in terms of these physical quantities. The equilibrium function must be written such that is possible to retrieve all the macroscopic moments using (4.4). One way to find the proper f_i^{eq} is by *moment matching*. This consist of writing the equilibrium function as an *ansatz* written as

$$f_i^{\text{eq}} = \omega_i \rho (1 + a_1 v_{i\alpha} u_\alpha + a_2 v_{i\alpha} v_{i\beta} u_\alpha u_\beta - a_3 u_\alpha u_\beta) \tag{F.28}$$

where ω_i are the weights that complement the velocity set. Then the constants a_1, a_2 and a_3 are found such that using the conditions for $v_{i\alpha}$ and ω_i described in (4.5) the macroscopic variables are obtained. For the case of fluids we have

$$a_1 = \frac{1}{c_s^2} \quad ; \quad a_2 = \frac{1}{2c_s^4} \quad ; \quad a_3 = \frac{1}{2c_s^2} \tag{F.29}$$

where c_s^2 constant appears once again due to (4.5), but finding the second order tensor, after doing the math we find that this matches the momentum flux tensor

$$\sum_i v_{i\alpha} v_{i\beta} f_i^{\text{eq}} = c_s^2 \rho \delta_{\alpha\beta} + \rho u_{i\alpha} u_{i\beta} = \Pi_{\alpha\beta} \tag{F.30}$$

thus, the constant c_s^2 appearing in (4.5) matches with the c_s^2 of (2.42) and f_i^{eq} is

$$f_i^{\text{eq}} = \omega_i \rho \left(1 + \frac{v_{i\alpha} u_\alpha}{c_s^2} + \frac{v_{i\alpha} v_{i\beta} u_\alpha u_\beta}{2c_s^4} - \frac{u_\alpha u_\beta}{2c_s^2} \right) \tag{F.31}$$

The equilibrium function is important to recover the required forms of the moments involved in the partial differential equations to solve, thus, its form is crucial in order to make this method to work. In the following sections we will describe another Lattice-Boltzmann model where the equilibrium function is different such that another kind of moments are obtained and therefor satisfying another set of equations if we introduce some restrictions to the algorithm.